

2013

A Comparative Study on the Modulatory Effects of Inhibition in the Mammalian and Avian Sound Localization Circuits

Matthew J. Fischl
Lehigh University

Follow this and additional works at: <http://preserve.lehigh.edu/etd>

 Part of the [Integrative Biology Commons](#)

Recommended Citation

Fischl, Matthew J., "A Comparative Study on the Modulatory Effects of Inhibition in the Mammalian and Avian Sound Localization Circuits" (2013). *Theses and Dissertations*. Paper 1483.

This Dissertation is brought to you for free and open access by Lehigh Preserve. It has been accepted for inclusion in Theses and Dissertations by an authorized administrator of Lehigh Preserve. For more information, please contact preserve@lehigh.edu.

A Comparative Study on the Modulatory Effects of Inhibition
in the Mammalian and Avian Sound Localization Circuits

by

Matthew J. Fischl

A Dissertation

Presented to the Graduate and Research Committee

of Lehigh University

in Candidacy for the Degree of

Doctor of Philosophy

in

Integrative Biology

Lehigh University

May 20th, 2013

© 2013 Copyright
Matthew J. Fischl

Approved and recommended for acceptance as a dissertation in partial fulfillment of the requirements for the degree of Doctor of Philosophy

Matthew J. Fischl

A Comparative Study on the Modulatory Effects of Inhibition in the Mammalian and Avian Sound Localization Circuits

22 April 2013

Defense Date

22 April 2013

Approved Date

Dissertation Director
R. Michael Burger

Committee Members:

Matthias Falk

Julie Haas

Yong Lu

ACKNOWLEDGMENTS

There are many, many people that have contributed to this document and my career at Lehigh. The following acknowledgements are not a complete list, but for the sake of brevity I cannot thank everyone individually.

I would first like to thank my wife for supporting me unconditionally in my doctoral endeavor and tolerating unpleasant employment so that we could live comfortably. I am incredibly lucky to be married to such a beautiful and caring person. I love you.

I would next like to acknowledge the hard work and patience of my advisor Dr. R. Michael Burger. Mike, you have taught me how to be a scientist. Your critical feedback has improved my scientific work in innumerable ways. Your support and compassion over the course of my time at Lehigh will never be forgotten. Thank you for always urging me to be the best I could be.

I would also like to thank the members of my dissertation committee, Dr. Yong Lu, Dr. Matthias Falk and Dr. Julie Haas. Yong, your advice and analytical eye has had a major influence on my research. Matthias, your questions and conversations have really made me feel that my research was interesting and important. Julie, I am indebted to you for agreeing to join my committee given the short notice. Thank you for your vital input.

The entire department of biological sciences deserves acknowledgement. This includes all of the groups such as the graduate committee who endowed me with two fellowships during my research, the faculty who have all helped train me through their coursework and seminars, and the administrators who have answered the same questions repeatedly over my career here. This department has been a very fostering environment.

I thank my family and friends for all of their love and support. Many of you have helped me to maintain my sanity during this process by lending an ear or offering a beer.

To my mother and father, thank you for always encouraging me and never stifling my inquisitions or ambitions. I am grateful for all of the sacrifices you made so I could further my education.

I would also like to thank everyone for their generous contributions to the Heather Oehling MDS foundation. Special thanks to Kandi Kulp (Schrader) and Jen Snekser for organizing the benefit and thanks to all of the celebrity bartenders for volunteering their time. Helping my wife return to health while continuing my graduate studies was the most difficult time in my life. Your donations relieved us from a tremendous debt.

Lastly, I would like to acknowledge everyone who has called me smart, gifted, intelligent, astute or otherwise encouraged me to embrace my nerdiness. Thank you for convincing me I could achieve this goal.

TABLE OF CONTENTS

List of Figures	vi
List of Tables	vii
List of Abbreviations	viii
Abstract	1
CHAPTER I: Introduction to sound localization circuitry	3
CHAPTER II: Modulation of synaptic input by GABA _B receptors improves coincidence detection for the computation of sound location	26
CHAPTER III: Synaptic physiology of inhibitory inputs in the superior olivary nucleus	72
CHAPTER IV: Slowly emerging glycinergic transmission enhances inhibition in the temporal processing pathway of the avian auditory system	91
CHAPTER V: Glycinergic transmission modulates inhibition in the avian brainstem	112
CHAPTER VI: Summary and Concluding Remarks	129
References	133
Vita	145

LIST OF FIGURES

<u>Figure #</u>	<u>Figure Title</u>	<u>Page #</u>
Figure 1.1:	Schematic representations of the generation of sound localization cues.....	5
Figure 1.2:	Schematic representation of features of the Jeffress model.....	7
Figure 1.3:	Fossil evidence suggests the tympanic ear evolved separately in birds (Aves) and mammals.....	9
Figure 1.4:	Schematic representation of the mammalian auditory system.....	12
Figure 1.5:	Avian auditory brainstem schematic.....	14
Figure 1.6:	Auditory space is represented by a neural place code in birds.....	16
Figure 1.7:	Schematic of ITD encoding in mammals.....	18
Figure 1.8:	Precisely timed inhibition imparts the ITD tuning in MSO neurons necessary for the two-channel encoding model.....	20
Figure 1.9:	Inhibitory feedback from the SON modulates response properties of brainstem neurons.....	23
Figure 2.1:	GABA _B R activation suppresses evoked EPSCs in MSO principal neurons.....	41
Figure 2.2:	Activation of GABA _B Rs suppresses IPSC amplitude and slows kinetics.....	43
Figure 2.3:	Modulation of GABA _B Rs effects rates of depression of EPSCs during repetitive stimuli.....	46
Figure 2.4:	Depression rates of IPSCs are affected by modulation of GABA _B Rs during repetitive stimuli.....	48
Figure 2.5:	ITD sensitivity is modulated by GABA _B R activation.....	50
Figure 2.6:	Blocking GABA _B R activity broadens sITD tuning curves.....	53
Figure 2.7:	Model parameters for excitatory and inhibitory inputs.....	55
Figure 2.8:	IPSC kinetics and PSC amplitude reduction independently shape ITD tuning in the E/EI model.....	58
Figure 2.9:	GABA _B R dependent improvements in ITD selectivity are maintained over a range of input parameters in the E/EI model.....	61
Figure 3.1:	Evoked IPSCs in the SON contain GABAergic and glycinergic components.....	84
Figure 3.2:	Spontaneous postsynaptic currents are modulated by blockade of both GABA and glycine receptors.....	86
Figure 4.1:	Glycine receptors are expressed in all four auditory brainstem nuclei.....	101
Figure 4.2:	Exogenous glycine application evokes strychnine sensitive currents in the SON, NM and NL.....	103
Figure 4.3:	High frequency stimulation evokes glycinergic transmission in NM.....	105
Figure 4.4:	Blocking GlyRs decreases the ability of evoked IPSPs to suppress action potentials in NM.....	107
Figure 5.1:	Pre-application of glycine suppresses evoked IPSC trains in the SON.....	120
Figure 5.2:	Evoked IPSCs are suppressed by glycine pre-pulse in NM.....	122
Figure 5.3:	Suppression of mini IPSC amplitudes after glycine application is eliminated by strychnine.....	123
Figure 5.4:	Manipulation of Cl ⁻ ion flux alters the suppression profile of glycine prepulse in the NM.....	125

LIST OF TABLES

<u>Table #</u>	<u>Table Title</u>	<u>Page #</u>
Table 2.1:	Depression variable values for depression of EPSG and IPSP magnitude in the computational model expression $G_{input}=G_{initial}(a+(b*\exp(c*t)))$	71
Table 3.1:	Raw data values for evoked, spontaneous and miniature IPSCs during <i>in vitro</i> whole cell voltage clamp experiments.....	82

LIST OF ABBREVIATIONS

A	ampere
ACSF	artificial cerebrospinal fluid
AP5	D-2-amino-5-phosphonopentanoic acid
AVCN	anteroventral cochlear nucleus
BAC	baclofen
bIPD	best interaural phase difference
bitD	best interaural time difference
CF	characteristic frequency
CGP	CGP55845
Cl-	chloride ion
CN	cochlear nucleus
CON	control
contra	contralateral
dB	decibel
DNQX	6,7-dinitroquinoxaline-2,3-dione
E#	embryonic day #
eIPSC	evoked inhibitory postsynaptic current
EPSC	excitatory postsynaptic current
EPSCG	excitatory postsynaptic conductance
EPSP	excitatory postsynaptic potential
Fig	figure
FR	firing rate
GABA	γ -Aminobutyric acid
Gly	glycine
GlyR	glycine receptor
GLYT2	glycine transporter 2
Hz	hertz
IgG	immunoglobulin G
ILD	interaural level difference
IPSC	inhibitory postsynaptic current
IPSCG	inhibitory postsynaptic conductance
ipsi	ipsilateral
IPSP	inhibitory postsynaptic potential
ITD	interaural time difference
K+	potassium ion
LNTB	lateral nucleus of the trapezoid body
LSO	lateral superior olive
LVA	low voltage activated
M	molar
MNTB	medial nucleus of the trapezoid body
MSO	medial superior olive

nVIII	auditory nerve
NA	nucleus angularis
NL	nucleus laminaris
NM	nucleus magnocellularis
P#	postnatal day #
PSC	postsynaptic current
PSP	postsynaptic potential
REC	recovery
s or sec	second
sIPSC	spontaneous inhibitory postsynaptic current
sIPSP	spontaneous inhibitory postsynaptic potential
sITD	simulated interaural time difference
SN	strychnine
SON	superior olivary nucleus
SPL	sound pressure level
SR	SR95531
strych	strychnine
TTX	tetrodotoxin
V	volts
VGAT	vesicular GABA transporter
VIAAT	vesicular inhibitory amino acid transporter
V_{rev}	reversal potential
Ω	ohm

Abstract

Sound localization is a critically important task for many animals including humans. Due to physical constraints acting on the circuits that process sound localization cues, many neural specializations have evolved. One of the key features and the focus of this dissertation is inhibitory input. To assess the impact of inhibition, I employ in vitro patch clamp techniques to observe cellular and synaptic physiology in brainstem circuits dedicated to sound localization processing.

Using a mammalian model, I test the impact that GABA_B receptor (GABA_BR) activation has on the inputs to the medial superior olive (MSO), the first area where sound localization computations take place. Activation of GABA_BRs modulates both excitatory and inhibitory inputs such that the magnitude of these inputs is decreased and the time course of inhibitory inputs is slowed. The functional significance of this modulation was tested using a bilateral stimulation protocol, which simulates the coincidence of in vivo excitatory inputs. Here, activation of GABA_BRs increased the sensitivity of MSO neurons to simulated interaural time disparity (ITD), the main cue for low frequency sound localization. To expand on these results, a computational model was used to show that each GABA_B dependent modulation had a beneficial impact on ITD sensitivity in the MSO.

In an avian system, I described the synaptic activity involving the superior olivary nucleus (SON), which provides the main inhibitory input in the avian sound localization circuit. At the SON itself, synaptic transmission consists of both GABA- and glycinergic components where glycine release is the result of co-release with GABA. I also show that functional glycine receptors localize at brainstem nuclei and that high frequency

stimulation results in the release glycine onto nucleus magnocellularis neurons, a feature of the avian brainstem that has not been observed previously.

In related experiments, I evaluate possible interactions that may occur when both GABA and glycine receptor systems are activated simultaneously. Here, a pre-activation of GlyRs leads to a decrease in conductance through the GABA_AR likely due to changes in Cl⁻ ion concentrations which manipulate the driving force of the ion.

CHAPTER I

Introduction to sound localization circuitry

For many vertebrate species, sound localization is an integral task for survival and social communication. Unlike the senses of touch and vision where the sensory surface is topographically organized such that neurons that respond to stimuli from a given location are next to each other, there is no place code on the sensory surface in hearing that correlates to the position of a sound in space. Therefore, sound location must be computed in the brain. This computation is performed by comparing sounds at the two ears. The binaural cues that are available include differences in timing and intensity that are created when a sound originates from a place lateral to a listener's midline. These cues are often small which has led to the evolution of many specializations in the circuits that perform sound localization computations. Inhibitory inputs play a key role in maintaining sensitivity to the cues used for sound localization over the broad range of auditory stimulus magnitudes experienced by listeners.

Sound Localization Cues

Sound localization in the horizontal plane (azimuth) is localized using two main binaural cues mentioned above, the timing and intensity differences created by lateralized sounds. These cues are used differentially across the range of sound frequencies. High frequency sounds defined as wavelengths shorter than the width of a listener's head will be attenuated as they travel around the head and therefore be louder in the ear closer to the sound source. This cue is called interaural level difference (ILD). For low frequency sounds, wavelengths are longer than the width of the head and will not be significantly attenuated. However, a lateralized sound will impinge on the ear closer to the source

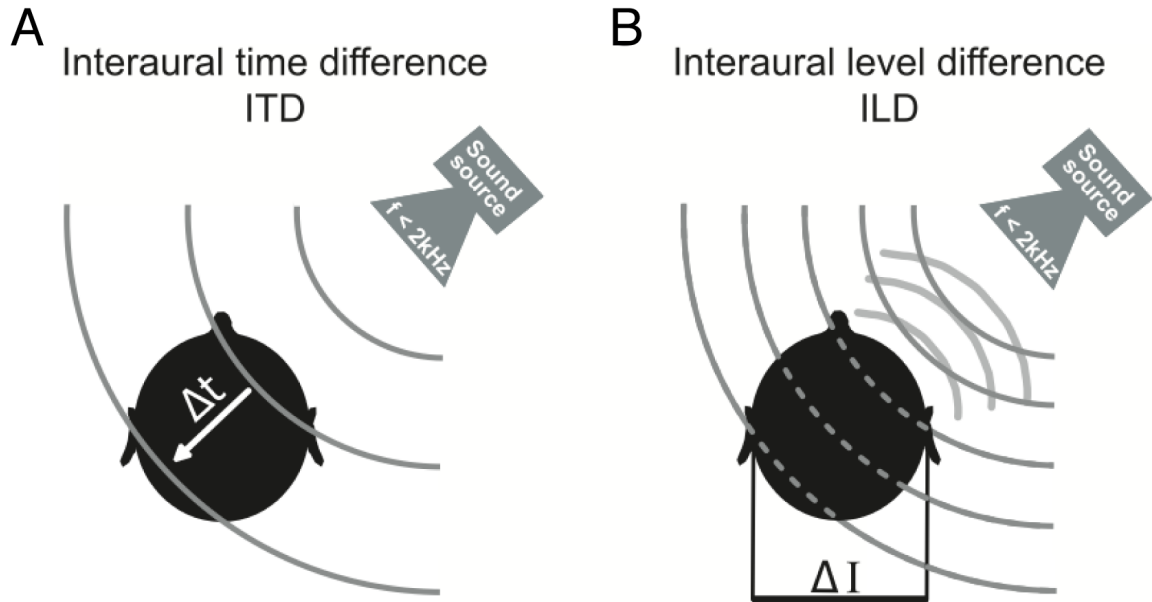


Figure 1.1: Schematic representations of the generation of sound localization cues. A. Interaural time disparity (ITD) is the difference in arrival time of a sound between the two ears. This is the primary cue used for low frequency sound localization. B. Interaural level difference (ILD) is the difference in intensity of a sound at the two ears. This results from a sound being attenuated as it travels around the head and is the primary cue used in the localization of high frequency sounds. Modified from Grothe et al. 2010.

first, then moments later the other ear. This difference in timing is the main cue used to localize low frequency sound and is called interaural time difference (ITD) (Fig 1.1).

These two cues vary systematically with the location of a sound source where there is no difference for a sound originating from directly in front of an individual and the maximum difference occurs at 90° lateral to a listener's midline (Thompson 1882, Rayleigh 1907). This study focuses on ITD processing in two animal models with good low frequency hearing; the gerbil, a mammal, and the chicken, an avian.

Jeffress Model of Sound Localization

A model circuit for ITD discrimination was proposed in 1948 by Lloyd Jeffress (Jeffress 1948). The model relies on three main features of the circuit: time-locked inputs, coincidence detectors, and a series of delay lines with varying input lengths to the coincidence detectors (Fig 1.2). Since ITD is a timing cue, temporal features of sound stimuli must be preserved (i.e. time-locked input). Phase-locking is a response property of auditory neurons whereby they fix their spiking output to a certain phase of the stimulus waveform (Fig 1.2A). “Coincidence detectors” are neurons that respond maximally when they receive input from both ears simultaneously. These neurons are found in the medial superior olive (MSO) in mammals and the nucleus laminaris (NL) in birds and receive phase-locked excitatory input from both ears. The “delay lines” refer to the anatomical arrangement of axons leading to the coincidence detector such that the combination of the conduction times down the axon and the ITD will cause a small

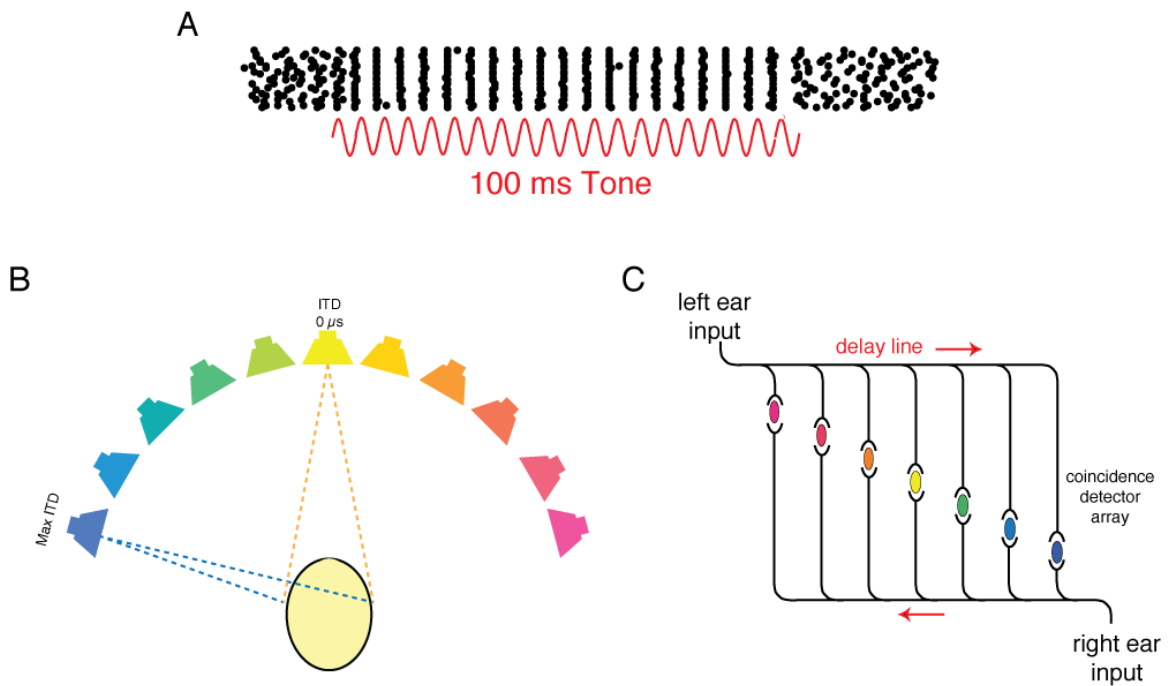


Figure 1.2: Schematic representation of features of the Jeffress model. A. Example of a neuron phase-locking to a tonal stimulus. Raster plot shows that the neuron fires predictably at a certain phase of the pure tone stimulus. Phase-locking provides the time locked inputs necessary for this model. B. ITDs vary systematically with position in the horizontal plane. C. Representation of the Jeffress model circuit where coincidence detecting neurons are innervated by an array of delay lines with varying axon lengths. The pairing of ITD and varying conduction times results in the maximum activation of one or a few coincidence detecting neurons. Color coding of the neurons matches the speaker location (B) that would theoretically evoke maximum response. B & C modified from Seidl et al. 2010.

number of neurons to receive coincident binaural input. A coincidence detecting neuron responding maximally to an ITD of zero should theoretically have equal conduction times from each ear. This model has been an integral part of sound localization research and shares many features with biological circuits in both birds and mammals (barn owl: Carr and Konishi 1990, chicken: Overholt et al. 1992, Seidl et al. 2009). While recent work has strengthened the relationship between the avian circuit and the Jeffress model, studies in the mammalian system have begun to depart from this view.

Animal Models and Evolution

For this research, gerbils and chickens were used as animal models. Both of these vertebrates possess hearing organs that have a tympanic membrane or eardrum. Fossil records indicate that the tympanic ear appeared approximately 200 million years ago after the divergence of mammals and birds. No common ancestor of mammals and birds has been discovered that possessed this anatomical feature leading scientists to believe that it has evolved independently in each group (Fig 1.3). Therefore, sound localization circuits have also evolved independently in mammals and birds (Clack 1997, 2002). The physical nature of sound and small head size of most mammals and birds has constrained the evolution of hearing systems such that convergent evolution had lead to similar systems in both vertebrate groups. Many features that are now considered hallmarks of sound localization circuitry are found in gerbils and chickens. Since the auditory system operates over a large range of intensities, many mechanisms contribute to the auditory systems ability to remain sensitive to low intensity stimuli but also respond dynamically

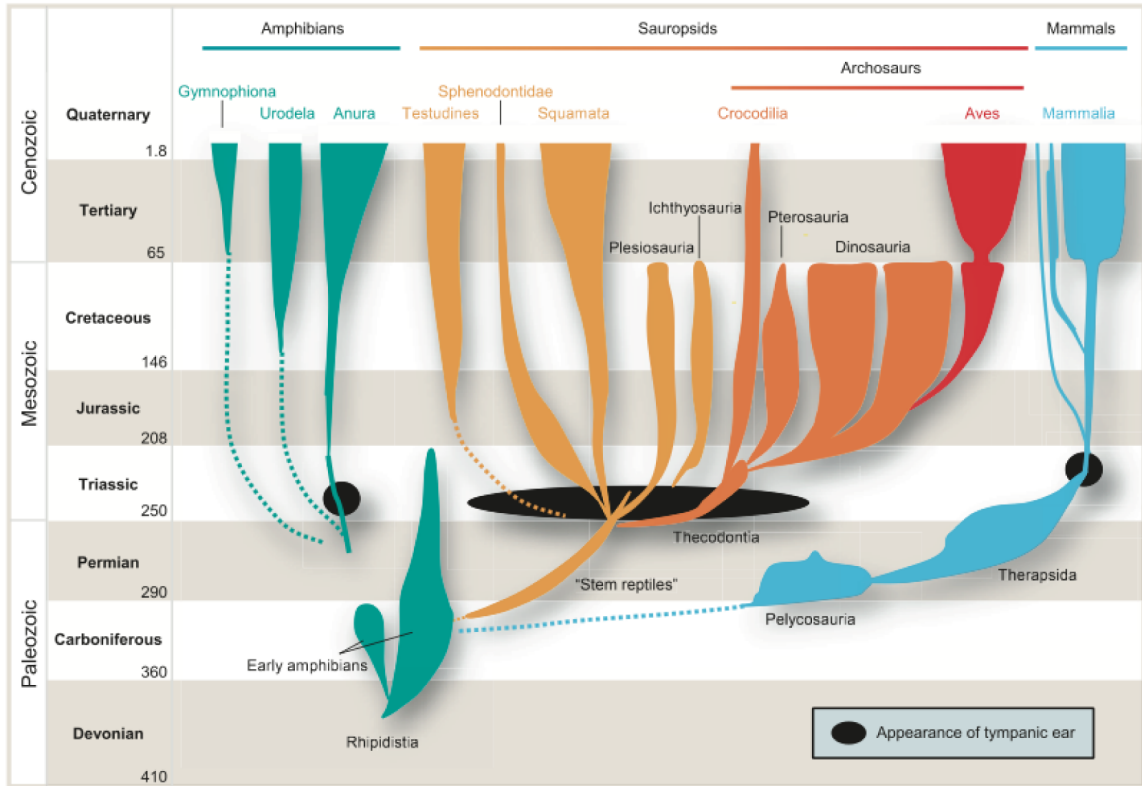


Figure 1.3: Fossil evidence suggests the tympanic ear evolved separately in birds (Aves) and mammals. Since no common ancestor of these two groups possessed a tympanic ear, sound localization mechanisms have also evolved separately. From Grothe et al. 2010.

at high intensities. These mechanisms include synaptic depression (Kuba et al. 2002, Cook et al. 2003), receptor desensitization (Raman and Trussell 1992), suppression of neurotransmitter release (Brenowitz et al. 1998) and populations of cells with a range of thresholds and spontaneous rates.

Neural Encoding of Sound

Due to the physical nature of sound (pressure waves of differing frequency and amplitude) and the evolution of the tympanic ear as a transduction mechanism, two key features of sounds that can be extracted by the hearing organ and transduced into electrical impulses are frequency and intensity. Frequency information is extracted initially in the cochlea. Physical characteristics of the basilar membrane (basilar papilla in the chicken) of the cochlea cause each frequency to resonate a specific area along the membrane's basal-apical extent. High frequencies displace the membrane near the base of the cochlea, low frequencies near the apex. This topographic representation of frequencies is called tonotopy. Tonotopic organization of neural response properties is generally maintained as a "place map" of frequency in the nuclei of the auditory brainstem and higher order auditory areas of the brain (von Bekesy 1970).

Intensity information is transduced from sound waves into electrical impulses (action potentials) in the cochlea as well. Hair cells along the basilar membrane depolarize with the displacement of the membrane via mechanically gated ion channels. More intense sounds cause greater displacement of the membrane, increased neurotransmitter release from the hair cells and increased activity of the auditory nerve

fibers. Generally, neurons in the auditory nuclei respond to greater intensity with increased firing rate up to a point of saturation.

Sound Localization Circuitry

In the mammalian ITD processing circuit (Fig 1.4), auditory nerve fibers enter the brainstem and synapse with bushy cells in the ventral cochlear nucleus (CN). These neurons are specialized for temporal signaling and show an improvement in phase-locking vector strength over their auditory nerve fiber inputs (Joris et al. 1994). Spherical bushy cells project ipsilaterally to innervate the MSO (Warr 1966, Osen 1969, Cant and Casseday 1986, Smith et al. 1993) while globular bushy cells project contralaterally to the medial nucleus of the trapezoid body (Smith et al. 1991). This synapse called the Calyx of Held is one of the largest synapses in the brain and is specialized in order to convert the excitatory signal from the CN into an inhibitory signal while maintaining temporal precision and minimizing latency (Held 1893, Morest 1968, Smith et al. 1998, von Gershdorff and Borst 2002). MSO neurons have bilaterally oriented dendritic arbors where ipsilaterally derived inputs synapse on the lateral dendrite and contralaterally derived inputs synapse on the medially oriented dendrite (Ramon y Cajal 1907, Rautenberg et al. 2009). The MSO is innervated bilaterally by excitatory inputs from spherical bushy cells of the ventral cochlear nucleus. MSO neurons also receive their main inhibitory input from the ipsilateral MNTB which is driven by globular bushy cells in the contralateral ventral CN (Morest 1968, Wenthold et al. 1987, Smith et al. 1991). The MSO also receives ipsilateral inhibitory input from the lateral nucleus of the

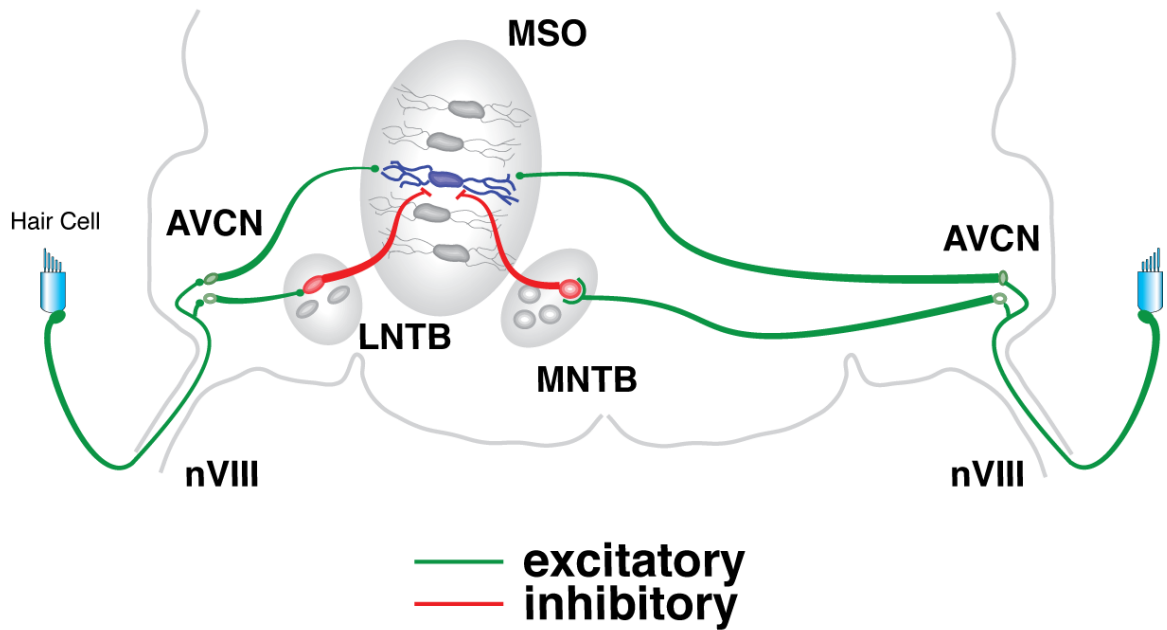


Figure 1.4: Schematic representation of the mammalian auditory system. Coincidence detecting neurons in the medial superior olive (MSO) receive bilateral excitatory input from bushy cells in the anteroventral cochlear nucleus (AVCN). Additionally they receive their primary inhibitory input from the ipsilateral medial nucleus of the trapezoid body (MNTB) which switches contralaterally derived excitation from the AVCN into inhibition. The MSO also receives an inhibitory input from the ipsilateral lateral nucleus of the trapezoid body.

trapezoid body (Cant and Hyson 1992). The MSO integrates all of these inputs and the strength and timing of each plays a role in the output of the neuron. MSO neurons send projections to the dorsal nucleus of the lateral lemniscus and the inferior colliculus for higher order processing (Thompson and Schofield 2000).

In birds, auditory nerve fibers enter the brainstem where they bifurcate to innervate the cochlear nuclei, the NA and the NM (Parks and Rubel 1975) (Fig 1.5). The NA provides glutamatergic input to the SON in the brainstem and higher order auditory nuclei involved in intensity discrimination. The NM is a relay in the timing circuit involved in ITD discrimination. NM neurons receive large secure synapses from the auditory nerve which provide phase-locked glutamatergic excitatory input (Koppl 1994, Carr and Koppl 1997, Konishi 2003). NM then relays phase-locked signals to both the ipsi- and contralateral NL. Anatomical studies show that while NM sends similar length projections to innervate the ipsilateral NL, its contralateral projections to the NL increase in length along the medio-lateral axis of the nucleus. Only the contralateral projection pattern bears a semblance to the delay lines modeled by Jeffress (Parks and Rubel 1975, Seidl et al. 2010). NL neurons have symmetric dendritic arbors that are innervated dorsally by the equal length axons from the ipsilateral NM and ventrally by axons increasing in length medial to lateral by the contralateral NM. NL provides sound location information to the inferior colliculus and other higher auditory nuclei. NL also provides input to the ipsilateral SON. The SON is the major source of inhibitory feedback for the auditory brainstem. It receives input from the ipsilateral NA and NL and

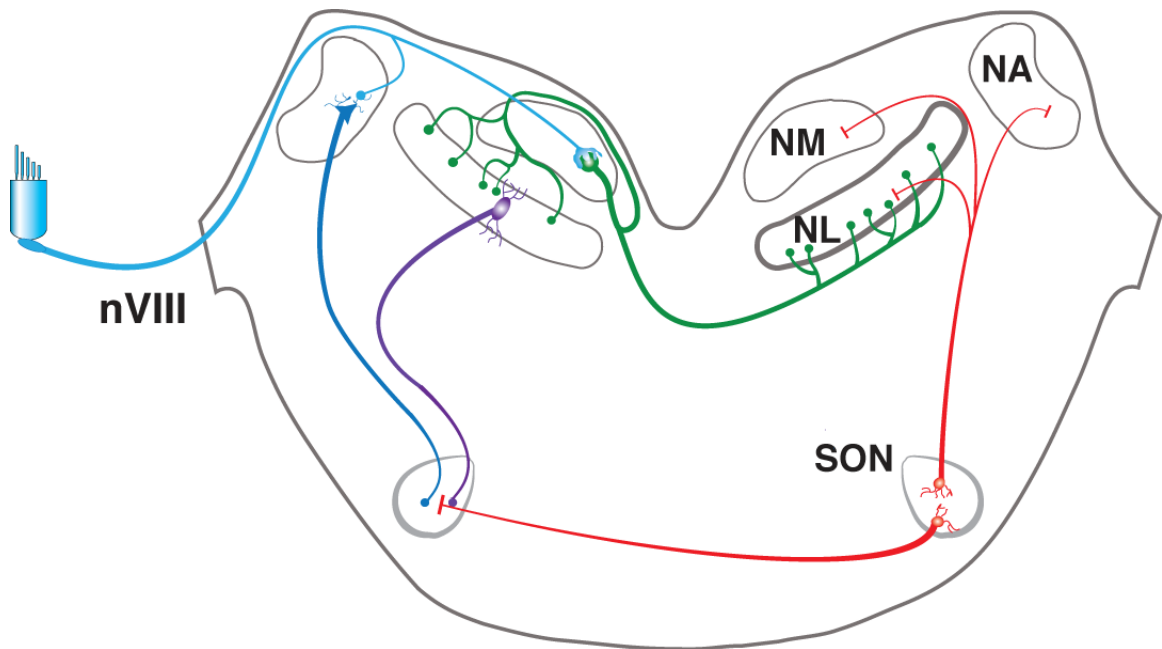


Figure 1.5: Avian auditory brainstem schematic. Auditory nerve (nVIII) fibers enter the brainstem and bifurcate to innervate the cochlear nuclei, nucleus magnocellularis (NM) and nucleus angularis (NA). Coincidence detecting neurons in the nucleus laminaris receive bilateral excitatory input from the NM. NA and NL innervate the superior olivary nucleus (SON). The SON provides inhibitory feedback ipsilaterally to the NM, NL and NA and also sends a projection to the contralateral SON.

the contralateral SON, and provides descending inhibitory feedback to the ipsilateral NA, NM and NL as well as ascending inhibition to the contralateral SON (Lachica et al. 1994, Conlee and Parks 1986, Burger et al., 2005.)

ITD computation

Although many characteristics of the ITD circuit are similar between mammals and avians, the current view is that the computation of ITDs is fundamentally different in the two groups. While avians are observed to follow the tenants of the Jeffress model, many studies involving the mammalian ITD circuit have yielded results that are at odds with the delay line theory.

The avian system, as described mainly through studies in barn owls and chickens, is remarkably similar to the Jeffress model. Delay lines are evident in the NM's contralateral projection to the coincidence detecting neurons in the NL (Parks and Rubel 1975, Young and Rubel 1983, Overholt et al. 1992, Seidl et al. 2010). These delay lines have been shown to impart a systematic arrangement of peak ITD responses in NL in both *in vitro* and *in vivo* experiments (Carr and Konishi 1988, 1990, Overholt et al. 1992, Joseph and Hyson 1993, Koppl and Carr 2008). It is therefore expected that the auditory space map is created by the peak ITD responses of a few neurons tuned to discrete location in the horizontal plane around a listener. Recent data supporting this model is shown in Figure 1.6 along with a schematic representation of the ITD circuit in birds.

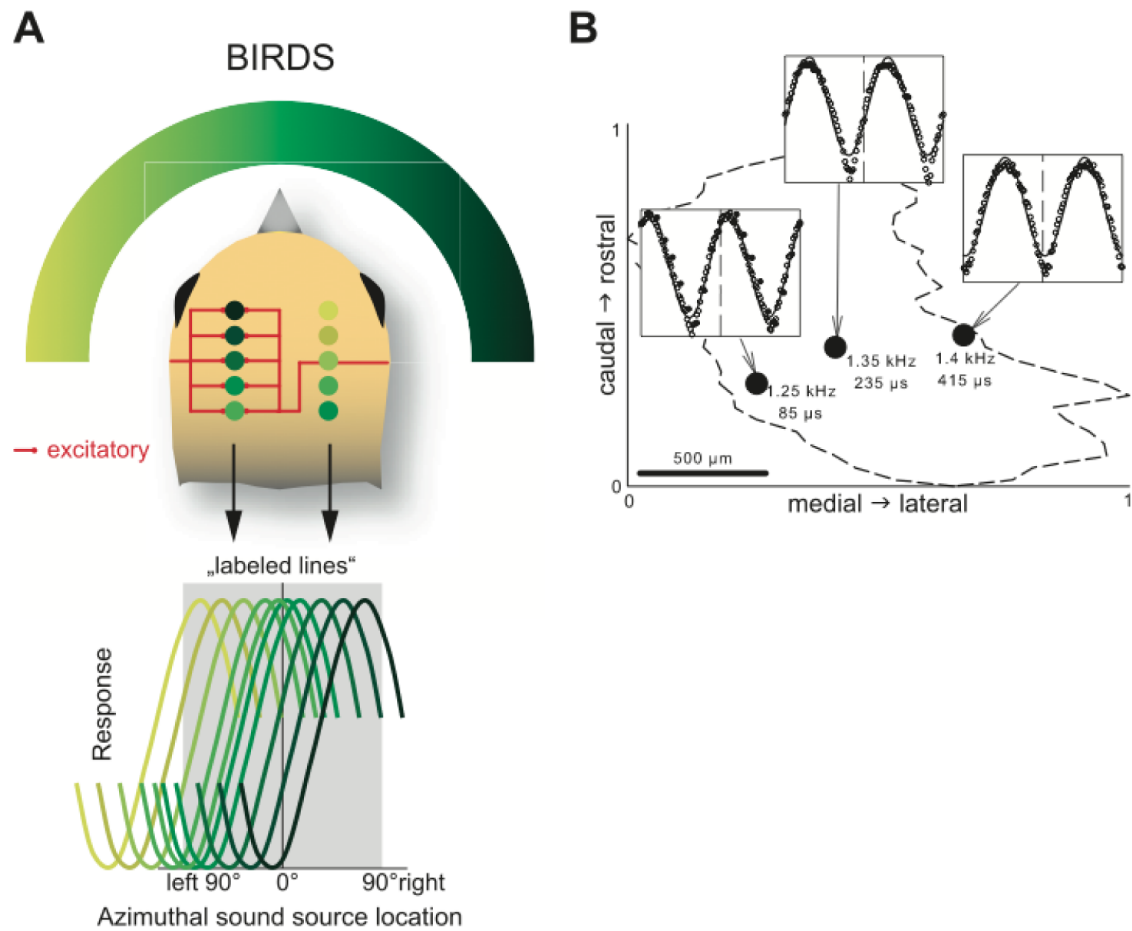


Figure 1.6: Auditory space is represented by a neural place code in birds. A. Schematic of the avian ITD circuit where delay lines to coincidence detecting neurons impart each neuron with a unique ITD function (lower panel) whose peak falls within the physiologically relevant range of ITDs. B. *In vivo* recordings from the NL show the systematic arrangement of best ITDs from medial to lateral in one isofrequency band. Adapted from Grothe et al. 2010. Panel B originally from Koppl and Carr 2008.

In mammals, the ITD circuit abides by the first two points in the Jeffress model, time-locked inputs and binaurally innervated coincidence detecting neurons. But anatomical evidence for the existence of delay lines in the mammalian circuit has led to mixed conclusions and no systematic arrangement has been confirmed over the population (Smith et al. 1993, Beckius et al. 1999). Additionally, the majority of neurons in the MSO display peaks in their ITD functions at delays outside of the physiologically relevant range of ITDs that the animal could experience (McAlpine et al. 2001, Brand et al. 2002, Pecka et al. 2008). These best ITDs (bITD) correlated with the characteristic frequency of the neuron such that there was a decrease in bITD as CF increased. A comparison of the phase difference (bIPD) in relation to the CF revealed that the bIPD was remarkably similar for the population ($bIPD = 0.12 \pm 0.04$ cycles). This shift in the ITD function towards the contralateral ear aligned the slope of the function at the midline (0 ITD) such that the steepest part occurs through the physiologically relevant range of ITDs experienced by the listener (Brand et al. 2002). This arrangement allows for the greatest degree of spike rate modulation to occur with physiologically relevant ITDs. These discoveries lead to the development of the two-channel model where the average response of the population of neurons in each hemisphere is compared and the specific ratio of activity in between the hemispheres represents specific positions in the azimuth (McAlpine et al. 2001, Hancock and Delgutte 2004, Siveke et al. 2006, Pecka et al. 2008). A schematized view of the two-channel model is shown in Figure 1.7.

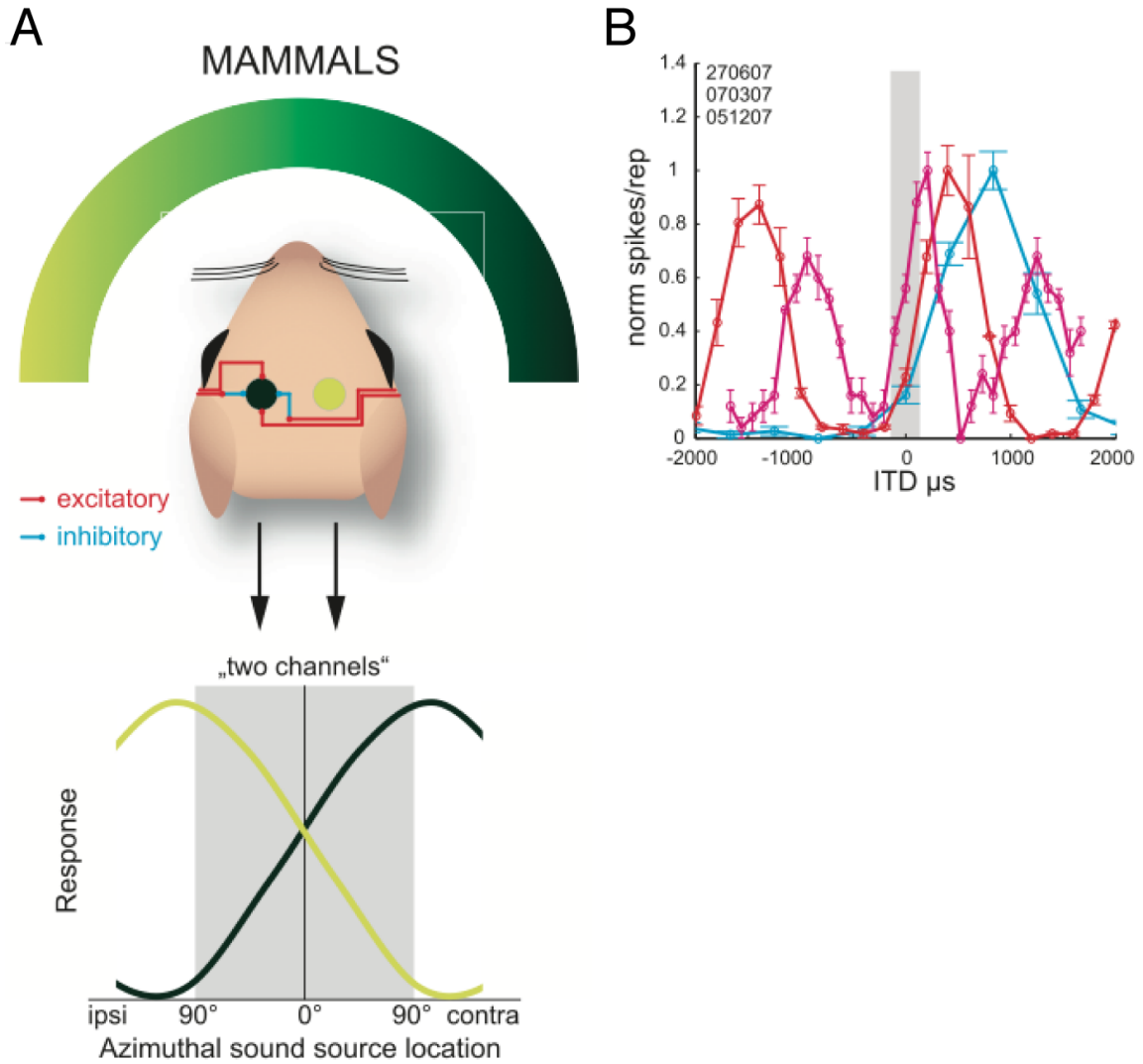


Figure 1.7: Schematic of ITD encoding in mammals. A. Integration of the inputs in the MSO results in populations of neurons that fire preferentially with sounds that lead in the contralateral ear. The source is determined by a comparison of spiking in the population in each hemisphere. B. ITD tuning curves from three neurons in the gerbil MSO show peaks outside the physiologically relevant range, but slopes in the physiologically relevant range. Modified from Grothe et al. 2010, B originally from Pecka et al. 2008.

Role of Inhibition in ITD processing

As previously mentioned the principal mode of inhibitory neurotransmission is different between the two systems, glycinergic feed-forward inhibition in mammals, and GABAergic feedback inhibition in avians. However, to begin the discussion on inhibition in ITD processing let us first look at a shared role in both systems. Neurons in the cochlear nuclei of mammals and birds provide the phase-locked inputs to the coincidence detecting neurons. At the cochlear nuclei, feedback inhibition has several functions. These include increasing frequency selectivity, maintaining firing rates below saturation during high intensity stimuli, and improving the phase-locking ability above that of the auditory nerve fiber inputs (mammal: Caspary et al. 1994, Kopp-Scheinflug et al. 2002, Dehmel et al. 2010, Kuenzel et al. 2011; bird: Koppl 1997, Fukui et al. 2006, Fukui et al. 2010). These modulatory effects ensure high fidelity in the output to the coincidence detectors.

In mammals, glycinergic transmission works on a cycle-by-cycle basis where precisely timed inhibition modulates the response of MSO neurons to phase-locked excitatory input. The impact of the timing of inhibition was shown in several *in vivo* studies in the gerbil MSO where pharmacological block of glycine receptors with strychnine resulted in increased firing rates and a shift of the peak of the ITD tuning curve towards 0ITD (Brand et al. 2002, Pecka et al. 2008). The conclusion from these studies was that the contralaterally derived glycinergic inhibition from the MNTB preceded the contralateral excitation and was responsible for shifting the ITD tuning curve towards the contralateral ear (see Fig 1.8 for further description). This temporal

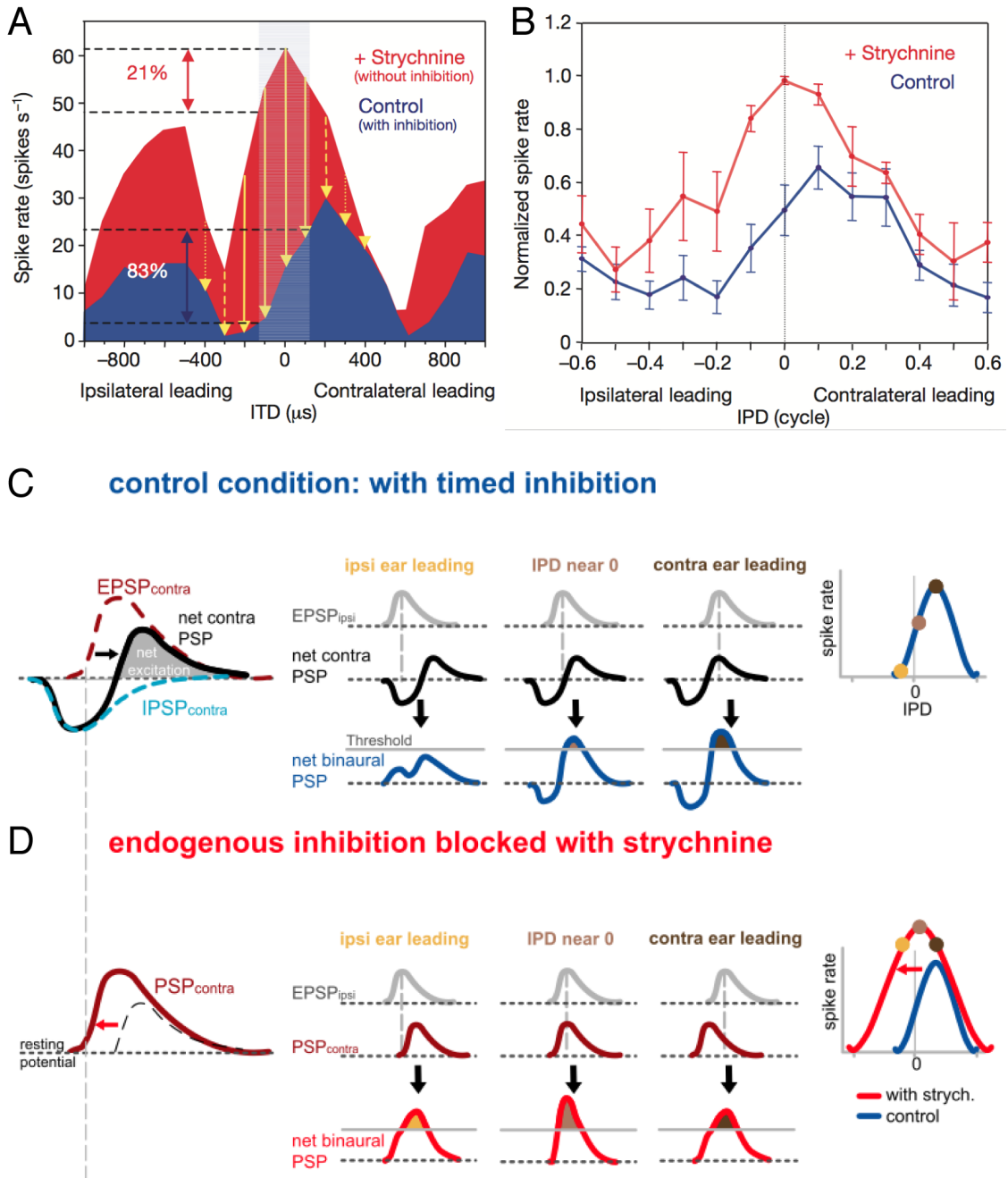


Figure 1.8: Precisely timed inhibition imparts the ITD tuning in MSO neurons necessary for the two-channel encoding model. A. ITD turning curves from an MSO neuron in control and GlyR block reveals shift of the curve towards zero ITD in strychnine. B. Population data for MSO neurons shows the peak of the ITD tuning curve in strychnine and the steep part of the slope around zero in control. C. Schematic representation of the integration of inputs in the MSO in the control condition showing how timing of inhibitory input shifts the peak of the tuning curve towards sounds leading in the contralateral ear. D. Integration scheme when inhibition is blocked resulting in a peak at zero ITD. Adapted from Pecka 2008.

integration of the glycinergic inhibition with the bilateral excitation sets up the 2-channel model for ITD discrimination in the mammalian circuit.

In the avian system the vast majority of research has focused on GABAergic inhibition. In the neurons known to be directly involved in ITD processing, the NM and NL, high cytosolic concentrations of Cl⁻ result in the efflux of Cl⁻ ions during activation of GABA receptor channels. Therefore, opening of Cl⁻ channels caused by GABA input will lead to an efflux of Cl⁻, taking negative charge out of the neuron and depolarizing it (Hyson 1995, Lu and Trussell 2000, 2001, Monsivais and Rubel 2001). This depolarization has an inhibitory effect because it activates low voltage activated (LVA) K⁺ channels at NM and NL. This K⁺ conductance has a shunting action, effectively lowers the input resistance, speeds up the membrane time constant and decreases the ability of non-coincident inputs from resulting in spike transmission (Bruckner and Hyson 1998, Funabiki et al. 1998, Kuba et al. 2002, Howard et al. 2010) (Fig 1.9). Additionally, the slight depolarization of the GABAergic inhibition presumably causes inactivation of sodium channels and raises the spiking threshold (Monsivais et al. 2001).

In addition to the GABA_A receptor system, metabotropic GABA_B receptors are also prevalent in the avian auditory brainstem nuclei (Burger et al., 2005b). GABA_B receptor activation in the NM has a suppressive effect on excitatory postsynaptic currents (EPSCs). This suppression has been shown to preserve phase-locking ability of NM neurons at higher frequencies by limiting neurotransmitter release and reducing the short-term depressive effects of high frequency stimuli (Brenowitz et al., 1998).

SON as a Gain Control

Sound localization circuitry operates over a very broad range of input intensities and ITD selectivity in the NL is maintained even at high stimulus intensities (>70dB) (Pena et al. 1996.) It is therefore likely that the feedback inhibition from the SON plays a role in this maintenance. The SON receives input proportional to sound intensity from the NA and provides inhibitory input to its ipsilateral targets the NA, NM and NL and the contralateral SON (Fig 1.10). The ipsilateral feedback loop and reciprocal connection form an inhibitory circuit that has been implicated as the source of gain control in this system (Burger et al. 2005a, Dasika et al. 2005, Hyson 2005) and is capable of equalizing imbalances in intensity that occur. In an *in vivo* study, Nishino et al. (2008) found that lesioning the SON reduced ITD selectivity in the ipsilateral NL in the chicken. Additionally, pharmacologically blocking GABA_A receptor mediated inhibition to the NM caused increased spiking and decreased phase-locking in NM neurons *in vivo* (Fukui et al. 2010). Both the data from the model by Dasika et al. (2005) and the two *in vivo* studies support the idea that the SON functions to balance inputs to the NL.

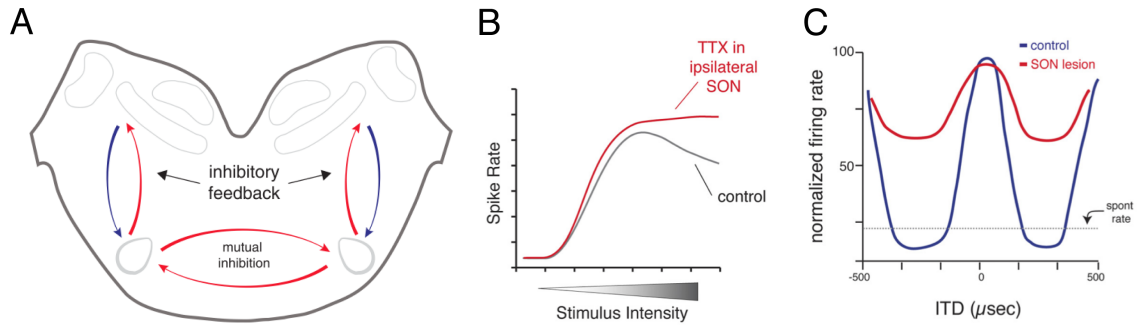


Figure 1.9: Inhibitory feedback from the SON modulates response properties of brainstem neurons. A. Schematic of the avian brainstem representing the inhibitory feedback loops in each brain hemisphere coupled by the reciprocal inhibitory connection between the superior olivary nuclei. B. Depiction of rate vs. intensity functions in the NM in control and after lesioning of the ipsilateral SON reveals inhibitory feedback during high intensity stimuli modulates the output of NM neurons. C. Schematized representation of ITD tuning curves from neurons in the NL shows a compression of the tuning curve with ipsilateral SON lesion. Adapted from Burger et al. 2011.

Rationale

The research in this dissertation broadens our understanding of inhibition in a circuit that relies on the maintenance of temporal features of sound. In the first group of experiments I examined the role of inhibitory modulation of inputs at the site of coincidence detection in the mammal. This approach allowed me to investigate mechanisms involved in sound localization that may be applicable to humans. In the second group of experiments I evaluate the nature of inhibitory feedback across several nuclei in the avian circuit in order to understand how a single major inhibitory input could possibly serve multiple computational functions.

Providing consistent input to coincidence detectors over a broad range of stimulus intensities is an important task in these circuits. The inhibitory feedback loop involving the reciprocal connectivity of the SONs in the avian system aids in this task. However, in the mammalian system, the inhibition is primarily feed forward. In the alternative branch of the sound localization circuit where ILDs are processed, Magnusson et al. (2008) observed the activity dependent release of GABA from lateral superior olive neurons that functioned as a retrograde signal to modulate presynaptic transmitter release. In the mammalian system, I test the hypothesis that GABA_BR activation modulates inputs to the MSO in a way that improves ITD selectivity using pharmacological manipulations during *in vitro* patch clamp experiments on gerbil brainstem tissue. This work was supported by computational modeling that resolved subtle aspects of GABA_B modulation.

Previous studies of inhibition in the avian brainstem have revolved around the unique depolarizing GABAergic inhibition seen in the timing nuclei (NM and NL).

However, a recent paper comparing the inhibitory input to the NM, NL and NA showed that inhibition in the NA contains both GABA- and glycinergic components (Kuo et al. 2009). Additionally, using immunohistochemistry, they showed that presynaptic terminals at NM, NL and NA stain positively for glycine. This was a surprising discovery since glycinergic transmission has never been observed in the NM or NL. Building off of these recent discoveries, I first focused on detailing the synaptic physiology of inhibitory inputs in the SON and show that similar to results in the NA, inhibition in the SON is mediated by both GABA and glycine transmission. I then looked at glycine receptor staining and function in the NM where glycine transmission had not been documented. I observed that prolonged high frequency stimulation evokes a slowly emerging glycinergic component of inhibition. In the final chapter I discuss the possible interactions that may arise at neurons where both GABA and glycine transmission occur.

CHAPTER II

Modulation of synaptic input by GABA_B receptors improves coincidence detection for the computation of sound location

Abstract

Interaural time disparities (ITDs) are the primary cues for localization of low frequency sound stimuli. ITDs are computed by coincidence detecting neurons in the medial superior olive (MSO) in mammals. Several previous studies suggest that control of synaptic gain is essential for maintaining ITD selectivity as stimulus intensity increases. Using P7-P24 acute brain slices from Mongolian gerbils, I confirm that activation of GABA_B receptors reduces the amplitude of excitatory and inhibitory synaptic currents to MSO and, moreover, show that the decay kinetics of IPSCs are slowed in mature animals. During repetitive stimuli, activation of GABA_B receptors reduced the amount of depression observed, while PSC suppression and the slowed kinetics were maintained. Additionally, I utilized physiological and modelling approaches to test the potential impact of GABA_B activation on ITD encoding in MSO neurons. Current clamp recordings from MSO neurons were made while pharmacologically isolated excitatory inputs were bilaterally stimulated using pulse trains that simulate ITDs *in vitro*. MSO neurons showed strong selectivity for bilateral delays. Application of both GABA_B agonists and antagonists demonstrate that GABA_B modulation of synaptic input can sharpen ITD selectivity. I confirmed and extended these results in a computational model that allowed for independent manipulation of each GABA_B dependent effect. Modelling suggests that modulation of both amplitude and kinetics of synaptic inputs by GABA_B receptors can improve precision of ITD computation. Our studies suggest that *in vivo* modulation of synaptic input by GABA_B receptors may act to preserve ITD selectivity across various stimulus conditions.

Introduction

Interaural time disparities (ITDs) are the primary cues animals use to localize low frequency sounds. ITD values available to an animal depend largely on head width and are on the order of tens to hundreds of microseconds. Neurons in the medial superior olive (MSO) of mammals compute ITDs by performing cross-correlation between inputs that are phase-locked to the stimulus waveform (Goldberg & Brown 1969, Yin & Chan 1990). These inputs are both excitatory and inhibitory and derive from both ears, although the dominant inhibitory input is glycinergic and is evoked from stimulation of the contralateral ear via the ipsilateral medial nucleus of the trapezoid body (MNTB) (Kuwabara & Zook 1992, Cant & Hyson 1992, Grothe & Sanes 1993, Smith et al. 2000, Pecka et al. 2008, Grothe et al. 2010). As ITDs vary, MSO neurons show robust rate modulation resulting from the convergence of these inputs (Goldberg & Brown 1969, Yin & Chan 1990). While the phase-locked nature of each input is stable or even improves with increases in stimulus intensity, the firing rate for each input fibre increases several fold over a 30-50 dB range of intensities (Joris et al. 1994, Kopp-Scheinflug et al. 2008), suggesting that MSO neurons are likely to receive summed synaptic conductances that vary greatly in magnitude with stimulus intensity. Thus, a computational challenge for neurons that cross correlate intensity dependent inputs is the maintenance of stable ITD selectivity over a large range of input magnitudes.

Despite these challenges, it is known that coincidence-detecting neurons in birds and mammals maintain stable ITD selectivity over a large range of stimulus intensities

(Pena et al. 1996, Pecka et al. 2008, Pecka et al. 2010). Behavioural performance in human and non-human primate studies confirms that localization ability improves over the first ~20 dB above threshold and remains stable at higher sound intensities (Su & Recanzone 2001, Recanzone & Beckerman 2004).

The precision of ITD selectivity relies on several mechanisms in the ITD circuitry that preserve computational fidelity. These may include receptor desensitisation (Kuba et al. 2002, Cook et al. 2003), EPSP normalisation by voltage-gated conductances (Scott et al. 2010) and as recently shown, GABA_B receptor (GABA_BR) dependent suppression of synaptic inputs in both birds (Brenowitz & Trussell 1998, Lu et al. 2005) and mammals (Magnusson et al. 2008; Hassfurth et al. 2010). Inhibitory feedback circuits have been shown to influence ITD processing circuitry in birds (Pena et al. 1996, Burger et al. 2005a, Nishino et al. 2008, Fukui et al. 2010), and may operate similarly at the level of the cochlea in mammals (Darrow et al. 2006) but its influence on ITD coding in mammals has not yet been demonstrated.

In this report, I confirm recent results showing that GABA_BR activation suppresses the magnitude of synaptic input to the MSO (Hassfurth et al. 2010). Additionally, I demonstrate that this alters the decay kinetics of inhibitory postsynaptic currents (IPSCs). I also describe the effects of GABA_BR activation and block on synaptic depression during repetitive stimuli. I tested the hypothesis that these effects could contribute to the preservation of ITD selectivity using two complementary approaches. *In vitro* current clamp experiments showed that pharmacological manipulation of GABA_BR signalling strongly influenced simulated ITD tuning. These results were confirmed and extended using a computational model that demonstrated that the small changes in IPSC

kinetics observed with GABA_BR activation may influence ITD selectivity. IPSC decay dependent influences on ITD selectivity were robust over a broad range of input conditions where IPSC delay and magnitude values were varied.

Methods

In vitro brain-slice preparation

All procedures were approved by Lehigh University's Institutional Animal Care and Use Committee. Mongolian gerbils at postnatal day 7 to 24 (P7-P24) were anesthetized with isoflurane and rapidly decapitated. The brainstem containing auditory nuclei was removed, blocked, and submerged in oxygenated artificial cerebrospinal fluid (ACSF) (containing in mM: 125 NaCl, 2.5 KCl, 25 glucose, 1.25 NaH₂PO₄, 25 NaHCO₃, 2 CaCl₂, 1 MgCl₂, 0.4 ascorbic acid, 3 myo-inositol, 2 pyruvic acid) at 22°C. Chemicals were obtained from Sigma-Aldrich, St. Louis, MO unless otherwise indicated. Following cerebellum removal the brainstem was placed dorsal surface (4th ventricle) down on the stage of a vibrating microtome (Microm 650V, Walldorf, Germany). Horizontal sections (100-200 µm) containing the MSO were obtained and submerged in an incubation chamber of continuously oxygenated ACSF and incubated at 37°C for approximately one hour. Slices were then kept at room temperature until used for recording.

Brainstem slices were placed in a custom recording chamber on a retractable chamber shuttle system (Sisky Design Instruments, Oregon, USA) and neurons were visualised with a Nikon FN-1 Physiostation microscope using infrared differential interference contrast optics. Video images were captured using a CCD camera (Hamamatsu C7500-50, Hamamatsu City, Japan) coupled to a video monitor. The recording chamber was continuously perfused with ACSF at a rate of 2-4 ml/min. An

inline feedback temperature controller and heated stage were used to maintain chamber temperature at $35 \pm 1^\circ\text{C}$ (TC344B, Warner Instruments, Hamden, CT, USA).

PSC Recordings

For PSC recordings, a concentric bipolar electrode with tungsten core (TM53CCINS, WPI, Sarasota, FL) was lowered to the tissue surface with a micromanipulator and placed in a position medial to the MSO near the MNTB. Here, the excitatory fibres from the contralateral AVCN as well as the inhibitory fibres from the ipsilateral MNTB could be stimulated. Principal MSO neurons were identified based on their characteristic bipolar morphology and low input resistance upon achieving a whole-cell configuration (Scott et al. 2005).

Patch pipettes were pulled from thick walled borosilicate glass capillary tubes (WPI 1B120F-4) to a resistance of 4-8 M Ω using a two-stage puller (Narashige PC-10, Tokyo, Japan) and back-filled with internal solution (containing in mM: 145 K-Glu, 5 KCl, 1 MgCl₂, 10 HEPES, 5 EGTA [pH adjusted to 7.2 with KOH]) used for both current and voltage clamp recordings. The potential values reported here were adjusted to include the calculated liquid junction potential of 15mV. For PSC recordings, 5 mM QX314 was added to the internal solution to prevent antidromic action potentials. In many cases, 0.4% biocytin was added to the internal solution to label the neurons following the protocol of Scott et al. (2005). MSO principal neurons had an average whole-cell capacitance of 44.6 ± 0.9 pF and an average series resistance of 13.5 ± 0.4 M Ω . In voltage clamp, series resistance was compensated at 60-80%. EPSCs were recorded during bath application of SR95531 (20 μM) and strychnine (500 nM) to block

GABA_Aergic and glycinergic inputs respectively. Membrane voltage was clamped at -75 mV using a Multiclamp 700B amplifier, digitized with a Digidata 1440 data acquisition board and recorded using Clampex software (Molecular Devices, Sunnyvale, CA). Excitatory PSCs (EPSCs) were evoked with 50 μ sec stimulus pulses (Isoflex, A.M.P.I. inc., Israel). Stimulus magnitude (range 10-90 V) was gradually increased until PSC amplitudes stabilised at their maximum amplitude. After collection of control data, GABA_BR activity was modulated by bath application of the agonist (\pm)baclofen (10 μ M or 0.1 μ M) or the antagonist CGP55845 (2 μ M) (Tocris Biosciences, Minneapolis, MN) and the stimulus protocols were subsequently repeated. Then the drugs were washed out and data were collected until control conditions recovered or the recording was lost. To isolate inhibitory inputs, ACSF containing kynurenic acid (4 mM) or a cocktail of 6,7-dinitroquinoxaline-2,3-dione (DNQX) (40 μ M) and D-2-amino-5-phosphonopentanoic acid (AP5) (50 μ M) (Tocris Biosciences, Minneapolis, MN) was used to block glutamatergic input. Measures of IPSC amplitudes and kinetics did not differ between kynurenic acid and DNQX/AP-5 treatment groups (data not shown). Membrane voltage was clamped at -25 mV for IPSC data collection.

PSC amplitudes and kinetics were analyzed using Clampfit software. Rise and decay time constants, expressed hereafter as tau (τ) values, were calculated from single exponential fits to PSCs. Baclofen, CGP55845 and recovery condition amplitudes were normalized to control PSCs, and treatment groups were assessed for statistical significance using paired Student's t-tests. In addition to the unitary stimulus protocols, 10 pulse trains at several frequencies (50-200hz) were also used to assess the role of

GABA_BRs in synaptic depression of EPSCs and IPSCs. The degree of depression of the PSC response was calculated with the following equation:

$$\% \text{ depression} = [1 - (\text{mean amplitude of pulse 10} / \text{mean amplitude of pulse 1})] \times 100$$

Simulated ITDs, bilateral stimulation

ITDs were simulated *in vitro* using bilateral stimulation protocols (Funabiki et al. 1998, Overholt et al. 1992). Stimulating electrodes were placed medial and lateral to the MSO in order to stimulate contralateral and ipsilateral AVCN input fibres. Ionotropic inhibitory inputs were blocked with SR95531 (20 μ M) and strychnine (500 nM). Whole-cell current clamp protocols were used to monitor voltage responses during evoked synaptic activity. Stimuli consisted of 10-pulse trains delivered at 50 or 100 Hz. For both ipsilateral and contralateral inputs, stimulus magnitude was increased until a single unilateral stimulus pulse evoked near-threshold EPSPs. In each trial, unilateral stimuli were delivered prior to the pulse train to simulate "monaural" conditions and to confirm that there was little or no spiking evoked with unilateral stimuli. Following the "monaural pulses", pulse train stimuli were presented bilaterally with a range of timing offsets to simulate ITDs (e.g. ± 1 ms/0.1 ms interval for P7-P16 animals (Fig 5C), or ± 500 μ s/50 μ s interval for >P16 animals (Fig 6A)). A given simulated ITD (sITD) was presented pseudorandomly and multiple sequences were presented in each condition. Data collected for each sITD were summed over several trials. The stimuli were repeated under exposure to bath applied GABA_BR agonists or antagonists, baclofen (0.1 μ M) or

CGP55845 (2 μ M) respectively, or both. The drug was then washed out and the stimuli again repeated to obtain recovery data. Action potentials for each sITD were identified using a thresholding algorithm in Clampfit. All ITD tuning curves were constructed by fitting functions to the spike counts at each sITD for both the positive and negative halves of the ITD function. Best fits were achieved using the sum of two sigmoid functions, and halfwidth was calculated as the width of the fitted ITD curves at half maximal spike rate. The fit equation is as follows:

$$Fit = S_1(x) + S_2(-x)$$

$$S_i(x) = A_i + \frac{K_i - A_i}{(1 + Q_i e^{-B_i(x - M_i)})^{1/T_i}}$$

where A is the lower limit, K is the upper limit, B is the growth rate, and M is the time shift, T is a dimensionless fitting coefficient.

Data are reported and illustrated as mean \pm SEM unless otherwise stated.

Computational Modelling of MSO neurons

Model MSO neurons were constructed in NEURON as multi-compartment models substantially modified from that published by Zhou et al. (2005). Each model MSO neuron was composed of a soma, two dendrites, and an axonal segment that contained the spike initiation zone. I modified the Zhou et al. (2005) model to incorporate empirically derived values for synaptic inputs from the current study and made anatomical adjustments according to current understanding of MSO morphology (Scott et al. 2005, Rautenberg et al. 2009). Major modifications included: 1) the axon and spike

initiation zone originates from the centre of the soma compartment, 2) The ion channel density distributions and channel dynamics of MSO neuron voltage gated K⁺ and Na⁺ channels were recently characterized in two papers from the Golding laboratory (Scott et al. 2010, Mathews et al. 2010). Our model was populated with somatic and dendritic voltage gated channel densities that were arranged to reflect these recent findings as follows:

i) Potassium channel kinetics and density on the soma and dendrite compartments were adapted from Mathews et al. (2010):

$$g = g_{\max} * w^4 * z$$

$$w_{\infty}(v) = \frac{1}{1 + \exp((v + 57.34)/-11.7)}$$

$$z_{\infty}(v) = \frac{1 - 0.27}{1 + \exp((v + 67/g))} + 0.27$$

$$w' = \frac{w_{\infty}(v) - w}{\tau_w(v)}, \quad z' = \frac{z_{\infty}(v) - z}{\tau_z(v)}$$

$$\tau_w = 0.35 + \left(\frac{21.5}{6 \exp((v + 60)/7) + 24 \exp((v + 60)/50.6)} \right)$$

$$\tau_z = 10.7 + \left(\frac{170}{5 \exp((v + 60)/10) + \exp((v + 70)/g)} \right)$$

$$V_{rev} = -106mV$$

$$G_{kLV} = 17mmho/cm^2 @ soma$$

$$G_{kLV} = 3.58mmho/cm^2 @ dendrite$$

Where w and z are activation and inactivation respectively.

ii) Sodium channel kinetics and distribution on the soma were based on findings of Scott et al. (2010):

$$g = g_{\max} * m^4 * [(0.993 * h) + 0.007]$$

$$m_{\infty}(v) = \frac{1}{1 + e^{\frac{v+46}{-11}}}$$

$$h_{\infty}(v) = \frac{1}{1 + \exp((v + 62.5)/7.77)}$$

$$m' = \frac{m_{\infty}(v) - m}{\tau_m(v)}, \quad h' = \frac{h_{\infty}(v) - h}{\tau_h(v)}$$

$$\tau_m = \frac{1}{3 \left[0.141 + \left(\frac{-0.0826}{1 + \exp((-20.5 - v)/10.8)} \right) \right]}$$

$$\tau_h = \frac{1}{3 \left[4 + \left(\frac{-3.74}{1 + e^{\frac{-40.6 - v}{5.05}}} \right) \right]}$$

$$V_{rev} = 55mV$$

$$G_{NaLV} = 60mmho/cm^2 @ soma$$

$$G_{NaLV} = 0mmho/cm^2 @ dendrites$$

Where m and h are activation and inactivation respectively.

iii) I_h channel kinetics were identical to those used by Zhou et al. (2005), but channel density distribution on the membrane is modeled after Mathews et al. (2010).

Input model:

Each of the two dendrites in the model cell received input from 10 independent excitatory synaptic inputs, and the soma received input from 10 independent inhibitory synaptic inputs. The experimenter manipulated the vector strength, maximum firing rate, and peak synaptic conductance.

We modelled all synaptic conductance kinetics with a double exponential so that when normalized, PSG shape would closely approximate PSGs derived from recordings shown in the results as follows:

$$g_{uni} = k(\theta_1, \theta_2)(e^{-\frac{t}{\theta_1}} - e^{-\frac{t}{\theta_2}})$$

Where g_{uni} is the unitary synaptic conductance, $\theta_1 = 0.2598$ and $\theta_2=0.2639$ for EPSC's, $\theta_1 = 0.2723$ and $\theta_2 = 1.313$ for control IPSC's and $\theta_1 = 0.6484$ and $\theta_2 = 1.348$ for IPSC's under the influence of baclofen. k is set to normalize the curve. Reversal potential was 20 mV for EPSCs and either -70 mV (Zhou et al. 2005) or -90 mV (Magnusson et al. 2005) for IPSCs. Synaptic input magnitude was scaled in the simulations according to average sound intensity values. Synchrony of model inputs were set to 10 and 20 for EPSCs and IPSCs respectively. Expressed as vector strength values, these correspond to approximately 0.95 for AVCN fibers and 0.99 for MNTB fibers. GABA_BR input magnitude modulation was modeled by reducing synaptic conductance magnitude to the maximum value observed empirically in 10 μ M baclofen. The maximum suppression for mature neurons was approximately 40% for EPSCs and 60% for IPSCs. Synaptic depression of PSGs was modeled based on data illustrated in Figures 3&4 with the following function:

$$G_{input} = G_{initial}(a + (b * \exp(c * t)))$$

where “a” constrains the steady state amplitude; “b” constrains the initial amplitude; and “c” controls the rate at which the initial conductance ($G_{initial}$), which is set by the experimenter, declines with activity to the depressed input conductance (G_{input}), which is

the conductance provided to the model cell. Input variable values for the depression function are given in Table 1.

The MNTB provides a phase-locked, contralaterally derived, glycinergic inhibition to the MSO. The timing of these phase-locked inputs relative to the excitation is unknown. *In vivo* and *in vitro* observations suggest that inhibitory input shifts peak ITD selectivity toward the contralateral ear (Brand et al. 2002, Chirila et al. 2007, Pecka et al. 2008, 2010). I systematically varied the delay of the leading inhibition in an iterative modeling experiment. I found that when the inhibitory input leads the contralaterally evoked excitation by 1.0 ms, the model most effectively reproduced the peak ITD function shift into the contralateral hemifield (Peak model ITD value: 30 dB: +74 μ sec; 45 dB: +139 μ sec; 60dB: +127 μ sec). Thus, this delay was chosen for subsequent tests of the model. The effect of delay is demonstrated in the results and discussed in detail.

ITD selectivity in the model was measured using two metrics. First, I use the halfwidth of the ITD tuning curve that was constructed using the same fitting parameters as the sITD curves *in vitro* (see above). Additionally I calculated the firing rate modulation through the physiologically relevant range of ITDs experienced by a gerbil, ± 130 μ sec (Maki & Furukawa, 2005).

Results

In the following sections I first demonstrate the effect of GABA_BR activation on excitatory and inhibitory synaptic currents in MSO neurons. I evaluated GABA_BR dependent influences on both the magnitude and temporal aspects of these inputs as well as the effects on synaptic depression. I then tested whether the effects that I observed could influence the computation of ITD tuning using an *in vitro* current clamp assay. Finally, in order to further investigate the relative importance of each GABA_B dependent synaptic current modification, I developed a computational model for which each GABA_BR dependent change in synaptic input was evaluated separately.

Effects of GABA_B R activation on EPSC amplitude and kinetics

Our initial goal was to evaluate the influence of GABA_BR activation on inputs to the MSO under various stimulus conditions. First, pharmacologically isolated EPSCs and IPSCs were evoked via stimulation of the afferent fibre tracts medial to MSO in gerbils aged P7 through P24. Bath application of ACSF containing 10 μ M baclofen effectively reduced EPSC magnitude (Fig 2.1). Figure 2.1A shows average traces of EPSC recordings from a P18 MSO neuron in control, 10 μ M baclofen, 2 μ M CGP55845 and recovery conditions. EPSC amplitudes were affected across the age range but the degree of GABA_B dependent suppression declined significantly with age as was also observed by Hassfurth et al. (2010) (% suppression: P7-P16, $73.6 \pm 2.4\%$; >P16, $48.5 \pm 4.6\%$). However, as late as P24, the oldest age tested, reduction of EPSC amplitude by GABA_BR activation remained >40%. PSC amplitude and kinetics mature rapidly with

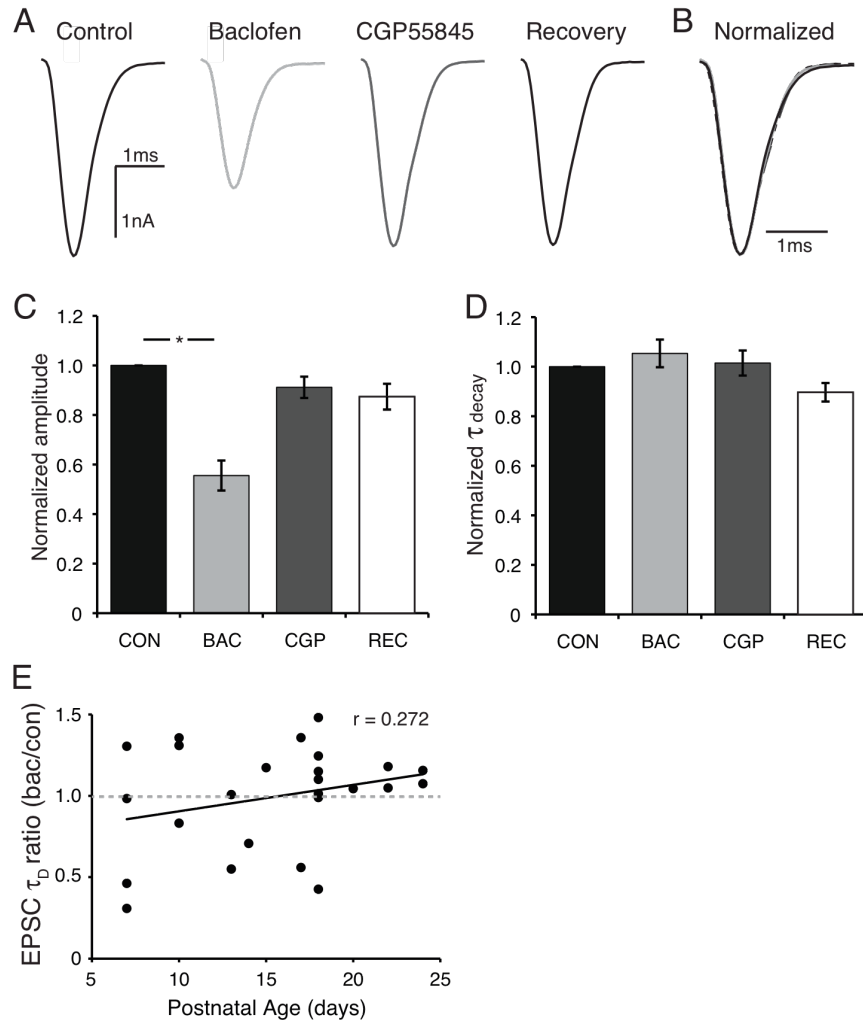


Figure 2.1: GABA_BR activation suppresses evoked EPSCs in MSO principal neurons.

A. Average of 10 EPSC traces from a P18 MSO neuron evoked via stimulation of contralateral AVCN fibers show amplitude suppression during baclofen (10 μ M) application and no change with application of CGP55845 (2 μ M). B. Normalized traces from panel A show no difference in kinetics between treatments. C. Baclofen significantly reduces amplitude of EPSCs ($p < 0.001$, $n = 16$) in P17-P24 MSO neurons, while CGP55845 has no effect ($p > 0.05$, $n = 11$). D. EPSC τ Decay values are unchanged by application of baclofen or CGP55845 ($p > 0.05$). E. Effect of baclofen on EPSC τ Decay does not correlate with age ($r = 0.272$, $p = 0.237$, $n = 26$), dashed line indicates ratio value of 1, indicative of no change in τ Decay with baclofen treatment. r -values are Pearson correlations.

age in MSO neurons following hearing onset around age P12 (Smith & Forsythe 2000, Scott et al. 2005). However, most of the maturational changes I observed in synaptic input asymptote at about P16, thus I divided our analysis into two age groups P7-P16 and P17-24. Population data for GABA_B dependent suppression are reported for P17-P24 neurons and are shown in Fig. 1C for EPSCs (baclofen suppression was $44.4 \pm 6.1\%$, $p < 0.005$, $n=16$). The amplitude suppression of EPSCs was also apparent at reduced concentrations of baclofen. Application of $0.1\mu\text{M}$ baclofen significantly suppressed EPSC amplitude by $20.6 \pm 5.1\%$ ($p < 0.05$, $n=4$). EPSC amplitudes measured in the presence of the GABA_B R antagonist, CGP55845, were not significantly different than control ($91.2 \pm 4.3\%$ of control, $p > 0.05$, $n=11$).

Measurements of EPSC kinetics were not influenced by GABA_BR activation. Figure 2.1B shows normalized average traces for the neuron from 2.1A demonstrating the stability of EPSC kinetics in all conditions. Average τ_{Rise} (data not shown) and τ_{Decay} (Fig. 2.1D: P17-P24 age group shown) were not different in the baclofen condition across the population (τ_{Rise} : Control, $0.48 \pm 0.06\text{ms}$; Baclofen, $0.37 \pm 0.06\text{ms}$, $p=0.79$; τ_{Decay} : Control, $0.50 \pm 0.04\text{ms}$; Baclofen, $0.52 \pm 0.05\text{ms}$, $p=0.96$, $n=16$), and unlike IPSCs (shown below), the ratio of baclofen/control τ_{Decay} values did not correlate with age (Fig. 2.1F). EPSC kinetics measured in the presence of CGP55845 were not significantly different than control (τ_{Rise} : $0.58 \pm 0.09\text{ms}$, $p > 0.05$; τ_{Decay} : $0.59 \pm 0.10\text{ms}$, $p > 0.05$, $n=11$).

IPSCs were also suppressed by GABA_BR activation. Figure 2.2A shows average traces from a P18 neuron. In contrast to EPSCs, IPSC suppression magnitude did not

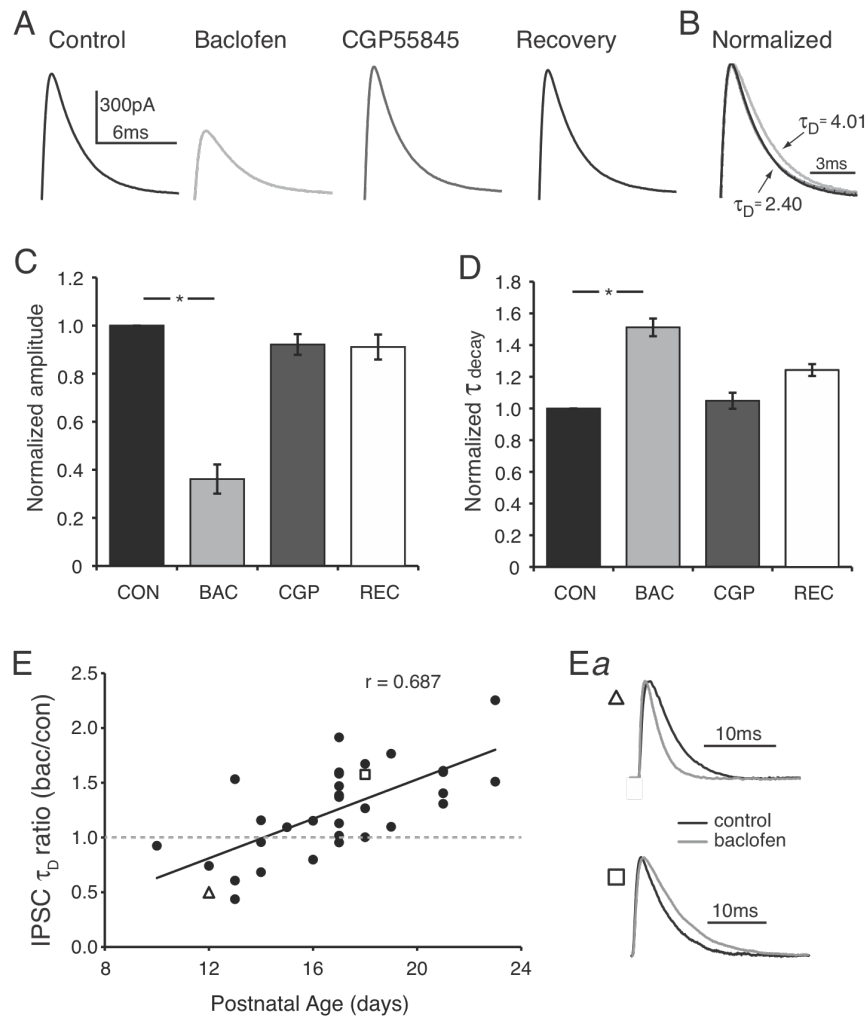


Figure 2.2: Activation of GABA_BRs suppresses IPSC amplitude and slows kinetics.

A. Average traces of IPSCs in each condition. B. Normalized average traces from panel A depict baclofen effect on IPSC kinetics. C. Population data from P17-P24 MSO neurons reveals that IPSC amplitudes were significantly reduced by application of baclofen ($p < 0.01$, $n = 18$), but remained unchanged in CGP55845 ($p > 0.05$). D. Baclofen significantly increased τ Decay kinetics ($p < 0.001$). E. Effect of baclofen on τ Decay correlates with age ($r = 0.687$, $p < 0.001$, $n = 30$). Ea. Normalized IPSC traces in control (black) and baclofen (grey) show a decrease in τ Decay at younger ages (top, triangle), and an increase in τ Decay at older ages (bottom, square) with GABA_BR activation. r -values are Pearson correlations.

change across the tested age range (data not shown). Figure 2.2C shows the average suppression for >P16 neurons at 10 μ M baclofen ($63.9 \pm 4.3\%$, $p < 0.001$, $n=18$). In the presence of 0.1 μ M baclofen, IPSC suppression remained prominent at $44.8 \pm 8.1\%$ ($p < 0.01$, $n=4$).

Unlike EPSCs, IPSC decay kinetics were influenced by baclofen (Fig. 2.2B,D,E). Furthermore, the effect of GABA_B activation on IPSC decay kinetics was strongly age dependent. Baclofen application increased the τ_{Decay} by $\sim 50\%$ (P17-23, $51.0 \pm 10.1\%$, $p < 0.0005$, $n=18$). Interestingly, Figure 2.2E shows the effect of baclofen on τ_{Decay} normalized to control values as a function of age. At early ages baclofen caused IPSCs to decay more rapidly, while at later ages GABA_B activation slowed decay ($r = 0.687$, $p < 0.001$, $n=30$, Pearson correlation). Figure 2.2Ea shows typical examples of IPSC kinetic changes under control and baclofen conditions for a P12 (*triangle*) and a P18 (*square*) neuron. Across the population of neurons aged P17 and above, the decay was significantly longer in the presence of baclofen compared to the control condition (P17-23, Control, $2.15 \pm 0.20\text{ms}$; Baclofen, $3.07 \pm 0.30\text{ms}$, $p < 0.0005$, $n=18$). IPSC amplitude and kinetic measures in the presence of CGP55845 were not significantly different than control (amplitude: $92.1 \pm 9.2\%$ of control, $p > 0.05$; τ_{Decay} : $1.95 \pm 0.27\text{ms}$, $p > 0.05$, $n=6$). τ_{Rise} values were not significantly different from control in either condition but did exhibit a trend toward slower kinetics (τ_{Rise} : control, $0.25 \pm 0.02\text{ms}$; baclofen, $0.29 \pm 0.03\text{ms}$; CGP55845, $0.24 \pm 0.02\text{ms}$; $p > 0.05$ for both).

GABA_B dependent influences on synaptic depression:

The excitatory and inhibitory inputs to MSO neurons are phase-locked and can sustain high firing rates (Yin & Chan 1990, Joris et al. 1994; Rhode & Greenberg 1994, Kopp-Scheinflug et al. 2008), conditions that typically induce synaptic depression (von Gersdorff et al. 1997, Smith et al. 2000, Hermann et al. 2007). Indeed, synaptic depression has been shown to contribute to ITD selectivity in coincidence detecting neurons (Kuba et al. 2002, Cook et al. 2003). GABA_B activation has been shown to reduce depression in avian cochlear nucleus neurons that process phase-locked information, especially at high stimulus frequencies (Brenowitz et al. 1998). In order to investigate GABA_B dependent effects on temporally patterned activity I evoked EPSCs and IPSCs with pulse trains at 50-200 Hz in the presence of baclofen or CGP55845 in 21 MSO neurons aged >P16.

Figure 2.3A shows typical EPSC responses evoked by 10 pulse trains at 100 Hz in a P18 MSO neuron. When the responses are normalized to the amplitude of the first peak, the effect of GABA_BR activation on reducing depression is evident (Fig 2.3B). The excitatory response to 100 Hz stimulus trains is shown in Figure 2.3C for each condition. I assessed depression by comparing the PSC amplitude of the 10th pulse relative to the response to the initial pulse (see Methods). Across the population EPSC amplitude depressed by $39.5 \pm 2.2\%$ in control ACSF (Fig 2.3C&D). Similar to results of our unitary stimulus protocols, inclusion of 10 μ M baclofen reduced the overall response amplitude including the first pulse (Fig 3A middle traces), however, depression was limited to $19.3 \pm 3.9\%$ ($p < 0.01$, $n=8$) during the train (Fig 2.3C&D). These findings are consistent with those reported in the avian cochlear nucleus (Brenowitz et al. 1998).

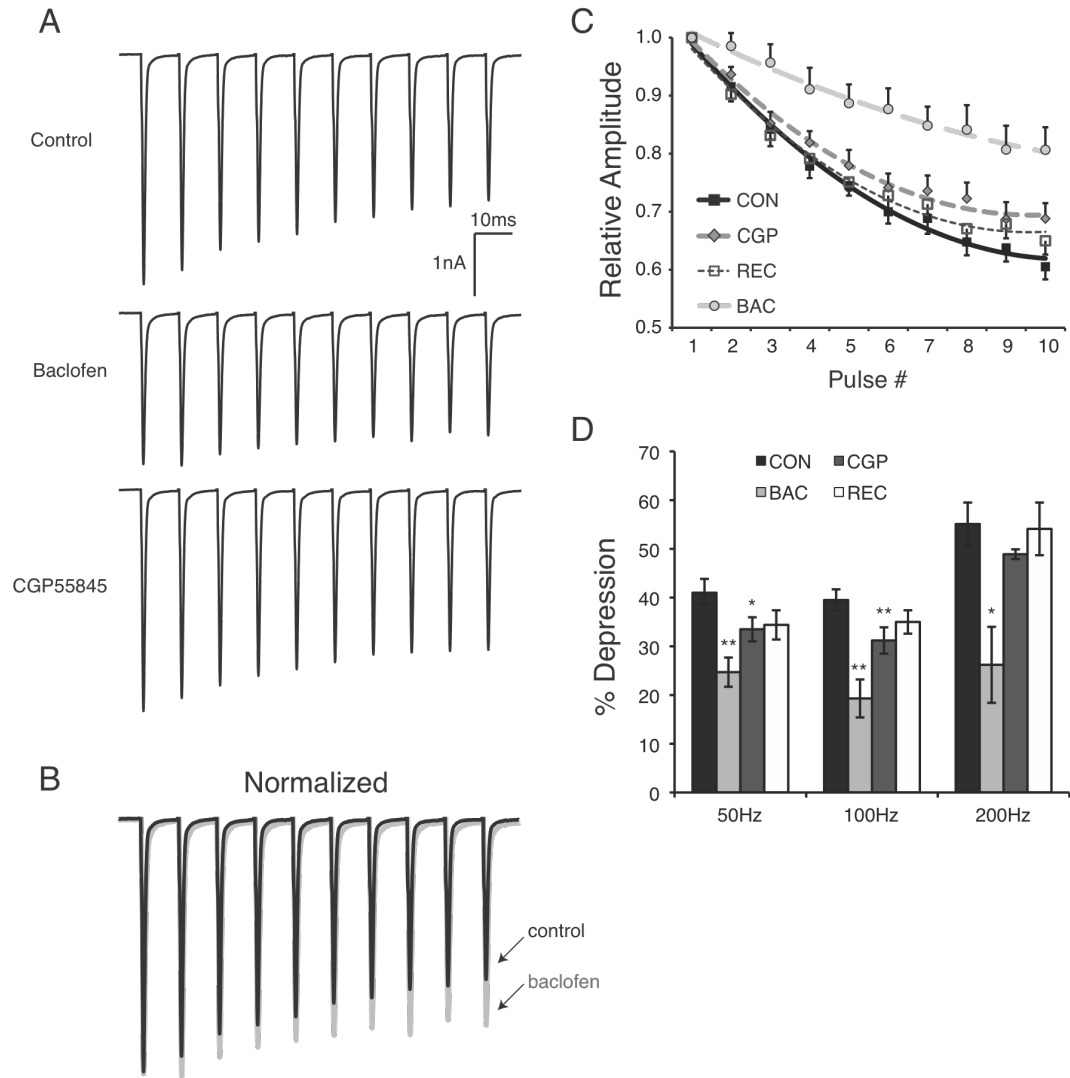


Figure 2.3: Modulation of GABA_BRs effects rates of depression of EPSCs during repetitive stimuli. A. Average of 20 trials of 100Hz stimulus trains. B. Normalized traces of control and baclofen condition show the reduction in depression during activation of GABA_BRs. C. Population data for depression at each pulse during the stimulus shows the reduction in depression during application of baclofen and CGP55845. The percent depression at the 10th pulse was significantly different from control with baclofen ($p < 0.01$, $n = 8$) and CGP55845 ($p < 0.01$, $n = 15$) application. D. Population data for percent depression values at three stimulus frequencies. EPSC trains in baclofen showed significantly less depression at all frequencies tested (50Hz, $n = 7$; 200Hz, $n = 3$). CGP55845 application also mildly but significantly reduced EPSC depression at 50 ($n = 7$) and 100Hz (at 200Hz, $p = 0.06$; $n = 3$). ** $p < 0.01$, * $p < 0.01$.

Washout of baclofen reversed this effect and depression returned to near control levels ($35.0 \pm 2.4\%$) (Fig 2.3C&D). Application of the GABA_BR antagonist CGP55845 did not change initial pulse response amplitude (Fig 2.3A), but did mildly reduced synaptic depression compared to control to $31.2 \pm 2.7\%$ ($p < 0.01$, $n=15$) (Fig 2.3C&D). This result suggests that in contrast to the single pulse stimulus protocol shown in Figures 2.1 & 2.2, the 100 Hz stimulus paradigm evokes endogenous GABA release and subsequent GABA_B activation in the control condition that is only revealed when the antagonist is applied. While variation of stimulation frequency (50, 100, or 200 Hz) influenced the overall magnitude of depression, GABA_BR pharmacological manipulations resulted in similar patterns with respect to depression at 50 and 200 Hz to those illustrated for 100 Hz (Fig 2.3D). Pulse-train stimuli also evoked depression in IPSCs that was similarly sensitive to GABA_B agonist and antagonist application. Figure 2.4A shows results for a P18 neuron stimulated at 50 Hz. The normalized IPSC traces (Fig 2.4B), as for EPSCs, show that the trailing pulses in the baclofen condition are less depressed relative to the control responses. In the control condition, IPSC amplitude was reduced by $55.1 \pm 5.4\%$ by the 10th pulse (100hz stimulus, $n=6$). The degree of depression was reduced in the presence of baclofen ($16.4 \pm 9.2\%$, $p < 0.01$, $n=6$) and moderately reduced in CGP55845 compared to control ($41.6 \pm 2.6\%$, $p < 0.05$, $n=4$). Washout of baclofen restored depression to near control levels ($41.1 \pm 2.7\%$) (Fig 2.4C&D). A similar pattern of modulation was seen with a 50Hz stimulus (Fig 2.4D). As previously described, IPSCs evoked using single pulse stimuli revealed a GABA_B dependent slowing of decay kinetics (Fig 2.2). Interestingly, this shift in τ_{Decay} values persisted throughout the train stimulus

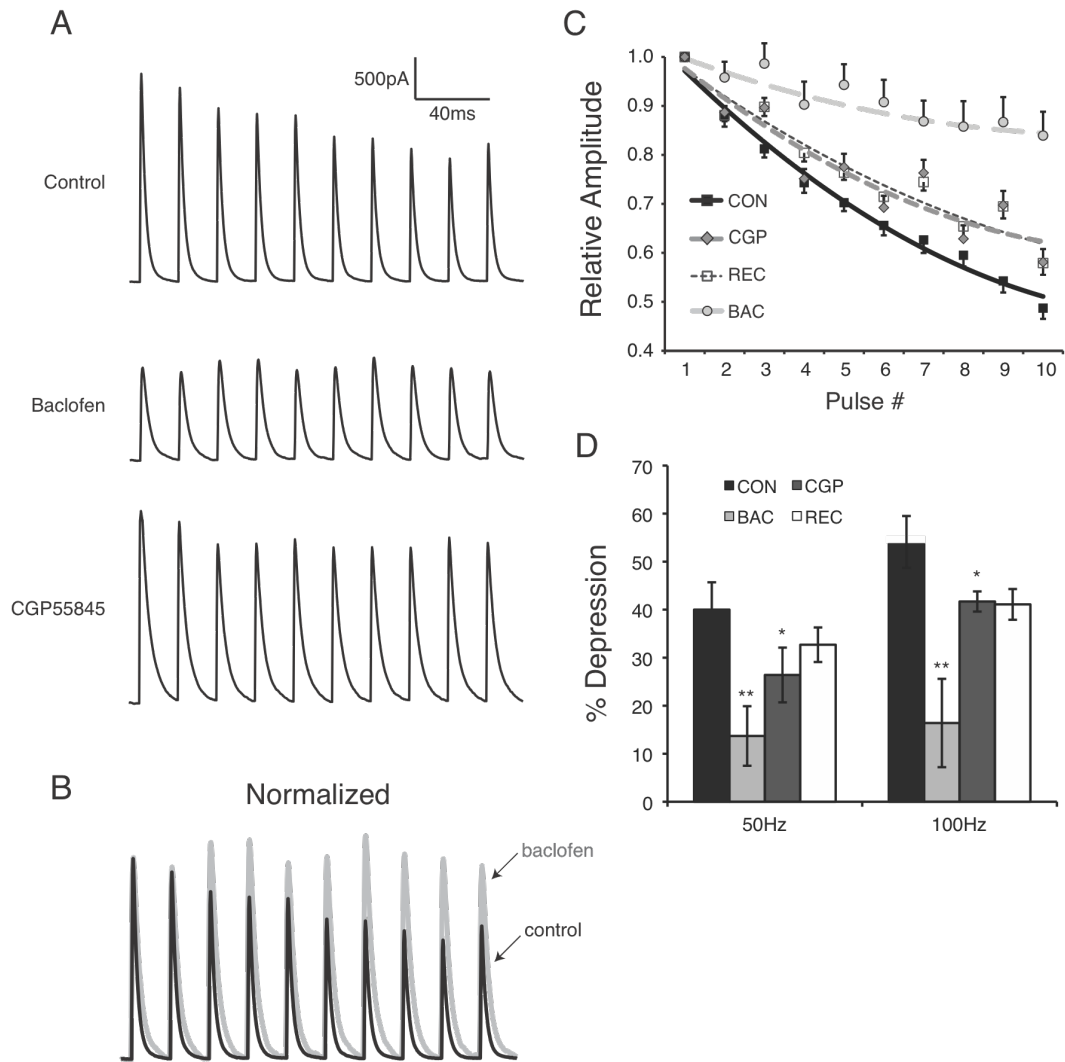


Figure 2.4: Depression rates of IPSCs are affected by modulation of GABA_BRs during repetitive stimuli. A. Average of 20 trials of 50Hz stimulus trains. B. Normalized traces of control and baclofen condition show the reduction in depression during activation of GABA_BRs. Additionally the slowing of IPSC kinetic seen in unitary responses are maintained in responses throughout the stimulus train (open arrowhead). C. Population data (100Hz trains) for depression at each pulse during the stimulus shows the reduction in depression during application of baclofen and CGP55845. Percent depression at the 10th pulse was significantly different from control in baclofen ($p < 0.01$, $n = 6$) and CGP55845 ($p < 0.05$, $n = 4$). D. Population data for percent depression at the two frequencies tested for IPSC train stimuli. Similar data patterns are observed at each frequency where both baclofen and CGP55845 reduced the amount of depression observed during the train (50Hz, $n = 5$). ** $p < 0.01$, * $p < 0.05$.

(Fig 2.4B). The IPSC τ_{Decay} of the 10th pulse was not significantly different than that to the first pulse within any condition (IPSC Control τ_{Decay} : pulse₁ 3.35 ± 0.47 , pulse₁₀ 3.32 ± 0.62 , $p=0.61$; Baclofen: pulse₁ 6.20 ± 1.16 , pulse₁₀ $6.00 \pm 1.04\text{ms}$, $p=0.31$). However, the kinetic shift observed was significant when τ_{Decay} of the tenth pulse response was compared between the baclofen and control conditions ($p<0.05$, $n=6$).

Effects of Baclofen on Simulated ITDs

GABA_B activation strongly modulates both IPSC and EPSC amplitudes. I sought to test whether these effects could function to influence ITD processing in MSO neurons. First, I simulated ITD-like conditions *in vitro* by stimulating the bilateral afferent inputs to MSO neurons recorded in whole-cell current clamp under excitation only conditions (Fig 2.5A). To prevent simultaneously evoking IPSPs from stimulation of neighbouring inhibitory fibre tracts, EPSPs were pharmacologically isolated with bath application of 20 μM SR95531 and 500 nM strychnine to block ionotropic GABAergic and glycinergic transmission, respectively. Afferent fibres were stimulated bilaterally with voltage pulse trains (10 pulses at 50 or 100 Hz) while the relative timing between the ipsilateral and contralateral stimulating electrodes was shifted pseudorandomly through a range of simulated ITD (sITD) values (see Methods). Stimulus amplitude was initially adjusted in the control condition so that postsynaptic potentials from each side resulted in PSPs that were near but below threshold. Each sITD value was sampled at least 10 times, and spike count data for each sITD value were summed. Figure 2.5B shows representative traces from a P13 neuron at two sITDs. Baclofen had a small effect on spike rate at the response maxima evoked at 0 μsec sITD. However, at the 200 μsec sITD, responses were strongly

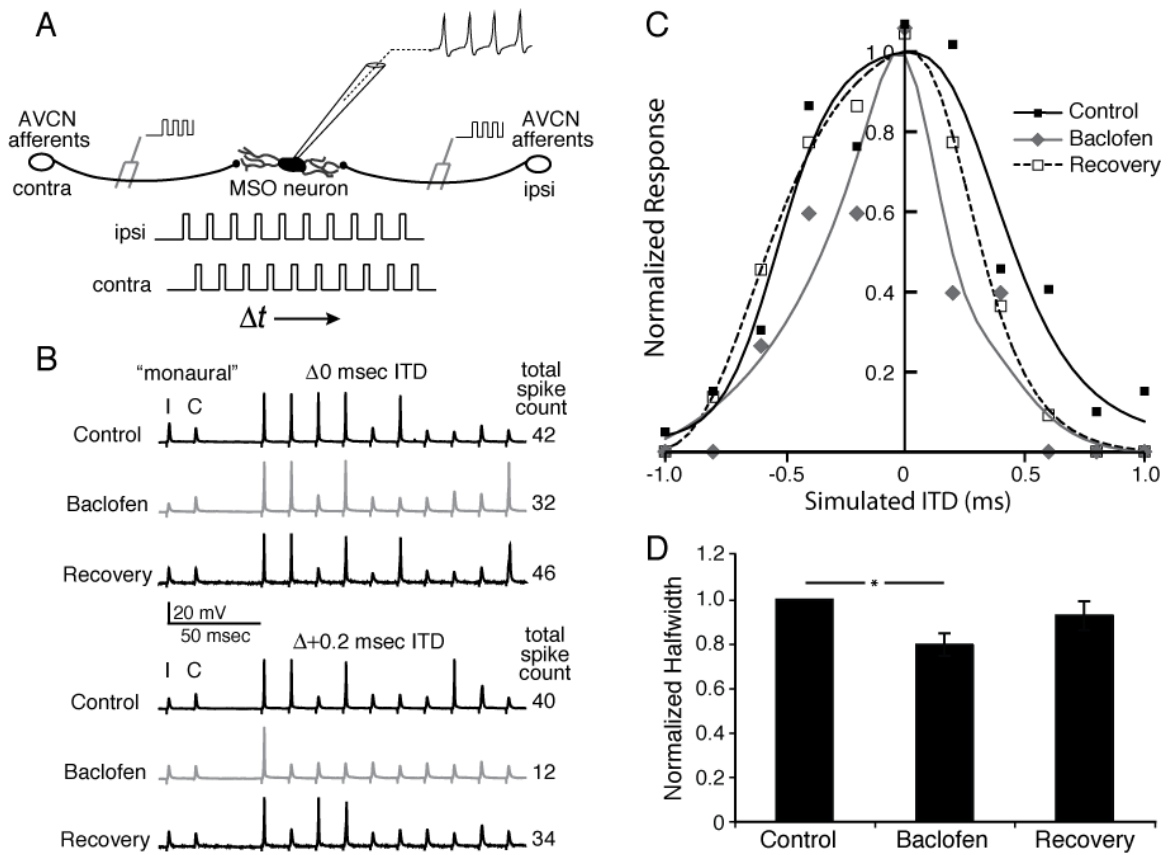


Figure 2.5: ITD sensitivity is modulated by GABA_BR activation. A. Schematic of bilateral stimulation protocol used to simulate ITDs in vitro (see Methods). B. Representative current clamp traces from the peak and +0.2 msec sITD time points from a MSO neuron (P13). Total spike counts are the sum of 10 trials at each simulated ITD. C. sITD tuning curves constructed using data from the neuron in B. D. Population data for sITD experiments show a significant decrease in sITD tuning curve halfwidth with application of 0.1 μ M baclofen that was recovered after washout ($p < 0.05$, $n = 25$).

suppressed during baclofen treatment. sITD tuning curves (Fig 2.5C) were constructed from spike count data that was normalized to the peak and fitted with a sigmoid function (see Methods). The peaks of all fitted sITD curves were centred at 0 μ sec ITD in order to directly compare halfwidths between conditions. Using this experimental paradigm, 25/31 neurons aged P11-19 tested showed ITD selectivity in the control condition. The ITD tuning curve halfwidth in control conditions decreased during development; the average halfwidth for P7-P16 neurons was $974 \pm 110 \mu$ sec while in the >P16 group, it was $382 \pm 21 \mu$ sec. This result mirrors changes in input resistance occurring over this time frame (series resistance, P7-P16: 14.3 ± 0.6 mV, n= 84; >P16: 11.8 ± 0.6 mV, n=39, $p < 0.01$). Bath application of ACSF containing 0.1 μ M baclofen effectively decreased the range of ITDs that would evoke discharges in 22/25 cells. ITD tuning curve halfwidth was reduced by $19.5 \pm 5.4\%$ over the entire population, (Fig 2.5D, $p < 0.001$) and was similar in both P7-P16 ($15.3 \pm 8.0\%$, n=14) and P17-P24 ($24.9 \pm 6.9\%$, n=11) MSO neurons ($p = 0.39$).

While spike counts under baclofen were reduced throughout the stimulus trains by 24.4% on average, analysis of responses to each pulse revealed that response probability was most labile for later pulses in the train compared to the initial pulses. These results are consistent with the depression of EPSC amplitude. For example, in the control condition at 0 μ sec sITD the initial pulse evoked a spike in $99.2 \pm 1.1\%$ of trials, while in the presence of baclofen the initial response probability declined slightly to $93.3 \pm 3.3\%$. However, for the 10th pulse the control probability was $58.5 \pm 10.4\%$ while the baclofen

probability was $35.0 \pm 8.5\%$. These results are consistent with the known role of depression in shaping ITD selectivity (Kuba et al. 2002, Cook et al. 2003).

To further confirm the observed GABA_B dependence of changes in halfwidth, I utilized the *in vitro* sITD approach during application of the GABA_BR antagonist CGP55845 (n=12) or sequential application of baclofen and CGP55845 (n=3). Data from a representative neuron that was exposed to antagonist alone is shown in Figure 2.6A. Figure 2.6B shows the population's increase in halfwidth with CGP55845 application ($134.7 \pm 11.9\%$ of control, $p < 0.01$, n=12). Figure 2.6C shows a representative neuron for which agonist and antagonist were presented sequentially. In this P18 neuron, baclofen caused a reduction in halfwidth to 64.3% from control baseline levels (*indicated by dashed line*) within 8 minutes. Co-application of CGP55845 followed by withdrawal of baclofen caused a stepwise broadening of ITD tuning to 131% of control when CGP55845 was presented alone. Finally, washout with normal ACSF caused ITD tuning halfwidth to return to the baseline control levels. In the three cells tested in this manner, baclofen reduced sITD halfwidth to $72.4 \pm 4.6\%$ of control while CGP55845 broadened tuning curves to $125 \pm 2.9\%$ of control. The increase in sITD halfwidth observed with agonist application is consistent with our PSC recordings, which suggest that a basal level of endogenous GABA_BR activation is evoked by high frequency train stimuli from endogenous sources under control conditions.

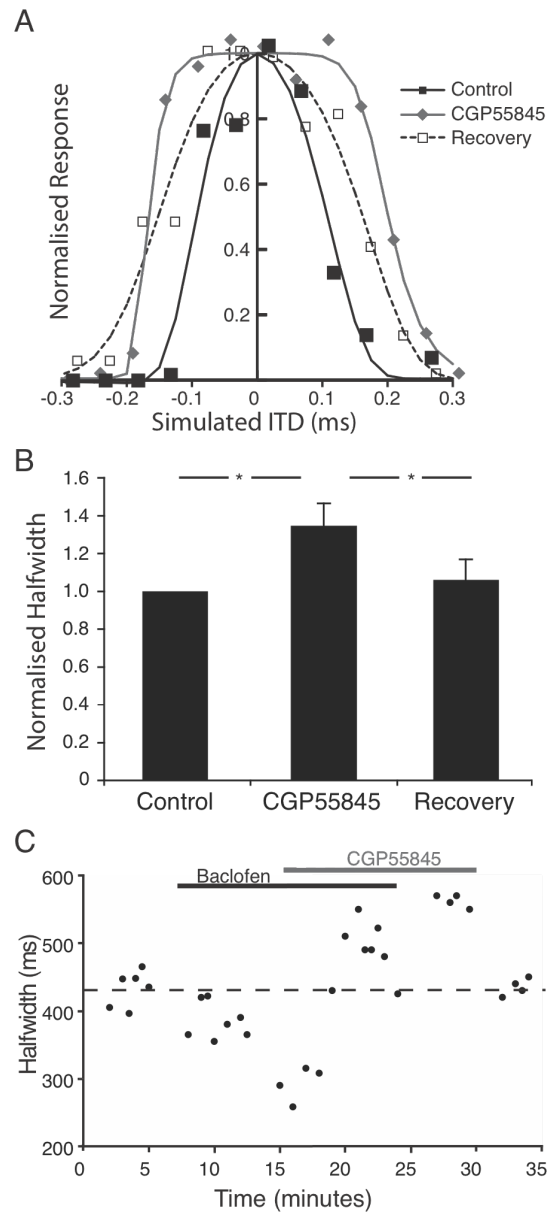


Figure 2.6: Blocking GABA_BR activity broadens sITD tuning curves. A. CGP55845 (2 μ M) application (diamond symbols) broadens sITD tuning curves relative to control (square symbols) in a P18 neuron. Recovery from inactivation is shown with open squares. B. Population data shows significant broadening of sITD halfwidth during CGP55845 application (* indicates $p < 0.01$, $n = 12$). C. Sequential application of baclofen and CGP55845 demonstrates the time course of the effect on ITD halfwidth.

Computational modelling of GABA_BR activation

The results presented thus far suggest that GABA_BR activation modulates both the magnitude of excitatory and inhibitory inputs to MSO as well as the kinetics of inhibition. Increased response selectivity to sITDs in baclofen suggests that GABA_B modulation of EPSCs may sharpen ITD tuning *in vivo*. In order to explore the relative contributions of input magnitude and IPSC kinetic modulation by GABA_BRs to ITD selectivity, I generated a computational model of an MSO neuron in which these effects could be independently controlled.

We utilized the model neuron architecture developed by Zhou and colleagues (2005) as a framework for our MSO model, but I made significant alterations to the inputs, the voltage dependent membrane properties, and anatomical characteristics based on both recent empirical data (Mathews et al. 2010, Scott et al. 2010) and data from the current study (see Methods). For the input model I simulated firing characteristics of bushy cells of the AVCN and principal neurons of the MNTB, which represented bilateral excitatory and contralateral inhibitory input respectively. Model synaptic inputs included intensity dependent entrainment (spikes per cycle) with fixed synchrony values for each bushy cell input based on published anteroventral cochlear nucleus (AVCN) rate-intensity data from Joris et al. (1994) (Fig 2.7A). In simulations that included inhibition, our model included a contralaterally evoked glycinergic input based on gerbil MNTB rate-intensity data from Kopp-Scheinflug et al. (2008) (Fig 2.7B). Stimuli were 500 ms, 200 Hz tones at three intensity values; 30, 45, and 60 dB SPL designated low, moderate, and high intensity which correspond to near threshold, mid dynamic range, and

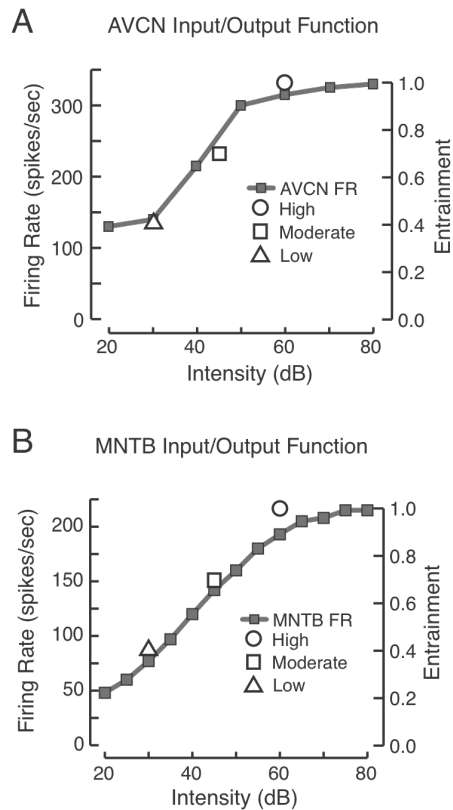


Figure 2.7: Model parameters for excitatory and inhibitory inputs. A. Modeled excitatory input rates are derived based on published AVCN input/output functions adapted from Joris et al., (1994) solid line. Data are expressed as both firing rate and entrainment values. Computational ITD simulations utilized three sample intensities on the entrainment curve to simulate MSO input near threshold (30 dB triangle), at moderate intensity (45dB square) and high intensity near saturation (60 dB circle). B. Input/output function for gerbil MNTB neurones adapted from Kopp-Scheinflug et al., 2008. The same three intensity conditions are sampled as in the excitation only model shown in panel A.

saturated firing rates respectively (Fig 2.7). Synaptic depression was modeled with functions based on data illustrated in Figures 2.3 & 2.4 (see Methods).

We tested the contributions of the three known influences of GABA_B modulation relevant to the model. GABA_BRs modulate the amplitude of both EPSCs and IPSCs and also modulate the kinetics of IPSCs. In order to assess the effect of the amplitude and kinetic modulation of PSCs on ITD encoding separately, I modelled the system in four conditions at each test intensity: 1) *control conditions*, in which there was no GABA_B modulation on any input; 2) *kinetic-only conditions*, in which the IPSC kinetics were changed to match the GABA_B modulated conditions (i.e. Fig 2.2Ea), but the PSC amplitudes were unchanged; 3) *amplitude-only conditions*, in which EPSC and IPSC amplitudes were suppressed but the IPSC kinetics model was identical to the control condition; 4) finally, the *combined condition* modulation where EPSC and IPSC amplitudes were modulated as well as IPSC kinetics. Figure 8 *panels A-C* show the model output, normalized ITD functions, halfwidth changes and firing rate modulation (see Methods) at each of the three test intensities under each condition.

First, I modelled normal EPSC and IPSC amplitude and only included the GABA_B dependent modulation of IPSC decay kinetics. GABA_B modulated IPSC kinetics caused a small change or mild suppression of the peak output-firing rate in the low and moderate intensity conditions, but not the high intensity condition (Fig 2.8, *Aa-Ca, red triangles*). Surprisingly, at moderate and high intensities IPSC kinetic modulation alone was sufficient to narrow ITD halfwidth, and was more efficacious as intensity increased (Halfwidth change: 30 dB: +10.2%; 45 dB: -17.8%; 60 dB: -43.8%). The kinetic modulation also improved FR modulation versus control through the physiologically

relevant range at all intensities (Fig 2.8*Ad-Cd*). These results suggest that the temporal aspects of the IPSCs may play a major role in shaping ITD selectivity *in vivo*, and that the modulation by GABA_BRs of inhibitory input may actively shape ITD selectivity by changing kinetics.

Next I tested amplitude-only conditions, in which both the EPSC and IPSC amplitude were suppressed by GABA_BR activation (Fig 2.8*A-C*, *blue circles*), but IPSC kinetics were unchanged from controls. Suppression of PSCs for the simulations shown was at the maximum values observed in the voltage clamp recordings; 40% for EPSCs and 60% for IPSCs. Simultaneous suppression of inputs resulted in an expected strong reduction in peak output-firing rate at low and moderate intensities. Normalized ITD functions of the model show that amplitude suppression of both EPSCs and IPSCs resulted in improved ITD selectivity at each intensity. Halfwidth values are shown in Figure 2.8, *c panels*, and were improved by PSC amplitude suppression (Halfwidth reduction: 30 dB: 19.6%; 45 dB: 35.6%; 60 dB: 34.5%). FR modulation was also improved (Fig 2.8*Ad-Cd*). These results suggest that input amplitude suppression is sufficient to improve ITD selectivity alone even while inhibitory input is also reduced. Interestingly, amplitude modulation efficacy stabilized at or above the moderate intensity while the kinetic modulation reported above showed a linear increase in efficacy as intensity increased (Fig 2.8*D*). At high intensity, the kinetic only modulation was similar in efficacy to the amplitude only modulation in reducing ITD halfwidth (Fig 2.8*Cc*).

Finally, I simulated the combined GABA_BR activation effects that I documented on both EPSC and IPSC magnitudes and IPSC kinetics. When GABA_BRs were activated

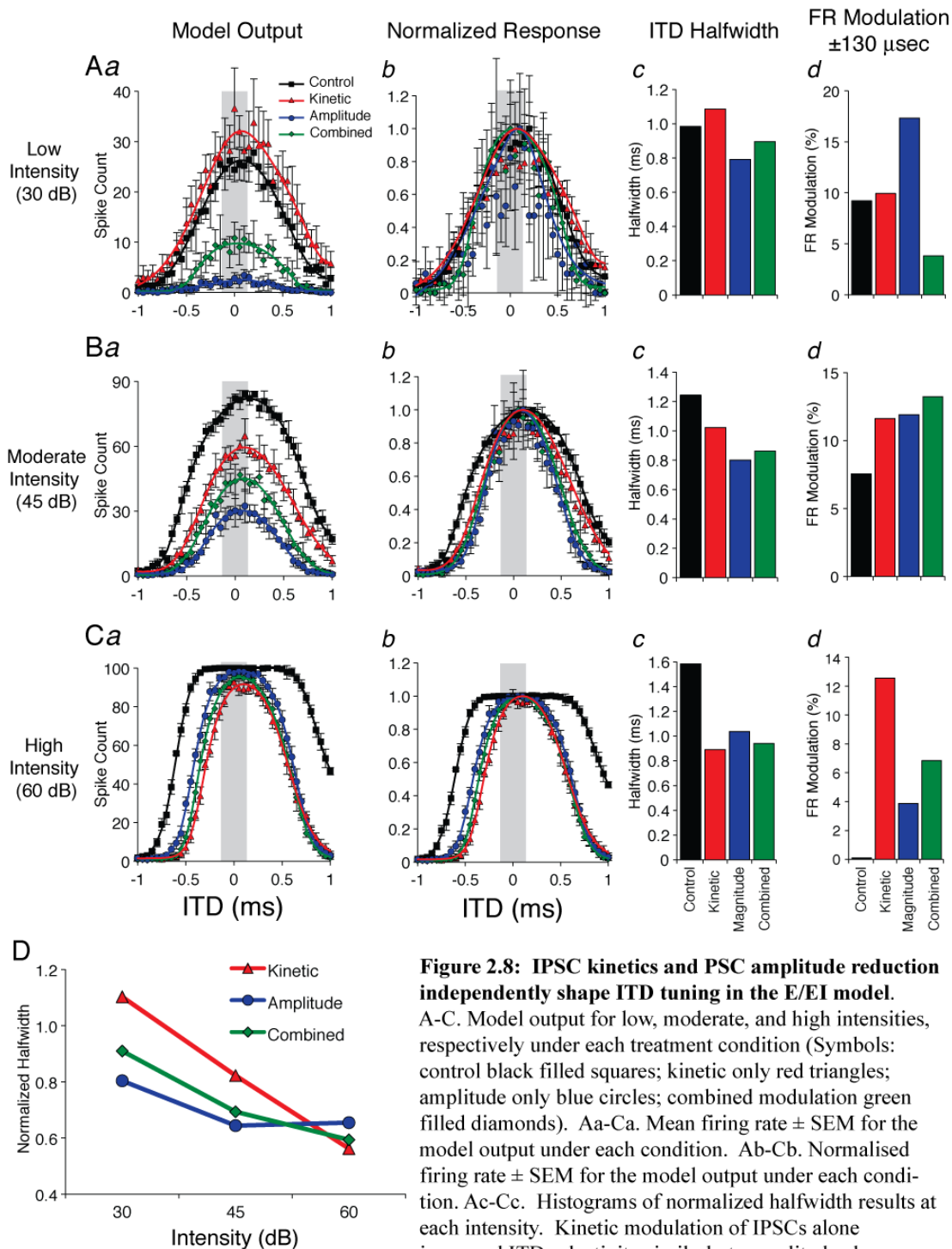


Figure 2.8: IPSC kinetics and PSC amplitude reduction independently shape ITD tuning in the E/EI model.

A-C. Model output for low, moderate, and high intensities, respectively under each treatment condition (Symbols: control black filled squares; kinetic only red triangles; amplitude only blue circles; combined modulation green filled diamonds). Aa-Ca. Mean firing rate \pm SEM for the model output under each condition. Ab-Cb. Normalised firing rate \pm SEM for the model output under each condition. Ac-Cc. Histograms of normalized halfwidth results at each intensity. Kinetic modulation of IPSCs alone improved ITD selectivity similarly to amplitude alone conditions at moderate and high intensities. Ad-Cd. Firing rate modulation for each condition for the biologically relevant range of ITDs ($\pm 130 \mu\text{sec}$) indicated by grey bars in columns a and b. Firing rate modulation increased in all GABA_B activated conditions relative to control at 45 and 60 dB. D. Comparison of the contribution of improvement in ITD sensitivity for each GABA_B dependent effect modelled at three intensities. The kinetic modulation of IPSCs has a greater impact on selectivity as intensity increases, while the amplitude modulation is most potent at low intensities. Interestingly, the combined influence of these modulations is fairly stable across intensity.

on all inputs, halfwidth of normalized responses was narrowed at all intensities (Halfwidth reduction: low: 9.0%; moderate: 30.7%; high 40.6%). Across intensity conditions, the combined GABA_B dependent modulation resulted in relatively stable narrowed ITD functions, and tended to increase in efficacy as intensity increased, but to a lesser degree than the kinetic only modulation (Fig 2.8D). This feature is interesting because it suggests that while kinetic or amplitude modulation influences halfwidth differentially across intensity, the net output when both are taken into account results in stable halfwidth reduction derived from GABA_BR activation. FR modulation was improved at moderate and high intensities in the combined modulation condition (Fig 2.8Ad-Cd). Overall, the results of model suggest that both IPSC kinetics and PSC suppression may play a role in maintaining ITD selectivity *in vivo*.

Model Tolerance to IPSC onset timing and relative E/I magnitude

Model parameters were chosen based on our current understanding of the cellular and synaptic physiology of the MSO and informed by *in vivo* observations of gerbil MSO neuron physiology. For the model output data presented thus far, IPSC inputs were presented with a 1.0 ms lead relative to contralateral excitation because model output best approximated the contralateral shift in peak ITD observed *in vivo* with this value (Brand et al. 2002, Pecka et al. 2010). The IPSC kinetic shift was a surprisingly potent modulator of ITD selectivity, but it is unclear to what extent this effect is a consequence of the particular model parameters that were chosen especially considering kinetic changes may be particularly sensitive to IPSC delay.

To test whether the GABA_B dependent improvements in ITD selectivity that I observed were robust independent of relative input timing, I systematically varied IPSC

lead-time in 0.2 ms intervals over a range comprising 1.4-0.6 ms. Over the range, the effect of delay on ITD selectivity was remarkably linear (Fig 2.9A). At all lead times tested, the GABA_B dependent IPSC kinetic shift narrowed ITD function halfwidth (Fig 2.9A, *open triangles*). Furthermore, the relative influence of IPSC kinetics and PSC magnitude was consistent and linear at every lead-time tested. These data indicate that the GABA_B induced shift in synaptic input features is predicted to have a robust influence on ITD selectivity in MSO neurons over a broad range of possible IPSC/EPSC arrival times.

The relative magnitude of excitation and inhibition received by MSO neurons *in vivo* and how these inputs vary with intensity remains unknown. However, *in vitro* measurements suggest that each MSO neuron receives at least 4-8 excitatory inputs and 2-4 inhibitory inputs. The summed conductance of excitation and inhibition are likely equal since each inhibitory input was estimated to have twice the conductance value of each excitatory input (Couchman et al. 2010). In order to test whether relative strength of excitation and inhibition would influence the GABA_B dependence of the results, the inhibition was manipulated in two ways. First I altered inhibitory strength by changing IPSC reversal potential, thus influencing the driving force on Cl⁻ current. Two reversal potentials for IPSCs, -70 mV (Zhou et al. 2005) or -90 mV (Magnusson et al. 2005) (-90 mV is shown in Fig 2.8), were modelled. This manipulation did not significantly affect the relative GABA_B dependent changes observed in ITD functions. Second, I adjusted the magnitude ratio of excitatory and inhibitory inputs in the model. Peak IPSC magnitude was tested at three values with respect to EPSC magnitude (Fig 2.9B). I

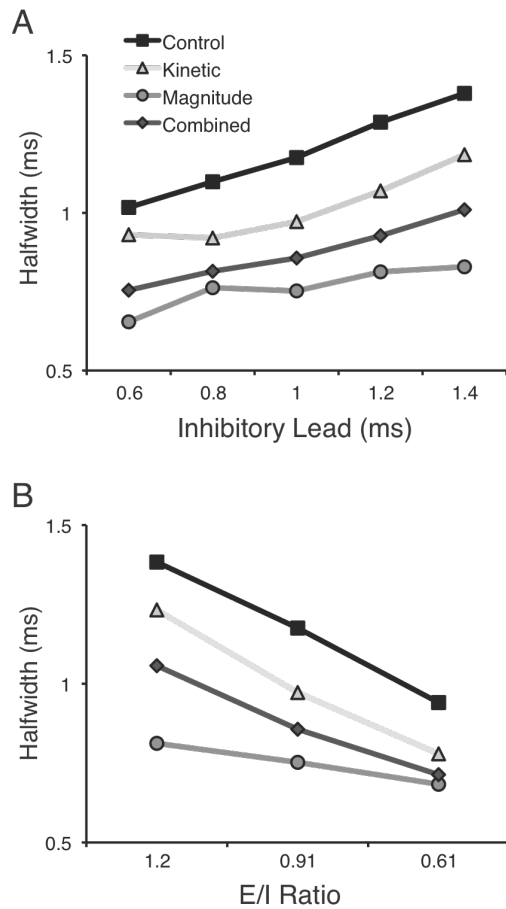


Figure 2.9: GABA_BR dependent improvements in ITD selectivity are maintained over a range of input parameters in the E/EI model. A. Halfwidth values for each condition at the five different inhibitory lead times. ITD selectivity improved with GABA_BR dependent modulations regardless of inhibitory lead time. B. Halfwidth values at the three different ratios of excitatory to inhibitory input magnitude. GABA_BR dependent changes in PSCs led to a decrease in halfwidth regardless of the relative input magnitude but ITD selectivity was greatest at the ratio where inhibition dominated.

found that regardless of the relative size of IPSCs and EPSCs, the GABA_B dependent IPSC kinetic shift and magnitude reduction resulted in greater ITD sensitivity compared to the control condition. Not surprisingly, as the magnitude of IPSCs increased, the influence of GABA_B dependent kinetic shifts also increased, but ITD selectivity was improved with GABA_BR activation at all IPSC magnitudes. Further, the relative contributions of GABA_B dependent changes in IPSC kinetics and PSC magnitude to ITD selectivity were similar regardless of the initial magnitude of the IPSCs.

Discussion

This report comprises four main findings. First, I demonstrated that both EPSC and IPSC amplitudes are modulated by GABA_BRs in the MSO and that the suppression of EPSCs is age dependent, consistent with data recently reported by Hassfurth et al. (2010). Second, IPSC decay kinetics are dependent on GABA_BR activation and the magnitude and direction of this effect changes during development. Third, I showed that synaptic depression of IPSCs and EPSCs in the MSO is reduced during GABA_BR activation. Fourth, I tested the hypothesis that PSC magnitude and/or kinetic modulation by GABA_B receptor activation improves coincidence detection in MSO neurons using both physiological and modelling approaches. Our model data also showed that GABA_B dependent changes in inhibitory kinetics are well suited to influence ITD computation and this effect may act independently of the input magnitude effects. Finally, the results from our model show robust tolerance to key features of the circuit such as the magnitude ratio and relative timing of excitation and inhibition.

GABA_B dependent EPSC amplitude modulation sharpens ITD selectivity

A principal finding of this study is that modulation of EPSC amplitude strongly influences ITD selectivity. Bath application of a low concentration of baclofen sharpened sITD selectivity in 22/25 neurons bilaterally stimulated with pulse trains. This result was consistent regardless of age. Since EPSC amplitude was reduced by activation of GABA_BRs, the temporal window during which these smaller synaptic events could sum to reach threshold was narrowed. Bath application of the GABA_B antagonist, CGP55845, significantly increased sITD halfwidth relative to both the baclofen and control conditions. While CGP55845 had no effect on unitary evoked EPSCs, I showed

that it did have an effect on the magnitude of EPSCs during the train stimuli by reducing synaptic depression. The latter result indicates that when using train stimuli in our experimental protocol, a low level of GABA_BR activation was endogenously evoked in the control condition. Thus, our estimate of GABA_B dependent suppression is likely to be conservative since it is based on baclofen application alone relative to control and did not include an estimate of stimulus induced GABA_B activation in the slice.

The sITD experiments also showed that GABA_B dependent suppression of PSCs was more potent for trailing spikes when compared to onset spikes. These data are consistent with the data presented in Figure 2.3, which showed substantial depression of EPSCs for ongoing stimulus trains. Baclofen application reduced EPSC depression overall but at the expense of the initial pulse response magnitude. Taken together, the PSC depression and spike output data suggest that the GABA_B dependent effects shown here will differentially influence the processing of ongoing sounds compared to computation of ITD at stimulus onset.

sITDs measured using the bilateral stimulation paradigm became more temporally selective over development. However, the contribution of GABA_B activation to sharpening sITD halfwidth was essentially stable over all ages that I tested. Halfwidth declined substantially with postnatal age in the control condition from 974 ± 110 μ sec in P7-P16 animals to 382 ± 21 μ sec in P17-P24 neurons. Despite this large change in control halfwidth, GABA_BR activation sharpened sITD tuning curves between 15-25% at every age tested. The developmental consistency of this result is interesting considering that several physiological properties of the neurons are rapidly changing during this period including PSC characteristics (Spirou & Berrebi 1997, Smith et al. 2000, Scott et

al. 2005, Couchman et al. 2010). It is possible that the reduction of GABA_B modulation of EPSCs that I observed is regulated to maintain a stable level of ITD selectivity throughout development.

In the computational model, I further investigated the dependence of the suppression of EPSCs on ITD tuning as a function of stimulus intensity. ITD tuning systematically improved with GABA_B activation, but did so at the expense of maximum firing rate (Fig 2.8 panels *Aa-Ca*). The low intensity sound condition under maximum GABA_BR activation yielded only a few responses near the peak of the ITD response.

It is a question then whether GABA_BR activation simply improves ITD selectivity by reducing overall spike rate. Both the *in vitro* data and the modelling data appear to refute that assertion. In the model, intensity dependent changes in spike rate under the control condition are indeed associated with a decrease in halfwidth (Fig 2.8) from 1.4 ms at 60 dB to 1.0 ms at 30 dB. However, GABA_B dependent reductions in halfwidth exceed those observed for spike rate alone, suggesting that coincidence detection depends on other features of the input characteristics beyond firing rate.

In this report, I used halfwidth and/or firing rate modulation as an assessment of ITD sensitivity. I showed that activation of GABA_BRs effectively improved selectivity by decreasing halfwidth of ITD tuning curves. Although in the model neuron at high intensity, our control ITD functions were rather broad relative to the biologically relevant range of ITDs, in our *in vitro* simulated ITD experiments, the animals age P17 and above had an average tuning curve halfwidth of ~380 μsec. ITD tuning curves for our modelling data were generally around 800 μsec with GABA_BR modulation included. Brand et al. (2002) showed that ITD tuning of MSO neurons *in vivo* is stimulus frequency dependent

with the broadest functions generated at low frequencies. Although *in vivo* data from low frequency MSO neurons are relatively rare, estimates of halfwidth from previous studies appear similar to our results (Brand et al. 2002, Pecka et al. 2008, Day & Semple, 2011). Additionally, the firing rate modulation through the biologically relevant range of ITDs improved with GABA_BR activation in our model. Our improvements were modest due to the limited peak shift (only ~100µs) I observed in the model which was about half of the shift observed *in vivo* (Brand et al. 2002, Pecka et al. 2008).

The finding that GABA_B activation strongly reduced responses in the MSO at low sound intensity has important implications for the proposed function of GABA_B dependent signalling in the system. It suggests that GABA_BR activation *in vivo* would most optimally be positively correlated with sound intensity. Such an arrangement would allow MSO neurons to encode ITDs at low intensity with larger, but more sparsely evoked EPSCs. Under low intensity conditions when GABA signalling is proportional to sound intensity, GABA_BR activation would be minimal and EPSC amplitude would be preserved. High intensity stimuli, however, would presumably recruit a stronger GABA signal, resulting in amplitude suppressed, but highly entrained EPSCs. Thus, the GABA_BR system could function to normalize summed excitatory synaptic current magnitude across a broad range of stimulus intensities assuming that the GABAergic signal is also activity dependent. Our data suggest such activity dependence is possible as blocking GABA_BRs had a noticeable effect on EPSC depression during trains of stimuli, but not during unitary stimulus protocols. *In vivo* recordings from MSO neurons in which GABA_B signalling is manipulated will be required to test this hypothesis.

It is of great interest to determine the source of acoustically driven GABA available to MSO neurons. MSO neurons are known to receive GABAergic terminals and to express GABA_A receptors into maturity (Korada & Schwartz 1999). However the origin of the putative GABAergic input is unknown. Interestingly, train stimulation in the presence of antagonist showed that GABA_B activation occurs under repeated stimulation of fibres medial to the MSO. This fibre bundle contains both excitatory AVCN and inhibitory MNTB fibres. Early in development MNTB neurons are known to co-release glycine, GABA, and glutamate (Smith et al. 2000, Nabekura et al. 2004, Gillespie et al. 2005). However, this co-release diminishes with age and the output of the MNTB is predominantly glycinergic by P17, although residual GABA release was still detected at this age (Nabekura et al. 2004). Some reports suggest that the superior periolivary nucleus, a GABAergic structure, provides input to the MSO, but these reports are not yet well substantiated by replication (*see review*: Thompson & Schofield, 2000). The lateral nucleus of the trapezoid body (LNTB), a known source of afferents to the MSO, also has a population of GABAergic cells (Spirou & Berrebi 1997). Finally, an intriguing possibility was recently revealed by Magnusson et al. (2008), which showed that in the neighbouring lateral superior olive (LSO), principal neurons appear to release GABA at dendritic terminals to modulate their presynaptic inputs via GABA_BR activation, although these neurons do not release GABA to their postsynaptic targets. However, recent results show that, in contrast to LSO, activation of GABA_BR in MSO does not depend on the activity of the MSO principal neurons themselves, which makes such a mechanism unlikely (Hassfurth et al. 2010).

The role of GABA_B dependent modulation of IPSCs

Our computational model is one of several in recent studies to probe the relative importance of inhibitory input in shaping ITD selectivity (Brand et al. 2002, Zhou et al. 2005, Leibold 2010). Glycinergic inhibition, from the MNTB and perhaps the LNTB is known to shape ITD function magnitude and shift the peak response toward the contralateral ear *in vivo* (Brand et al. 2002, Pecka et al. 2008, *reviewed in*: Grothe et al. 2010). The precise temporal pattern of phase-locked EPSCs and IPSCs evoked in MSO neurons *in vivo* remains unknown. However, several modelling and empirical studies in brain slices suggest that inhibition which leads excitation each stimulus cycle is most effective at replicating the *in vivo* observations (Brand et al. 2002, Zhou et al. 2005, Chirila et al. 2007, Leibold 2010). Jercog et al. (2010) found differences in contra- versus ipsilateral excitatory input kinetics which contributed to shifts in ITD tuning curves. They utilised a thick-slice *in vitro* preparation in which stimulation of intact afferent fibres from their origins in VCN evoked PSPs in MSO neurons. Using our bilateral stimulation protocol, with direct stimulation of AVCN fibres proximal to MSO neurons, I did not observe any significant differences in EPSP rise slopes (data not shown). In our current model, I used bilaterally symmetric PSCs with relative IPSC/EPSC timing derived from an iterative approach where I systematically shifted the relative timing until the model output best replicated published *in vivo* data from gerbil MSO recordings (Brand et al. 2002, Pecka et al. 2008, 2010). I found that inhibition leading by 1.0 ms was most effective at shifting the best ITD peak toward the contralateral ear to values that approximate *in vivo* observations. However, I also showed that the GABA_B dependent effects on PSC kinetics and/or magnitude described here

contribute similarly to ITD selectivity across a broad range of IPSC delays. The halfwidth declined at every delay of IPSC, but the degree of sharpening depended on the particular delay (Fig 2.9A).

Our model demonstrated that slowing the decay kinetics of the IPSC by ~40% (corresponding to the data shown in Fig 2.2E), was sufficient to sharpen ITD functions at all stimulus intensities. When the kinetic and amplitude suppression were modulated together, they modulated ITD sensitivity at a level intermediate to the two individual effects. Interestingly, the kinetic effect differed from the amplitude suppression effect in that the kinetic effect increased in efficacy with increased intensity. The narrowing of ITD functions was also associated with an increase in the firing rate modulation through the physiological range of ITDs (Fig 2.8 *panels c and d*).

In a recent study, Couchman et al. (2010) showed that EPSC and IPSC magnitudes are likely to be similar in the mature MSO. Our modelling tested the GABA_B dependent effects over a range of relative EPSC/IPSC magnitudes and showed their effects to be similar regardless of input ratio. These results suggest that the GABA_B dependent modulation of IPSC kinetics in conjunction with PSC amplitudes may have robust important functions in ITD processing.

The developmental dependence of shift in IPSC decay kinetics was a novel and unexpected finding in this study. GABA_B receptor activation shortened IPSC decay in young animals while extending it in older animals. This occurs in the context of a process of speeding IPSC decay over the same time frame (Smith et al. 2000) due primarily to a transition from mixed GABAergic/glycinergic MNTB input to one dominated by glycine during this period of development. A variety of factors have been

shown to influence evoked PSC kinetics in several systems including reduction of quantal content leading to better synchrony (Brenowitz et al. 1998), phosphorylation state of GABA_A receptor (Hahner et al. 1991), and competitive occlusion of current among glycine and GABA receptors (Li et al. 2003). Some of these have even been shown to depend on GABA_B activation such as the reduction in IPSP duration during GABA_BR blockade (Price et al. 2008) and the speeding up of EPSC decay time constants (Otis & Trussell 1996). The exact mechanism of this change in MSO neurons was not a central focus for this study, and our experiments did not address which, if any of these multiple factors may contribute to the observed kinetic effects. Resolution of these mechanisms will be a focus of future investigation.

Summary and Conclusions

Control of synaptic gain is a general problem confronting all neurons that must make stable and accurate computations when input varies in magnitude. MSO neurons have several synaptic and intrinsic mechanisms that allow them to stabilize PSC amplitude. ITD computation is a remarkably demanding computation, where coincidence-detecting neurons in the avian nucleus laminaris (NL) and mammalian MSO modulate their firing rate several fold with sub-millisecond variation in ITD. These ITD computations in MSO neurons are sensitive to changes in synaptic gain as our model showed prominent degradation of ITD selectivity as stimulus amplitude increased in the absence of compensatory mechanisms. *In vivo*, however, ITD coding is remarkably stable with changes in stimulus intensity in both NL and MSO, suggesting that mechanisms to reduce the impact of changes in input firing rate exist. Inputs to MSO

neurons are highly synchronized to the stimulus waveform at all intensities, but as intensity increases, firing rate can increase 300-400% for each input fibre. While it is unknown precisely how many inputs impinge on each MSO neuron from each ear, the size of the summed synaptic conductance may vary widely over changes in stimulus intensity. I have demonstrated that GABA_BRs are a possible mechanism that components of the MSO circuitry may use to normalize synaptic strength, preventing saturation under intense stimulus conditions, and preventing failures during low amplitude stimuli.

Table 2.1: Depression variable values for depression of EPSC and IPSC magnitude in the computational model expression $G_{input} = G_{initial}(a + (b * \exp(c * t)))$

	<u>Control</u>		<u>GABA_BR activation</u>	
	EPSC	IPSC	EPSC	IPSC
a	0.428785	0.467342	0.686903	0.88245
b	0.574672	0.531022	0.336557	0.118218
c	-0.0675269	-0.0440469	-0.686903	-0.0466922

Chapter III

Synaptic physiology of inhibitory inputs in the superior olivary nucleus

Abstract

Inhibitory input provides an important mechanism for modulating activity in the circuit that performs computations necessary for accurate sound localization. Neurons in the superior olivary nucleus (SON) in the avian brainstem provide the main inhibitory input to this circuit. Studies involving inhibition in the avian brainstem have focused on the depolarizing GABAergic inhibition provided by the SON to its targets while few experiments have addressed the physiology of the SON itself, or its inputs. This study describes the characteristics of inhibitory synaptic transmission at the SON, which receives a putative inhibitory input from the contralateral SON. On the synaptic level, I found in all SON neurons that I sampled, evoked and spontaneous IPSCs were modulated by both GABAergic and glycinergic inhibition, similar to recently published observations of inhibition at the nucleus angularis (NA). Immuno-histochemical evidence and analysis of sIPSCs revealed that SON cells receive a mixture of both purely GABAergic terminals, as well as terminals from which GABA and glycine are co-released. Additionally, SON neurons had a staining pattern similar to the terminal staining where some cells were immunopositive for GABA and others were co-labeled for GABA and glycine. Evidence for glycinergic signaling within the SON is a novel result that may have important implications for the role of inhibition in the auditory brainstem.

Introduction

In the avian brainstem, inhibition is an integral part of maintaining sensitivity to interaural time disparities (ITDs), the main cue for localizing low frequency sounds. In the sound localization circuit, ITDs are processed by coincidence detecting neurons that receive input from both ears. These neurons are located in the nucleus laminaris (NL) in birds (Parks and Rubel 1975, Sullivan and Konishi 1986, Carr and Konishi 1990, Peña et al. 1996, Burger and Rubel 2008, Grothe et al. 2010, Burger et al. 2011). In order to accurately process ITDs, input to the NL must be precisely timed and consistent over a broad range of input intensities. Inhibitory input plays a key role in modulating inputs to ensure accurate computations.

The main source of inhibitory input in this circuit is the superior olivary nucleus (SON). The SON provides inhibitory feedback to ipsilateral targets, nucleus magnocellularis (NM), nucleus angularis (NA) and NL as well as feed-forward inhibition to the contralateral SON (Carr et al. 1989, Lachica et al. 1994, Westerberg and Schwarz 1995, Yang et al. 1999, Burger et al. 2005a). Investigation of inhibition in this system has focused on the depolarizing GABAergic inhibition observed at the targets of the SON involved in ITD computations (mainly NM and NL). *In vitro* experiments have demonstrated that this inhibition improves both phase-locking in NM and ITD sensitivity in NL by minimizing the time window where two inputs can sum to reach threshold (Bruckner and Hyson 1998, Funabiki et al. 1998, Yang et al. 1999, Monsivais et al. 2000, Kuba et al. 2002, Howard et al. 2007). *In vivo* experiments confirm these results. Lesioning of the ipsilateral SON resulted in a decrease in the ability of NM neurons to

phase-lock to auditory stimuli (Fukui et al. 2010). The same lesioning protocol also decreased ITD selectivity in NL neurons due to compression of the dynamic range of the ITD tuning curves (Nishino et al. 2008).

Despite the breadth of investigation on the impact the SON has at its target nuclei, little is known about the physiology of the SON itself. Using a combination of *in vivo* and *in vitro* methods our lab described the response properties of SON neurons to acoustic stimuli, and the synaptic physiology of inhibitory inputs to the SON (Coleman et al. 2011). The main findings of the *in vivo* experiments are detailed below in order to preface the *in vitro* synaptic physiology results, which are the focus of this chapter.

Response properties of SON neurons to acoustic stimuli

The responses of SON neurons to monaural acoustic stimuli were tested by presenting 50ms tone bursts at the neuron's best frequency. Spiking was assessed using *in vivo* extracellular recording techniques. Response patterns to these stimuli were diverse and fell into several groups. The vast majority of neurons in the SON were driven by acoustic stimulation (~95%). Of these cells, two-thirds exhibited a sustained pattern with a peak response near the onset of the stimulus tone followed by continued firing throughout the stimulus. The other one-third had an onset pattern where they fired only a few spikes at the onset of the stimulus. Approximately 5% of SON neurons were inhibited by acoustic stimulation. These neurons typically had high spontaneous firing rates that were suppressed during the stimulus tone.

Neurons that exhibited the sustained response pattern were tested for phase-locking ability at best frequency. Approximately 50% of these neurons showed

significant capability to phase-lock. This was a surprising result given previous reports suggesting the intrinsic properties of SON neurons were not apt for preservation of temporal aspects of stimuli (Lachica et al. 1994, Yang et al. 1999, Monsivais et al. 2000).

The impact of inhibition on acoustically driven responses was assessed by pharmacological block of GABA and/or glycine receptors by iontophoresis of receptor antagonists. GABA_A receptor block resulted in an increase in firing rate and a decrease in phase-locking efficiency. Glycine receptor block yielded similar results, suggesting that glycinergic transmission occurs at the SON and like GABAergic inhibition, acts to modulate the responses to acoustic stimuli.

Glycinergic transmission in the avian brainstem

The *in vivo* results regarding the modulation of response properties by glycine were intriguing considering the recent discovery of glycinergic transmission as a component of inhibition in the NA of chickens (Kuo et al. 2009). In addition to the physiological demonstration of synaptic glycine transmission, immunohistochemical analysis also revealed the presence of glycine in presynaptic terminals at the NM, NL and NA. Here, glycine co-localized in terminals that were also immunopositive for GABA. Coleman et al. (2011) confirmed these results and established that glycine also co-localized with GABA in presynaptic terminals surrounding SON neurons. Additionally, both transmitters are observed in the cell bodies of some SON neurons indicating that the SON is the likely source of glycine in this circuit.

This chapter is a detailed description of the *in vitro* experiments published in Coleman et al. (2011). These experiments describe the synaptic physiology of inhibitory

inputs to the SON. I demonstrate that inhibition here is similar to that in the NA where inhibitory postsynaptic currents are mediated by both GABA- and glycinergic components. Further, I provide evidence for the hypothesis that glycinergic inhibition here is the result of the co-release of GABA and glycine from the same vesicles.

Methods

In vitro brain-slice preparation

For synaptic physiology, 12 white leghorn chickens aged E17-P5 were rapidly decapitated and the brainstem containing auditory nuclei was removed, blocked, and submerged in oxygenated artificial cerebrospinal fluid (ACSF) (containing in mM: 130 NaCl, 3 KCl, 10 glucose, 1.25 NaH₂PO₄, 26 NaHCO₃, 3 CaCl₂, 1 MgCl₂) at 22°C. The brainstem was placed rostral surface down on the stage of a vibrating microtome (Microm 650V, Walldorf, Germany). Coronal sections (150-200 µm) containing the SON were collected, submerged in an incubation chamber of continuously oxygenated ACSF and incubated at 37°C for approximately one hour. Slices were then maintained at room temperature until used for recording.

Brainstem slices were placed in a custom recording chamber on a retractable chamber shuttle system (Siskiyou Design Instruments, Oregon, USA) and neurons were visualized with a Nikon FN-1 Physiostation microscope using infrared differential interference contrast optics. Video images were captured using a CCD camera (Hamamatsu C7500-50, Hamamatsu City, Japan) coupled to a video monitor. The recording chamber was continuously perfused with ACSF at a rate of 2-4 ml/min. An inline feedback temperature controller and heated stage were used to maintain chamber temperature at 35 ± 1°C (TC344B, Warner Instruments, Hamden, CT, USA).

IPSC Recordings

For evoked IPSC recordings, a concentric bipolar electrode with tungsten core (WPI TM53CCINS, Sarasota, FL) was lowered to the tissue surface with a micro-manipulator and placed in a position dorsomedial to the SON. Principal SON neurons were identified based on their characteristic round morphology. Patch pipettes were pulled from thick walled borosilicate glass capillary tubes (WPI 1B120F-4) to a resistance of 4-8 M Ω using a two-stage puller (Narishige PC-10, Tokyo, Japan) and back-filled with internal solution (containing in mM: 130 CsCl, 1 CaCl₂, 1 MgCl₂, 10 EGTA, 10 HEPES, 2 ATP, 0.3 GTP, 10 phosphocreatine, pH adjusted to 7.3 with CsOH). 5 mM QX314 was added to the internal solution to prevent antidromic action potentials. In many cases, 0.4% biocytin was added to the internal solution to label the neurons following the protocol of Scott et al. (2005). SON principal neurons had an average whole-cell capacitance of 36.7 ± 14.3 pF and an average series resistance of 10.2 ± 4.1 M Ω . In voltage clamp, series resistance was compensated at 60-80%. Evoked and spontaneous IPSCs were recorded during bath application of 6,7-dinitroquinoxaline-2,3-dione (DNQX) (40 μ M) and D-2-amino-5-phosphonopentanoic acid (AP5) (50 μ M) in order to block glutamatergic input. Membrane voltage was clamped at -60 mV using a Multiclamp 700B amplifier. The signal was digitized with a Digidata 1440 data acquisition board and recorded using Clampex software (Molecular Devices, Sunnyvale, CA). IPSCs were evoked with 50 μ sec stimulus pulses with a stimulus isolation unit (Isoflex, A.M.P.I. Inc., Israel) through a bipolar electrode. Stimulus magnitude (range 10-90 V) was gradually increased until IPSC amplitudes stabilized at their maximum. Spontaneous IPSC data was collected by recording 30-60 second epochs while clamping

the membrane at -60mV. Miniature IPSCs were also collected in the presence of 1 μ M TTX to block the contribution of presynaptic action potentials to spontaneous events. In our recordings, no significant differences were observed between spontaneous and miniature events in any condition and therefore the data were pooled (Oleskevich and Walmsley 2002), and will be referred to as sIPSCs hereafter. After collection of control data, SR95531 (20 μ M) and strychnine (500nM) were sequentially applied to block GABA_A and glycine receptors (GlyRs) respectively. In several cells, SR95531 and strychnine were applied simultaneously during data collection. IPSC amplitudes and kinetics were analyzed using Clampfit software. Rise and decay time constants, expressed hereafter as tau (τ_{rise} and τ_{decay}) values, were calculated from standard exponential fits from 10-90% of the peak of IPSCs. τ_{decay} values were obtained using either single or double exponential fits. Goodness of fit was determined by comparing the sum of the squared errors. Double exponential fits were chosen if the sum of the squared errors was less than half that of the single exponential fit. A weighted τ_{decay} value was calculated for double exponential fits using the equation:

$$\text{weighted } \tau = \tau_1 (A_1/A_1+A_2) + \tau_2 (A_2/A_1+A_2)$$

as in Kuo et al. (2009). Spontaneous IPSC frequency (Hz) was also calculated. Drug and recovery condition amplitudes and kinetic measures were normalized to control and each treatment group was assessed for statistical significance using paired Student's t-tests. Data in the results are expressed as percent of control \pm standard deviation. Error bars in figures represent standard error of the mean. Raw data values for evoked, spontaneous, and miniature IPSCs are found in Table 3.1.

Results

Evoked inhibitory synaptic transmission in the SON is mediated by both GABAergic and glycinergic components

The *in vivo* experiments demonstrated modulation of SON response properties with application of both glycine and GABA_A receptor antagonists. Both antagonists increased acoustically driven spike rates and diminished the precision of phase locking. To further characterize inhibitory transmission in the SON, I used *in vitro* whole cell voltage clamp techniques to record evoked and spontaneous IPSCs while pharmacologically manipulating GABAergic and/or glycinergic transmission.

IPSCs were evoked by placing a stimulating electrode on input fibers dorsomedial to the border of SON while excitatory inputs were blocked with 40 μ M DNQX and 50 μ M AP5. Evoked IPSCs (eIPSC) were observed in 20/21 neurons tested. eIPSC amplitude was variable with an average peak amplitude of -975 ± 957 pA (Table 3.1). In order to isolate the GABAergic component of eIPSCs, 500 nM strychnine was bath applied. Peak eIPSC amplitude was reduced in 12/12 cells on average to $50.6 \pm 16.8\%$ of the control value (Fig 8A). Similarly, blocking GABA_A receptors with SR95531 (20 μ M) reduced eIPSC amplitude to $45.2 \pm 19.4\%$ of control (n = 14). Simultaneous application of both SR95531 and strychnine completely abolished eIPSCs in 9 of 13 cells. The residual current for the population was $5.3 \pm 6.9\%$ of control (Table 3.1). In addition to amplitude modulation, changes in the eIPSC waveform kinetics were also evident (Fig

Table 3.1: Raw data values for evoked, spontaneous and miniature IPSCs during in vitro whole cell voltage clamp experiments

Condition	Peak Amp. (pA)	Area (pA)	Halfwidth (ms)	τ Rise (ms)	τ Decay (ms)	Frequency (Hz)
<i>Evoked IPSCs</i>						
Control (n = 20)	-947 ± 957	-4339 ± 3557	3.92 ± 2.29	1.56 ± 0.83	4.41 ± 2.93	--
Strychnine (n = 12)	-510 ± 611	-2807 ± 2513	5.45 ± 3.26	1.70 ± 0.85	7.03 ± 3.55	--
SR95531 (n = 14)	-310 ± 216	-741 ± 353	2.35 ± 1.03	1.23 ± 0.77	2.34 ± 0.88	--
SN + SR (n = 13)	-35.6 ± 48.0	-135 ± 108	--	--	--	--
Recovery (n = 15)	-676 ± 672	-3227 ± 2584	3.83 ± 2.25	1.53 ± 0.58	5.35 ± 3.82	--
<i>Spontaneous IPSCs</i>						
Control (n = 18)	-114 ± 48.2	-428 ± 192	1.93 ± 0.61	0.91 ± 0.22	4.35 ± 1.61	7.45 ± 6.51
Strychnine (n = 12)	-73.3 ± 35.6	-329 ± 147	2.32 ± 1.10	0.99 ± 0.31	6.48 ± 4.41	8.49 ± 4.58
SR95531 (n = 16)	-95.3 ± 53.6	-278 ± 169	1.39 ± 0.43	0.84 ± 0.37	2.91 ± 1.69	1.87 ± 1.38
Recovery (n = 14)	-103 ± 61.5	-398 ± 209	2.09 ± 1.00	1.06 ± 0.55	5.59 ± 4.10	7.76 ± 6.75
<i>Miniature IPSCs</i>						
Control (n = 6)	-141 ± 48.7	-496 ± 112	2.26 ± 0.48	0.90 ± 0.33	4.71 ± 1.26	11.3 ± 7.02
Strychnine (n = 5)	-63.1 ± 17.2	-244 ± 60.4	2.11 ± 0.44	1.06 ± 0.32	7.46 ± 1.12	9.11 ± 6.61
SR95531 (n = 5)	-92.2 ± 41.2	-308 ± 113	1.81 ± 0.26	0.87 ± 0.24	4.34 ± 1.01	1.81 ± 0.98
Recovery (n = 5)	-122 ± 84.6	-436 ± 255	2.20 ± 0.39	0.97 ± 0.20	5.09 ± 1.08	10.8 ± 6.51

Values indicate mean ± SD. SN Strychnine, SR SR95531

3.1A). I compared the halfwidth and τ_{decay} values of isolated GABAergic and glycinergic eIPSC components. Blocking GlyRs broadened the eIPSC and increased both the halfwidth ($145.3 \pm 59.9\%$ of control, $p < 0.05$, $n = 12$) and τ_{decay} ($158.1 \pm 72.1\%$ of control, $p < 0.05$, $n = 12$; Fig 3.1Cii, D). Blocking GABA_A receptors with SR95531 had a complementary effect on kinetics, narrowing the eIPSC waveform by reducing halfwidth ($65.3 \pm 25.6\%$ of control, $p < 0.01$, $n = 14$) and τ_{decay} ($66.5 \pm 19.7\%$ of control, $p < 0.01$, $n = 14$; Fig 3.1Ci,D). Area under the eIPSC waveform was also reduced in both drug conditions (strychnine: $60.7 \pm 22.1\%$ of control, $p < 0.01$, $n = 12$; SR95531: $31.1 \pm 22.4\%$, $p < 0.01$, $n = 14$; Fig 3.1B). These data suggest that both GABAergic and glycinergic transmission occur in the SON, that each contribute equally to the peak eIPSC amplitude, but that the GABAergic transmission provides the majority of the total eIPSC current.

Glycine and GABA are co-released at some inhibitory terminals in SON

Kuo et al. (2009) showed evidence suggesting that the most likely source of glycine in NA was from terminals that co-release GABA and glycine. Given our findings that both GABAergic and glycinergic synaptic transmission act on SON neurons, several possible input arrangements exist for these two modes of inhibition: 1) SON neurons could receive independent, purely GABAergic and purely glycinergic inputs, 2) these inputs could be provided by GABA/glycine co-release terminals as reported in NA (Kuo et al. 2009), or 3) there could be a mixture of single transmitter and co-release terminals. To differentiate between these possible input arrangements, I evaluated the properties

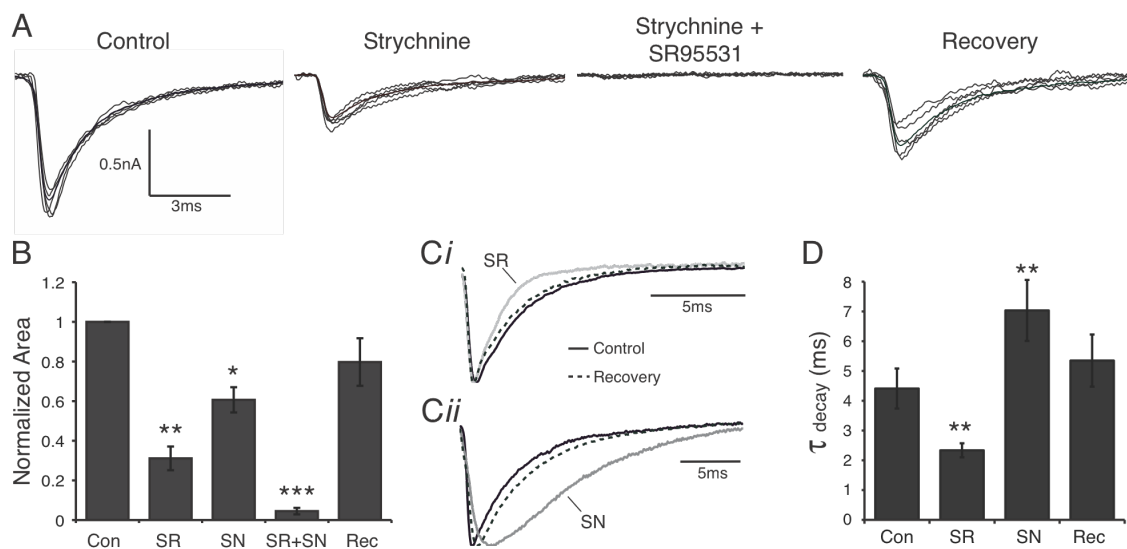


Figure 3.1: Evoked IPSCs in the SON contain GABAergic and glycinergic components.

A. Evoked IPSC (eIPSC) traces from a representative SON neuron during pharmacological treatments shows a significant decrease in amplitude with GlyR block (strychnine). B. Population data showing the effect of treatments on eIPSC area. C. Normalized eIPSC traces showing kinetic modulations during drug treatments (average of 10 traces in each condition). *Ci*. Bath application of SR95531, a GABA_A receptor antagonist results in faster eIPSC kinetics. *Cii*. Blockade of GlyRs with strychnine yielded slower eIPSC kinetics. D. Population data for τ decay values used for analysis of kinetics of eIPSCs. *Dashed line* represents normalized control value. *Significantly different from control, $p < 0.05$, ** $p < 0.01$. ***Significantly different from all other conditions, $p < 0.01$.

of spontaneous and miniature IPSCs. Statistical analysis of spontaneous and miniature events revealed no significant differences so the data sets were pooled and will be referred to as sIPSCs (see Methods).

We held SON cells at -60mV for 30 or 60 second epochs while blocking excitatory input with DNQX and AP5 in 24 neurons. sIPSCs were common with an average frequency of $8.42 \pm 6.25\text{Hz}$ (Table 3.1). Blocking GABA_A receptors significantly reduced the sIPSC frequency ($27.8 \pm 23.5\%$ of control, $p < 0.01$, $n = 21$), suggesting that many sIPSCs were purely GABAergic. SR95531 application also reduced the average peak amplitude of the remaining sIPSCs ($76.4 \pm 19.1\%$ of control, $p < 0.001$, $n = 21$) (Fig 3.2A,C,D). In contrast, strychnine application had no significant effect on sIPSC frequency, but there was a slight trend toward fewer events ($85.6 \pm 25.6\%$ of control, $p > 0.05$, $n = 17$; Fig 3.2C). However, peak sIPSC amplitude was significantly reduced ($66.2 \pm 32.3\%$ of control, $p < 0.01$, $n = 17$; Fig 3.2A,D). No sIPSCs were observed during simultaneous application of strychnine and SR95531 ($n = 13$). One additional observation was that during the control condition there was typically a few very large ($>400\text{pA}$) events as seen in Figure 3.2A. These events were absent in the drug conditions, but returned with recovery. These data taken together are consistent with an input arrangement where each SON neuron receives a substantial portion of purely GABAergic synaptic terminals, but few, if any, purely glycinergic terminals. Rather, the glycinergic component appears to be co-released with GABA at some terminals. I further analyzed the distributions of sIPSC kinetics in each condition to confirm these findings.

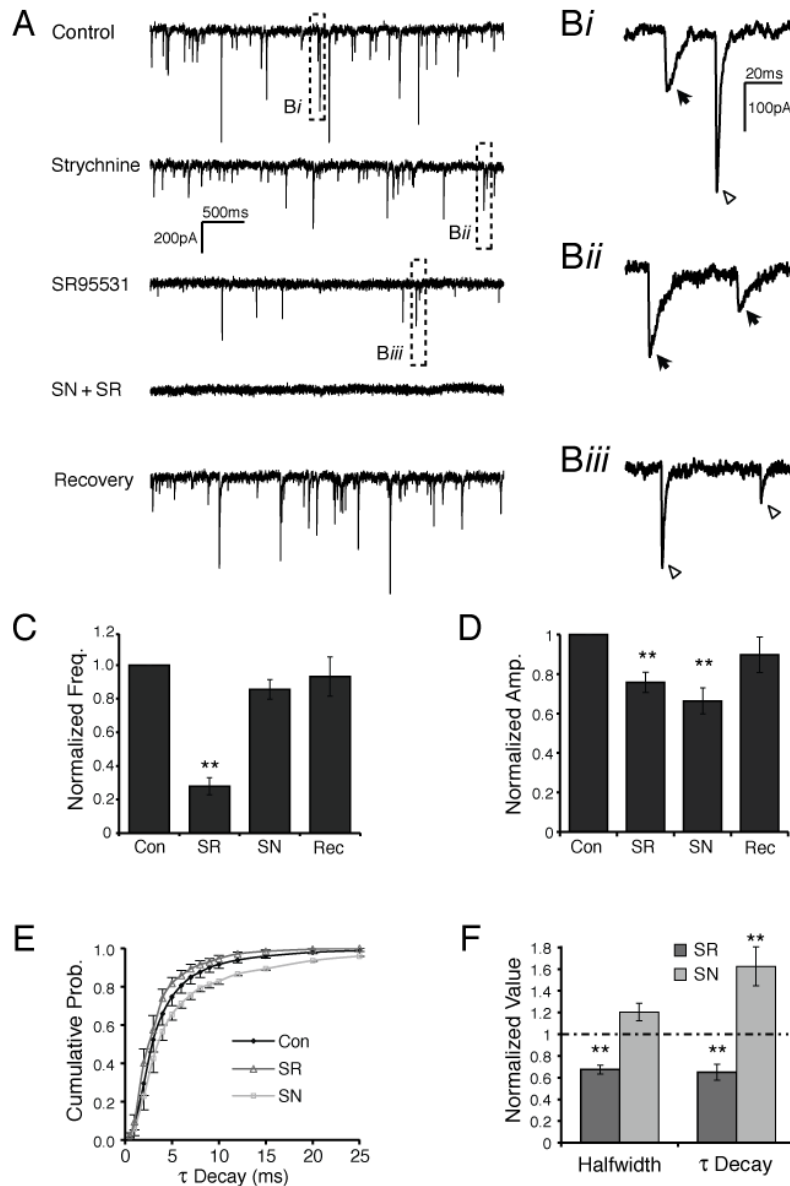


Figure 3.2: Spontaneous postsynaptic currents are modulated by blockade of both GABA and glycine receptors. A. Representative 5-s epochs of spontaneous (s)IPSC records in each experimental condition. B. Expanded 100-ms segments from the traces in A showing condition dependent decay kinetics. Bi. Control condition showing heterogeneous kinetic profiles including slow (arrow) and fast (arrowhead) events. Bii. Isolated GABAergic sIPSCs tended to have slower kinetics (quantified in F). Biii. Isolated glycinergic sIPSCs had faster kinetics. C. Population data for normalized frequency of sIPSCs. Frequency was significantly reduced during application of SR95531 but not strychnine. D. Population data for normalized amplitude of sIPSCs. Both SR95531 and strychnine significantly reduced sIPSC amplitude when bath applied. E. Cumulative probability analysis of τ decay values revealed a monophasic rise in control conditions that was significantly shifted to shorter or longer values in SR95531 and strychnine, respectively ($P < 0.01$, Kolmogorov-Smirnov test). F. Quantification of kinetic measures show a decrease in halfwidth and τ decay values in SR95531 and an increase in τ decay values in strychnine. Strychnine did not significantly change halfwidth.

* $P < 0.05$, ** $P < 0.01$, significantly different from control; pooled data include both sIPSCs and miniature IPSCs.

The evoked IPSC data show that isolated GABAergic and glycinergic conductances have very different decay kinetics. If sIPSCs arose from purely GABAergic or glycinergic terminals, then I would expect a bimodal distribution of sIPSC kinetics. However, τ_{decay} values for sIPSCs recorded in the control condition typically had a broad continuous distribution from slow to fast events. Figure 3.2Bi shows example events from the control condition in panel *A* illustrating this heterogeneity. The first event (*arrow*) has a slow decay, whereas the second event (*arrowhead*) is notably faster. Application of strychnine shifted the sIPSC population towards slower events (Fig 3.2Bii,E,F). Conversely, SR95531 application resulted in mostly faster sIPSCs (Fig 3.2Biii,E,F). Analysis of the cumulative probability plot for all τ_{decay} values from 14 cells in which both drugs were applied shows a monophasic rise in the control condition consistent with the broad and continuous distribution of values (Fig 3.2E). τ_{decay} kinetics of sIPSCs in both strychnine and SR95531 were significantly different from the control condition and different from each other (Kolmogorov-Smirnov test, $p < 0.01$). Taken together the observations of antagonist effects on τ_{decay} distributions in conjunction with their influences on sIPSC frequency and amplitude modulation shown above suggests that the most parsimonious model of SON input arrangements includes both purely GABAergic terminals and some GABA/glycine co-release terminals. While I cannot rule out the possibility that SON neurons receive some purely glycinergic terminals, our data do not support this hypothesis.

Discussion

Inhibitory inputs to the SON

Our *in vitro* data provide additional insights into the nature of GABA and glycinergic input to SON neurons. In all of the cells tested, I observed a GABAergic and glycinergic component during evoked IPSCs. Isolated GABAergic currents had a longer duration while the glycinergic component was shorter when compared to control. In the SON, the GABAergic component contributed about 65% of the total inhibitory current. Evoked IPSCs in the control condition were similar in kinetics but larger in magnitude than evoked IPSCs seen in the NA (Kuo et al. 2009) where GABA and glycine were suggested to be co-released. Our analysis of sIPSCs suggested a similar input arrangement of inhibitory transmission in the SON. I found that blocking GABAergic transmission resulted in a significant decrease in the frequency of spontaneous events, indicating that the SON receives many inhibitory inputs that are purely GABAergic. In contrast blocking GlyRs did not reduce sIPSC frequency, but did significantly reduce sIPSC amplitudes suggesting that the glycinergic component of sIPSCs was not independent of GABA release. Kinetic analysis of sIPSCs were consistent with a co-release model of GABA and glycine. First, if GABA and glycine were released in separate vesicles, one would predict a bimodal distribution of sIPSC decay kinetics reflecting each of the two putative sources of input. Instead I observed that sIPSCs in the control condition had a continuous distribution of τ_{decay} values. Second, sIPSC amplitude decreased significantly in both drug conditions consistent with GABA and glycine co-release. Finally, the control condition was the only condition where I saw very large

(>400pA) events (Fig 3.2A). I hypothesize that these larger events, which tended to have fast kinetics (data not shown), are the result of summation of co-released transmitters.

Role of Co-release in the Avian Brainstem

Co-release of GABA and glycine has been demonstrated at many synapses in the brain (Jonas et al. 1998, Tanaka and Ezure 2004, Dugué et al. 2005, Wojcik et al. 2006, Lu et al. 2008). Kuo et al., (2009) reported co-immunolocalization of GABA and glycine in NA, NM and NL, however, physiological recording of glycinergic transmission was only observed in the NA. Burger et al. (2005a) showed that many inhibitory terminals across NA, NM, and NL arise from collateral branches of single SON neurons. In the present study, I observed GlyR staining in the SON as well as mixed GABA/glycinergic synaptic transmission *in vitro*. In the mammalian auditory brainstem circuit one source of inhibitory input, the medial nucleus of the trapezoid body, is known to co-release GABA, glycine and glutamate from terminals innervating the lateral superior olive early in development (Gillespie et al. 2005). Release from MNTB terminals shifts to primarily glycinergic output following hearing onset (Kandler and Friauf 1995, Kotak et al. 1998, Kim and Kandler 2003, Nabekura et al. 2004, Gillespie et al. 2005). Our data suggest that co-release in the SON is not likely due to developmental processes since I observed the physiological and anatomical hallmarks of co-release in animals up to P23. Hearing onset is around E11 in chickens, and the auditory system is considered mature before hatching (by E18 for review see: Rubel and Fritzsche 2002). However, a comprehensive developmental study will be required to completely rule out further developmental changes that may occur throughout maturation.

While the source of the GABA/glycine co-release terminals remains unknown, an appealing hypothesis is that SON neurons are providing both GABA and glycine to their targets. Co-immunostaining for GABA and glycine was observed in NM, NA, and NL (Kuo et al. 2009), and the SON is known to provide the dominant inhibition to these targets. However, at present, it appears that the mode of inhibition in those targets is determined by the complement of receptors expressed by the postsynaptic cells. A similar multi-target co-release arrangement has been described in a mammalian hindbrain circuit (Dugué et al. 2005). This arrangement seems plausible in the avian auditory brainstem where the primary source of inhibition (SON) provides input to both nuclei that process timing information and areas involved in intensity processing (Takahashi and Konishi 1988). The kinetically slow GABAergic input to NM and NL has been shown to improve temporal selectivity and coincidence detection (Funabiki et al. 1998, Yang et al. 1999, Monsivais et al. 2000, Fukui et al. 2010). The functional significance of GABA/glycine co-release within the SON is at present unknown. The *in vivo* experiments performed in this study demonstrated that GABAergic and glycinergic inhibitory inputs modulated the response properties of SON neurons similarly. The sIPSC analysis strongly suggests that SON neurons receive mixed inhibitory inputs composed of both co-release and purely GABAergic terminals. The possibility for diverse functional roles for this complement of inhibitory circuitry in the avian auditory brainstem should be investigated in future studies.

CHAPTER IV

**Slowly emerging glycinergic transmission enhances
inhibition in the temporal processing pathway
of the avian auditory system**

Abstract

Glycinergic synaptic transmission is a prominent modulator in the mammalian sound localization circuit, for neurons specialized to encode temporal information. However, hallmarks of glycinergic signaling have been absent or rarely observed in studies of analogous neurons in birds. Previous physiological studies of these neurons indicate that GABA antagonist application completely blocks inhibition. Further, spontaneous or evoked glycinergic currents have not been observed. However, recent studies have shown that, glycine is indeed co-released with GABA in the auditory nuclei that are not generally associated with the temporal processing pathway, and that glycine can be immunohistochemically detected at terminals in all nuclei including those specialized for temporal processing; nucleus magnocellularis (NM) and nucleus laminaris (NL) (Kuo et al., 2009; Coleman et al., 2011). Here, I show immunohistochemical evidence of glycine receptor (GlyR) expression in NM and NL. Using whole-cell recordings in acute slices I demonstrate that exogenous glycine application evokes strychnine sensitive currents in NM and NL. Additionally, I show that synaptic stimulation at high but physiologically relevant frequencies evokes a slowly emerging glycinergic response in NM that increases in amplitude over the course of the stimulus. The glycinergic component represented approximately 30% of the inhibitory potential at the end of the 50-pulse stimulus. Further, I show that glycine transmission is computationally relevant for these neurons as its elimination results in reduced inhibitory efficacy for suppression of discharges evoked by current injection into NM neurons.

Introduction

Animals use differences in the arrival time of sound at each ear, or interaural time disparities (ITDs), to compute the location of low frequency sound sources. In vertebrates, ITDs are computed by binaural coincidence detecting neurons in the brainstem. Coincidence detecting neurons reside in nucleus laminaris (NL) in birds (Parks and Rubel, 1975; Sullivan and Konishi, 1986; Carr and Konishi, 1990; Pena et al., 1996; Burger et al., 2011) and in the medial superior olive (MSO) in mammals (Goldberg and Brown, 1969; Yin and Chan, 1990).

Inhibitory synaptic transmission is a key feature of sound localization circuitry, contributing to temporal precision over a broad range of sound intensities. In mammals, precisely timed feed-forward glycinergic input from the medial nucleus of the trapezoid body (MNTB) modulates the ITD selectivity of MSO neurons (Brand et al., 2002; Pecka et al., 2008). Until recently, investigation of avian systems has focused on slow, depolarizing feedback GABAergic inhibition from the superior olivary nucleus (SON) to its targets in the brainstem (Hyson et al., 1995; Yang et al., 1999; Monsivais et al., 2000; Monsivais and Rubel, 2001; Yamada et al., 2013), while observations of glycinergic transmission in these nuclei have been few and limited by several factors. For example, previous studies have shown that glycine immunoreactivity is sparse in NM and NL (Code and Rubel, 1989). Further, whole-cell recordings in these nuclei have indicated that both spontaneous and evoked inhibitory synaptic currents were completely blocked by application of GABA_A receptor antagonists (Funabiki et al., 1998; Yang et al., 1999; Monsivais et al., 2000; Lu and Trussell, 2000). Recent work has revealed glycinergic

transmission in other nuclei of this circuit in birds. Inhibitory input to the nucleus angularis (NA) (Kuo et al., 2009) and SON (Coleman et al., 2011) is marked by co-release of GABA and glycine at some synapses. These studies further showed that GABA and glycine co-localize in the terminals that synapse onto NA and SON neurons, but paradoxically also on neurons in NM and NL where glycinergic transmission was not observed electrophysiologically (Kuo et al., 2009; Coleman et al., 2011). Co-release of transmitter is long known to occur in developing synapses (Gillespie et al. 2005; Awatramani et al. 2005) but recently has been demonstrated in mature neurons (Kuo et al., 2009; Coleman et al., 2011). Recent work in the mammalian cochlear nucleus, where glycine is the dominant inhibitory transmitter, has shown GABA co-release when synapses are stimulated at high frequencies (Nerlich and Milenkovic, personal communication).

Here I report expression of GlyRs in all principal nuclei of the mature avian ITD computing circuit. Physiological tests show that these GlyRs are functional in NM and NL where glycinergic transmission has not been previously observed. Further, I demonstrate release of synaptically evoked glycine in response to long duration, high frequency stimulation in NM. Finally, I show that this glycinergic component contributes to the efficacy of inhibition in NM during high frequency stimulation.

Co-release of transmitter is long known to occur in developing synapses (Gillespie et al. 2005, Awatramani et al. 2005), but recently has been shown in mature neurons (Kuo et al. 2009, Coleman et al. 2011). Recent work in the mammalian cochlear nucleus, where glycine is the dominant inhibitory transmitter, has shown GABA co-

release when synapses are stimulated at high frequencies (Nerlich and Milenkovic, personal communication).

Here I show expression of GlyRs in all principal nuclei of the mature avian ITD computing circuit and that these GlyRs are functional in NM and NL where glycinergic transmission has not been previously observed. Further, I demonstrate release of synaptically evoked glycine in response to long duration, high frequency stimulation in NM. Finally, I show that the glycinergic component contributes to the efficacy of inhibition in NM during high frequency stimulation.

Methods

All procedures were approved by the Lehigh University Animal Care and Use Committee.

Immunohistochemistry

Immunohistochemical staining for GlyR followed protocols described in Coleman et al., (2011). Briefly, four P5 chickens were deeply anesthetized and transcardially perfused with PBS followed by 4% PFA in PBS, pH 7.4. Brains were removed and postfixed in 4% PFA overnight at 4°C. Brains were rinsed and blocked, then sectioned at 30 µm (HM650V, Microm). Sections were transferred to a solution (containing: 10mM sodium citrate; 0.05% Tween 20; pH 6.0) for antigen retrieval and maintained at 80°C in a water bath for 30 min. Sections were cooled to 27 °C, rinsed, then blocked in 10% normal goat serum for 1 hour. Sections were incubated overnight at 4°C in solution containing: 5% normal goat serum, anti-neurofilament (cat. # AB1987; 1:200, Millipore) and anti GlyR (cat#:146011, 1:1,000; Synaptic Systems). Sections were rinsed then incubated for 2h with secondary antibody conjugated to AlexaFluor 488 goat anti-mouse and AlexaFluor 633 goat anti-rabbit to label GlyR and Neurofilament, respectively (Invitrogen). Sections were mounted in Vectashield (Vector Laboratories) and confocal images were captured (LSM 510 Meta, Zeiss). Images were processed using Photoshop (Adobe Systems) to match pixel intensity distributions between color channels. No staining was observed when primary antibodies were absent or when GlyR antibody was preabsorbed with antigen peptide (Coleman et al., 2011).

Western blot analysis

Chicken lung, chicken brainstem, and gerbil brainstem tissue were homogenized in lysis buffer (10mM Tris-HCl pH 7.4, 0.32M sucrose, 5mM EDTA pH 8) supplemented with 0.1mM PMSF and complete EDTA-free protease inhibitor cocktail (Roche), mixed with an equal volume of 4% SDS, and sonicated. Membrane fractions were collected by centrifugation at 13,000 x g (4°C) for 20min with three washes in supplemented lysis buffer. Membranes were resuspended in modified RIPA buffer (25mM Tris pH 7.6, 150mM NaCl, 1% Triton X-100, 1% sodium deoxycholate, 1% SDS) supplemented with 1mM PMSF for 10min at room temperature and measured using the DC Protein Assay (Bio-Rad). 20µg of protein was separated by 10% reducing SDS-PAGE and then electrotransferred onto a 0.2µm PVDF membrane for Western analysis. Antibodies used: mouse anti-GlyR (1:500; Synaptic Systems, clone mAb4a); HRP-conjugated goat anti-mouse IgG (1:50,000; Promega). ECL-Plus (GE Healthcare) was used for chemiluminescent detection with Kodak BioMax film.

In vitro brain slice preparation:

For *in vitro* physiology, 42 white leghorn chickens aged E17-P5 were used. Brainstem slices were prepared and maintained as in Coleman et al., (2011).

In vitro whole-cell recordings:

Borosilicate capillary glass pipettes (1B120F-4, WPI) were pulled to a resistance of 4-8 MΩ using a two-stage puller (PC-10, Narishige) and back-filled with internal solution (for voltage clamp containing in mM: 105 CsMeSO₃, 35 KCl, 5 EGTA, 10 HEPES, 1 MgCl₂, 4 ATP-Mg, and 0.3 GTP-Na, pH 7.2 adjusted with KOH). In current

clamp experiments, CsMeSO₃ was exchanged for K-gluconate and CsCl for KCl. 5 mM QX314 was added to the internal solution to prevent antidromic spiking except during functional testing. These internal solutions yielded depolarizing inhibitory inputs observed in the avian brainstem. In voltage clamp, series resistance was compensated at 60-80% (Multiclamp 700B, Molecular Devices). The signal was digitized with a Digidata 1440 data acquisition board and recorded using Clampex software (Molecular Devices).

Inhibitory inputs were pharmacologically isolated in ACSF containing 6,7-dinitroquinoxaline-2,3-dione (DNQX) (40 μ M) and D-2-amino-5-phosphonopentanoic acid (AP5) (50 μ M) to block AMPA and NMDA receptors. GlyRs were blocked using strychnine (0.5-1 μ M). GABA_A receptors (GABA_ARs) were blocked using SR95531 (20 μ M). GABA_BRs were blocked with CGP55845 (2 μ M) during high frequency stimulation protocols. Pharmacological agents were supplied from Tocris except where indicated.

GlyR activation via pressure application of glycine

Pipettes for pressure application of glycine were pulled to a resistance of \sim 1M Ω and placed within 50 μ m of the neuron soma. 100ms glycine (Sigma) (0.5-1mM in ACSF containing DNQX and AP5) puffs were applied using \sim 2.5psi pressure injection (PLI 100A, Warner Instruments).

Synaptic activity in NM

Inhibitory postsynaptic potentials or currents were evoked with 50 μ sec stimulus pulses with a stimulus isolation unit (Isoflex, A.M.P.I. Inc.) through a concentric bipolar

electrode (TM53CCINS, WPI) placed to the ventrolateral perimeter of NM. Stimulus magnitude (range 10-90V) was gradually increased until amplitudes stabilized at their maximum. Stimulation protocols ranged from single events to trains of 50 pulses at frequencies of 200 and 333Hz. For 50-pulse trains, the glycinergic component was analyzed on a pulse-by-pulse basis where the average amplitude at each pulse was compared to control and GABA_AR block conditions. The average residual component remaining during block of both GABA_ARs and GlyRs was subtracted from each condition before comparisons were made.

Functional testing of glycinergic component

The functional test for glycinergic efficacy consisted of suprathreshold current injection trains (duration 0.5-0.6ms ranging from 950-1350pA) at 50 Hz for 50 pulses. During this train, synaptic inhibitory input was evoked at 200 Hz for 40 pulses (200ms) using a bipolar tungsten electrode. Spike probability was calculated and compared between control and strychnine conditions during the 250ms period initiated at the first pulse of inhibitory stimulation.

Results

GlyR immunohistochemistry in the auditory brainstem

Previous work has documented the existence of glycine immunopositive synaptic terminals apposed to neurons in several avian auditory nuclei, including NM and NL (Code & Rubel, 1989; Kuo et al., 2009; Coleman et al., 2011). These results were paradoxical considering glycine transmission has not been physiologically confirmed in NM and NL. However, other studies have shown postsynaptic responses from multi-transmitter releasing terminals is determined solely by the complement of receptors expressed by the postsynaptic neuron (Dugue et al., 2005). To resolve whether glycine signaling is indeed present in ITD processing nuclei, I investigated expression of GlyR in NM and NL (Fig. 1). GlyR immunoreactivity was robust in NM and NL (Fig. 1A-C) where subcellular staining appeared punctate and was absent from the nucleus. GlyR staining confirmed reports of glycinergic synaptic transmission in NA and SON (Kuo et al., 2009; Coleman et al., 2011) (Fig. 1D). Antibody specificity was confirmed using Western analysis (Fig. 1F) and antigen preabsorption (Coleman et al., 2011).

Exogenous glycine application evokes strychnine sensitive currents in NM and NL

Our immunohistochemical evidence suggested that GlyRs are expressed in NM and NL, nuclei specialized to process temporal features of sound. Since glycinergic transmission has never been observed in these nuclei, I tested whether glycinergic responses could be observed during exogenous glycine application. 100ms glycine puffs were applied to neurons in NM, NL and SON in the presence of glutamate and GABA receptor antagonists. Application of glycine evoked inward current that was almost

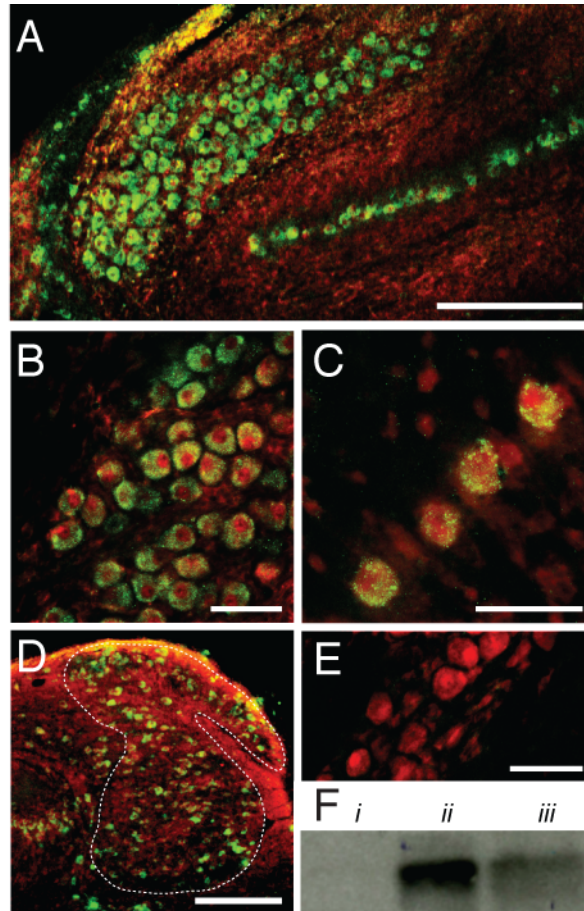


Figure 4.1: Glycine receptors are expressed in all four auditory brainstem nuclei. A. Low magnification confocal image of timing nuclei (NM, *left* and NL, *right*) neurons labeled for GlyR (green) and neurofilament (red). B. GlyR staining in the NM is robust in the somatic region. C. NL neurons are also immunopositive for GlyRs. D. Low magnification image of NA shows many neurons with GlyR staining. E. Image of NM neurons shows no GlyR staining when the primary antibody was omitted. F. Western blot analysis of GlyR antibody specificity shows no band in the chicken lung tissue (negative control, *Fi*) and bands in both gerbil (positive control, *Fii*) and chick brainstem (*Fiii*) tissues. Scale bars: A,D = 200 μm ; B,C,E = 50 μm .

entirely abolished during bath application of strychnine (0.5-1 μ M), a GlyR antagonist. Figure 2A shows the glycine response in control, strychnine, and washout conditions for an E19 NM neuron. Similar responses were observed for all neurons tested in the three nuclei (Fig. 2B) and were consistent across the age range (E18-P5). Kuo et al., (2009) demonstrated similar results for NA. Taken together with the immunohistochemical results, these data indicate that functional GlyRs exist in all four brainstem nuclei at ages considered mature for the chick auditory system.

High frequency stimulation evokes glycine release in NM

A number of studies have indicated that inhibitory transmission in the NM and NL are completely blocked by GABA_AR antagonists (Funabiki et al., 1998; Yang et al., 1999; Monsivais et al., 2000; Lu and Trussell, 2000). Indeed, I too saw little evidence of glycinergic activity in spontaneous events or responses evoked by single-pulse stimuli in current (Fig. 3A-B) or voltage clamp (not shown). However, few published studies of NM have evoked inhibitory synaptic transmission at stimulation rates approaching the highest acoustically driven rates observed *in vivo* for SON neurons. Previous work from our group suggests that SON neurons can reach spike rates exceeding 200Hz during intense acoustic stimulation (Coleman et al., 2011). Thus, I tested whether prolonged high frequency stimulation could evoke glycine release in the NM. Our protocol consisted of 50-pulse stimulus trains at 200 and 333Hz during whole cell recordings in voltage or current clamp. Figure 3C shows averaged IPSP traces from a representative NM neuron stimulated at 200Hz in each pharmacological condition. The GABA_AR antagonist SR95531 reduced but did not eliminate the evoked IPSP. The residual IPSP

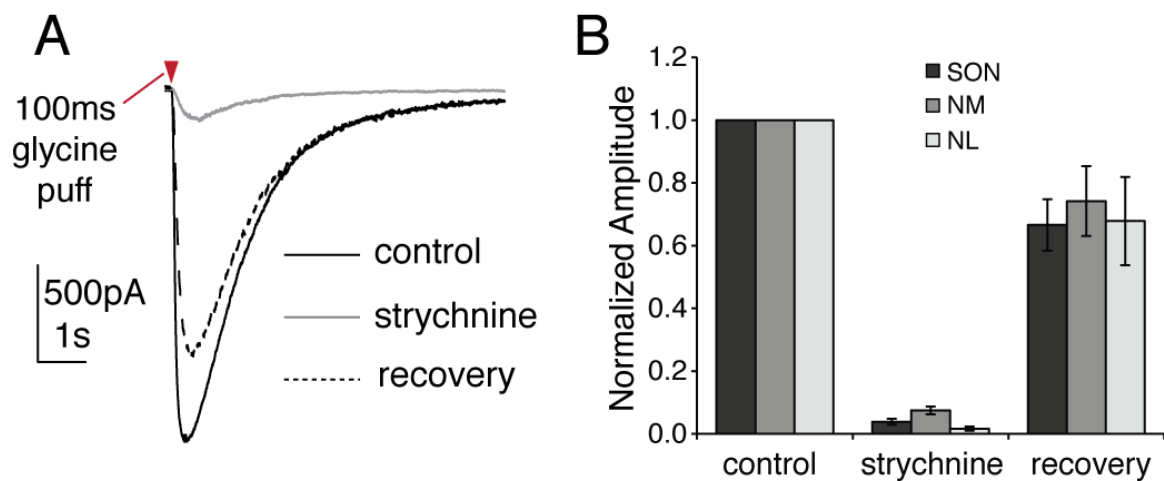


Figure 4.2: Exogenous glycine application evokes strychnine sensitive currents in the SON, NM and NL. A. Representative traces from an E19 NM neuron show the current response from a 100ms puff of glycine (1mM) onto the cell soma in control, strychnine and recovery conditions. B. Population data from the 100ms glycine puff reveals a similar trend during GlyR block and washout in the three brainstem nuclei tested.

appeared to accumulate over the course of the stimulus and reached approximately 30% of the control IPSP by pulse 50 (200Hz: $30.7 \pm 7.9\%$, n=4; 333Hz: $27.5 \pm 7.2\%$, n=4; Fig. 3D). This component was eliminated with the addition of 0.5mM strychnine and recovered after washout (Fig. 3C). IPSP amplitude recovered near control levels after SR95531 washout.

Evoked IPSCs followed a similar response pattern in voltage clamp. Again, application of SR95531 resulted in an incomplete suppression of the IPSC and the residual component was nearly abolished after the addition of strychnine. The glycinergic current was greatest at pulse 50 and represented ~15% of the control current at both 200 and 333Hz stimulus frequencies (200Hz: $14.5 \pm 1.8\%$, n=7; 333Hz: $14.4 \pm 3.5\%$, n=7). These results suggest that glycine contributes to inhibition in NM under high but physiologically relevant firing rates observed *in vivo* for SON neurons.

GlyR block reduces the efficacy of inhibition in NM

To test the functional efficacy of glycinergic input to NM, I used a protocol similar to Monsivais et al., (2000) (see Methods) where 50 Hz suprathreshold current pulse trains were injected into NM neurons to evoke spiking while inhibitory fibers were simultaneously stimulated during a 200 ms window (40 pulses at 200Hz) (Fig 4A,B). Representative traces are shown in Figure 4A for an NM neuron in each condition. Activation of inhibitory inputs in the control condition generally reduced spiking by at least 40% during the 250ms following the onset of evoked inhibition (see Methods). Strychnine application lead to a significant increase in firing rate during inhibitory input activation (control: $22.3 \pm 5.9\%$; strychnine $53.9 \pm 13.3\%$; n=4, p = 0.036; Fig 4B).

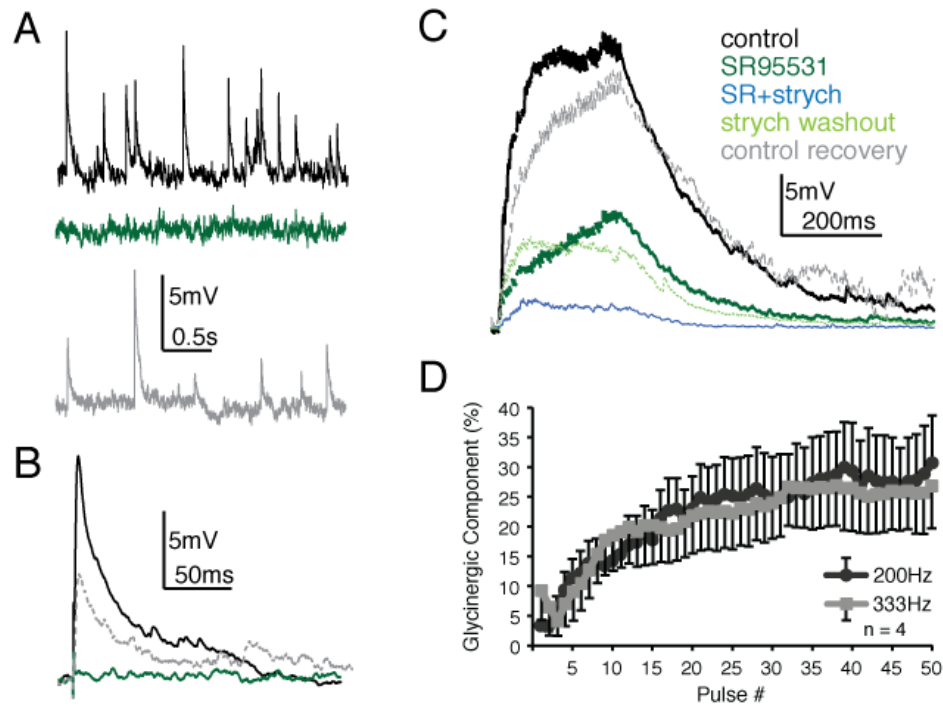


Figure 4.3: High frequency stimulation evokes glycinergic transmission in NM. A. Traces show miniature IPSPs that are completely abolished during SR95531 application confirming purely GABAergic events. B. Overlay of averaged IPSP traces again confirm purely GABAergic events evoked during single pulse stimulation. C. Averaged traces of IPSPs evoked using a 200Hz, 50-pulse stimulus in each pharmacological condition. GABAAR block reduces the summed IPSP amplitude leaving a residual component that is eliminated by GlyR block. Color code for pharmacological condition is the same for A-C. D. Population data for the average magnitude of the glycinergic component analyzed pulse-by-pulse during the high frequency train stimuli. The glycinergic component was calculated by dividing the IPSP amplitude at pulse n in SR95531 by the IPSP amplitude at pulse n in control.

These results suggest that glycine release evoked under physiologically relevant stimulus conditions contributes to the overall efficacy of the inhibition, and modulates the excitability of NM neurons.

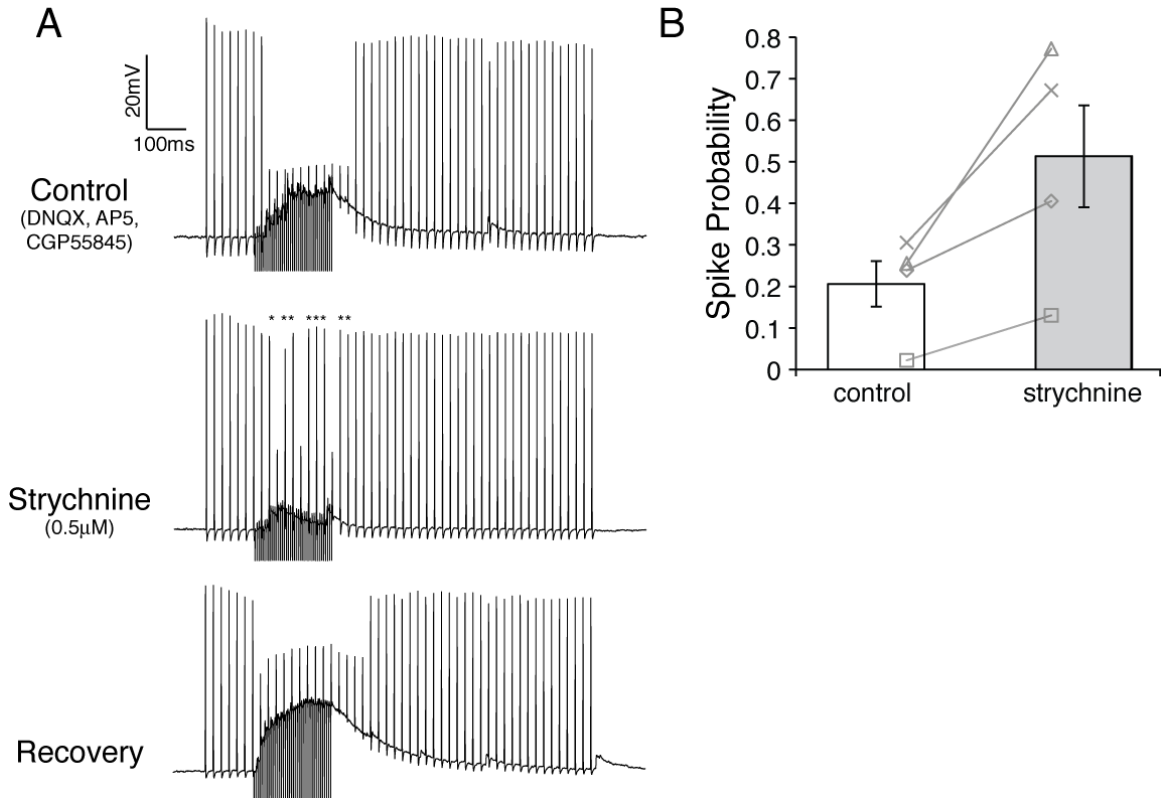


Figure 4.4: Blocking GlyRs decreases the ability of evoked IPSPs to suppress action potentials in NM. A. Representative current clamp traces from an E19 NM neuron in each pharmacological condition. Application of strychnine resulted in an increase in the firing rate during the inhibitory time window (asterisks in strychnine condition represent action potentials suppressed in the control). B. Population data for the spike probability during the inhibitory time window in control and strychnine conditions shows a significant increase in spike probability during strychnine application (n=4, p=0.035). Grey lines connect the spike probability at each condition for each cell tested.

Discussion

GlyR immunohistochemistry and receptor function

In this report, I show for the first time robust expression of GlyRs and evidence of synaptically evoked glycine release in nuclei specialized for temporal processing in the avian auditory system. Physiological evidence of glycine transmission in this circuit has only recently been documented (Kuo et al., 2009; Coleman et al., 2011). These studies demonstrated synaptically evoked GABA/glycine co-release in SON and NA. Together, these results indicate that anatomical pre- and postsynaptic hallmarks of glycinergic transmission observed in these nuclei are confirmed by electrophysiological evidence of glycinergic signaling in all nuclei of this circuit.

Glycinergic transmission in the brainstem

Previous studies suggested that glycinergic transmission accounts for approximately 50% of the amplitude of single-pulse evoked IPSCs in the NA and SON (Kuo et al., 2009; Coleman et al., 2011). In NM I confirmed previous results that glycine transmission is not evident from recordings of spontaneous release or release evoked by single-pulse stimuli. Rather, our results indicate that glycine transmission was only induced during high frequency stimulation. The glycinergic component built over the course of the response to comprise up to 30% of the total IPSP by the end of the train. Our protocols simulated high but physiologically relevant input frequencies, comparable to firing rates observed for SON neurons in response to intense acoustic stimuli *in vivo* (Coleman et al., 2011).

Role of glycine

Glycinergic transmission in NA and SON results from the co-release of GABA and glycine from inhibitory terminals. One function of glycine was described *in vivo* for SON where it aids in maintenance of phase-locking to acoustic stimuli (Coleman et al., 2011). The role of glycine in NM and NL has not yet been investigated *in vivo*. Given the results of the current study, I propose that glycinergic transmission would be recruited during intense stimulation when GABA release may be subject to synaptic depression (Lu et al., 2005). This hypothesis is plausible for several reasons. First, glycine and GABA are trafficked by the same vesicular transport protein, vesicular amino acid transporter (VIAAT *also known as VGAT*) (Wojcik et al., 2006). VIAAT has been localized at both GABA- and glycinergic terminals (Chaudhry et al., 1998; Dumoulin et al., 1999). Since terminals surrounding NM and NL neurons are immunopositive for both GABA and glycine, co-release is likely as has been shown in NA and SON (Kuo et al., 2009; Coleman et al., 2011). The fact that glycine is only released during high frequency stimulation may suggest that glycine is only recruited into vesicles by VIAAT when GABA is depleted in the terminal. Previous studies have demonstrated that transmitter transport into vesicles is concentration dependent. The relative abundance of GABA or glycine may suppress transport of the complimentary transmitter into vesicles (Burger, 1991). It was recently shown that glycinergic transmission can be suppressed, and GABA transmission potentiated via GLYT2 block or increase in GABA synthesis (respectively) in cartwheel cells that co-release GABA and glycine (Apostolides and Trussell, 2013). Thus, depletion of GABA during intense and prolonged inhibitory stimulation in NM may lead to the recruitment of glycine into vesicles to maintain the

inhibitory tone. Evidence for a similar mechanism has recently been observed in the mammalian cochlear nucleus where GABAergic transmission is recruited during high frequency stimulation of primarily glycinergic inputs to bushy cells (personal communication, Jana Nerlich and Ivan Milenkovic).

Source of glycine

The source of glycinergic terminals in NM and NL is unknown, but there are several candidates. The transmitter staining patterns of SON neuron somas suggests that high levels of both GABA and glycine are present in populations of these cells (Coleman et al., 2011). These neurons would seem to be the most likely glycine source, but it is odd that spontaneous glycine release occurs in NA and SON but not NM and NL, as these nuclei share SON collateral inputs (Burger et al., 2005). However, it is possible that different subsets of SON fibers project to subsets of target nuclei. Whether the GABA/glycine positive SON neurons are the population projecting to NM and NL is unresolved and requires further investigation.

Several studies have described the existence of a small population of cells between the NM and NL that are immunopositive for markers of GABA and glycine transmission (Müller, 1987; Carr et al., 1989; von Bartheld et al., 1989; Kuo et al. 2009). Yamada et al., (2013) showed that these neurons receive excitatory input from NM and provide inhibitory input to low frequency NL neurons. It is possible that glycine release was evoked from these cells in the current study. This is speculative, however, since the connectivity of these cells to areas other than NL is not fully characterized.

Summary

Our study demonstrates that functional GlyRs are expressed in four principal nuclei of the avian auditory brainstem and that glycinergic transmission is evoked in NM by high frequency stimulation. Importantly, the glycine was recruited at stimulus frequencies within the range of firing frequencies observed for SON neurons *in vivo*. Additionally, glycinergic transmission contributes to the efficacy of inhibition for suppression of spikes evoked by current injections into NM neurons. These findings indicate that glycinergic inhibition is more ubiquitous in the avian brainstem than previously understood, and that models of ITD processing in avian circuitry must incorporate glycinergic components of inhibition.

CHAPTER V

Glycinergic transmission modulates inhibition in the avian brainstem

Abstract

Co-transmission of several neurotransmitters from a single neuron is becoming increasingly prevalent as the physiology of many neuronal circuits is finely dissected. Recent studies have shown that glycine is co-released with GABA in avian auditory brainstem nuclei involved in the computation of interaural time disparities (ITDs), a cue used in sound localization processing (Kuo et al. 2009, Coleman et al. 2011). This circuit relies on inhibitory input to maintain the temporal precision necessary for ITD encoding. I utilize this circuit and perform *in vitro* whole-cell recordings to assess the consequences of glycine receptor (GlyR) activation on inhibitory transmission. To this end, I evaluated the effect of an exogenous glycine pre-pulse on synaptically evoked inhibitory currents in the nucleus magnocellularis (NM) and the superior olivary nucleus (SON). Activation of GlyRs reduced the amplitude of inhibitory postsynaptic currents evoked during a 100Hz train stimulus in both nuclei. This modulatory effect was blocked during application of strychnine and recovered after washout. Changes in the driving force of Cl⁻ ions was the likely cause of the observed occlusion as activation of GlyRs was insufficient to cause the occlusion and switching the direction of Cl⁻ ion flux resulted in an enhanced evoked IPSC amplitude. These results suggest that glycine transmission may provide a novel modulatory mechanism for inhibition in the sound localization pathway of birds.

Introduction

Inhibitory input plays an integral role in the maintenance of temporal precision in the avian sound localization circuit (Funabiki et al. 1998, Yang et al. 1999, Monsivais et al. 2000, Lu and Trussell 2000, Fukui et al. 2010). Recent work revealed a novel form of inhibition in this circuit that results from the co-release of GABA and glycine from the same vesicles (Kuo et al. 2009, Coleman et al. 2011). This mode of transmission occurs in some synapses at the nucleus angularis (NA) and superior olivary nucleus (SON) where GABA and glycine each account for approximately 50% of the total amplitude of evoked inhibitory postsynaptic currents (IPSCs). Glycine transmission was also observed in the nucleus magnocellularis (NM) where stimulation at high but physiologically relevant rates evoked a slowly emerging glycinergic component of the inhibition. This glycinergic component was functionally important as blocking glycine transmission reduced the efficacy of inhibition in the NM. An *in vivo* study showed that GlyR block reduced the ability of SON neurons to phase-lock to pure tone stimuli near best frequency. Beyond these two studies, the role of glycine and its co-release with GABA is not well understood in this circuit.

Co-release of GABA and glycine from the same vesicles is possible because they share a vesicular transport molecule (vesicular inhibitory amino acid transporter, VIAAT or VGAT) (Burger et al. 1991, McIntire et al. 1997, Sagne et al. 1997, Wojcik et al. 2006). The transmitters are loaded into the vesicles based on their concentration in the axon terminals, which is derived from the presence of synthesizing molecules and

membrane transporters (Eulenburg et al. 2005). Co-release of GABA and glycine is interesting from a postsynaptic point of view because both receptor channels transmit the chloride (Cl⁻) ion upon ligand binding.

In other systems where each mode of transmission is present, GABA and glycine receptors have been shown to interact. Several experiments indicate that there is a cross-suppressive effect when both receptors are activated simultaneously. Studies in spinal cord neurons of rat (Li et al. 2003) and frog (Kalinina et al. 2009) indicate an asymmetry of occlusion where activation of glycine receptors prior to GABAergic transmission yields a greater degree of suppression than the opposite condition (GABA preceding glycine). Other labs have suggested that these results are an artifact of alteration in driving force of Cl⁻ ions caused by changes in Cl⁻ ion concentration during receptor activation and ion flux (Karlsson et al. 2011).

I use the avian sound localization circuit to investigate how inhibitory synaptic transmission is affected by GlyR activation. I demonstrate that activation of GlyRs occludes synaptically evoked IPSCs in both NM and SON. By manipulating the driving force of Cl⁻ ions using voltage clamp protocols, I show that ligand binding and activation of GlyRs is not sufficient to induce suppression and that forcing Cl⁻ into the neuron during glycine application (thereby increasing the Cl⁻ driving force) results in an enhanced evoked response. These data indicate that activation of GlyRs during inhibitory transmission provides an additional level of modulation and tuning at synapses important in sound localization processing.

Methods

All protocols and procedures were approved by the Lehigh University Institutional Animal Care and Use Committee.

In vitro brain slice preparation:

Methods for slice preparation were identical to those in the previous two chapters (see Chapter 3 & 4 Methods).

In vitro whole-cell recordings

Patch pipettes were pulled from thick walled borosilicate glass capillary tubes (WPI 1B120F-4) to a resistance of 4-8 M Ω using a two-stage puller (Narishige PC-10, Tokyo, Japan) and back-filled with internal solution (containing in mM: 105 CsMeSO₃, 35 CsCl, 5 EGTA, 10 HEPES, 1 MgCl₂, 4 ATP-Mg, and 0.3 GTP-Na, pH 7.2 adjusted with KOH). 5 mM QX314 was added to the internal solution to prevent antidromic action potentials. In experiments where phosphatase 2B activity was blocked, cyclosporin A (0.5 – 1.5 μ M) was added to the internal solution. In voltage clamp, series resistance was compensated at 60-80%. Membrane voltage was clamped using a Multiclamp 700B amplifier. The signal was digitized with a Digidata 1440 data acquisition board and recorded using Clampex software (Molecular Devices, Sunnyvale, CA).

Effect of GlyR activation on IPSCs

Inhibitory transmission was pharmacologically isolated by using a control bath solution containing ACSF with 6,7-dinitroquinoxaline-2,3-dione (DNQX) (40 μ M) and

D-2-amino-5-phosphonopentanoic acid (AP5) (50 μ M) to block AMPA and NMDA glutamatergic transmission. Pipettes for pressure application of glycine were pulled to a resistance of \sim 1M Ω and were visually guided near (\sim 50 μ m) the surface of a patched cell. Glycine (500 μ M in ACSF containing DNQX and AP5) was applied using \sim 2.5psi pressure injection with a PLI 100A picoliter injector (Warner Instruments). Glycine was applied for a 10-second duration.

Synaptically evoked IPSCs were evoked with 50 μ sec stimulus pulses with a stimulus isolation unit (Isoflex, A.M.P.I. Inc., Israel) through a concentric bipolar electrode with tungsten core (WPI TM53CCINS, Sarasota, FL). For recordings in the NM, the stimulator was placed adjacent to the nuclei in a ventrolateral location and for the SON, a dorsomedial location was used. Presynaptic fibers were stimulated with pulse trains consisting of 15 pulses at 100Hz. Stimulus magnitude (range 10-90 V) was gradually increased until IPSC amplitudes stabilized at their maximum. The start of the 100Hz train began when the current response to the 10s glycine puff returned to baseline (usually within 5-8s in the long protocol). Peak amplitude during the train was used to compare treatment groups. In control, test (strychnine 1 μ M) and recovery, evoked responses were compared between the no glycine condition and the glycine pre-pulse condition using the equation:

$$1 - (\text{evoked amplitude with gly pre-pulse} / \text{evoked amplitude no gly}) \times 100\% = \% \text{ suppression}$$

This protocol and analysis was performed while holding the membrane voltage at three different potentials: -60mV, approximating V_{rest} (Figs 5.1 & 5.2); E_{Cl^-} , ranging from -25mV to -35mV (average: -28.3 ± 3.3 mV, $n=3$; derived empirically during the

experiment) (Fig 5.4A-E); and +20mV, to drive the flux of Cl⁻ ions into the neuron (Fig 5.4F-H).

The effect of GlyR activation on the amplitude of spontaneous IPSCs (sIPSCs) was also examined. A baseline amplitude of sIPSCs was acquired during a 15s interval prior to the application of glycine. After a 10s glycine pulse, the current was allowed to return to baseline and then the amplitude of sIPSCs was measured. sIPSC amplitude was obtained for each event using a search template in Clampfit. sIPSC amplitudes were averaged during 5s bins and compared to the pre-pulse average.

Results

GlyR transmission suppresses IPSC amplitude

The effect of glycine receptor activation on evoked IPSCs in the brainstem was evaluated by exogenous application of glycine paired with presynaptic fiber stimulation. The protocol consisted of a 10s pulse of glycine followed by a 15 pulse, 100Hz train of inhibitory presynaptic fiber stimulation via a bipolar tungsten electrode (Fig 5.1A depicts the protocol). I first performed this protocol on neurons from the SON where glycinergic transmission occurs at terminals that co-release GABA and glycine (Coleman et al. 2011). I compared the amplitude of the peak synaptically evoked IPSC with (Fig 5.1Bii) and without (Fig 5.1Bi) the glycine pre-pulse in control, strychnine and recovery conditions (example traces shown in Fig 5.1B). In the SON, a 10s glycine pre-pulse resulted in suppression levels of ~70% in the control and recovery conditions (control: $79.5 \pm 2.1\%$ suppression, $n=4$, $p=0.18$; recovery: $62.2 \pm 4.3\%$ suppression, $n=3$, $p=0.09$). The raw data averages for the evoked IPSC amplitudes are shown for each condition in Figure 5.1C. Note that in the strychnine condition the amplitude of the evoked IPSC is reduced due to the blockade of the glycinergic component present in the SON at this stimulation frequency. In every neuron tested, bath application of strychnine reduced the amount of suppression observed in the control condition ($8.4 \pm 14.3\%$ suppression, $n=4$, $p>0.05$ vs. no glycine condition, $p<0.01$ vs. control; Fig 5.1D).

In the NM, the results obtained using this protocol matched that of the neurons in the SON (Fig 5.2). The glycine pre-pulse significantly suppressed evoked IPSCs in the

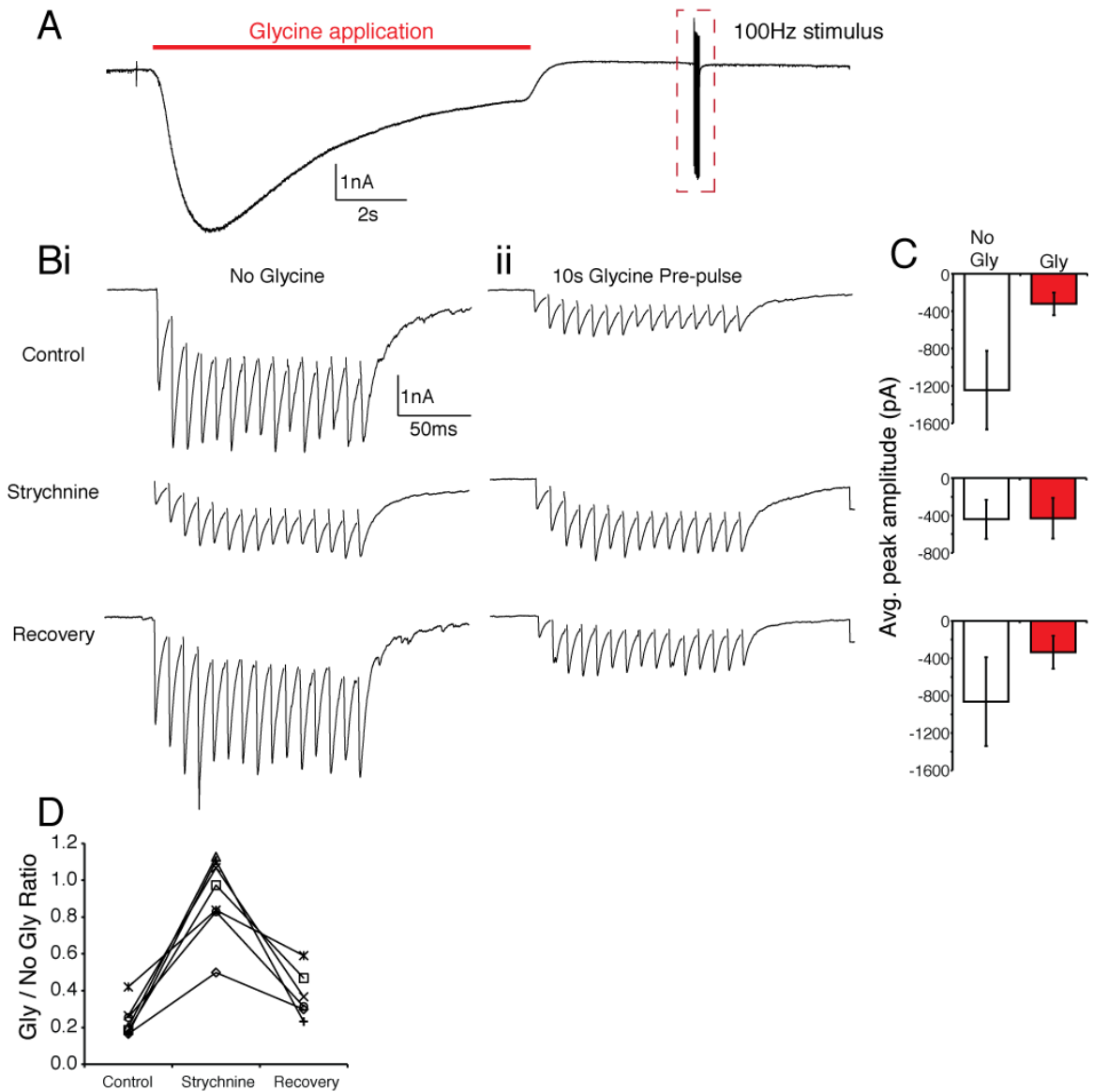


Figure 5.1: Pre-application of glycine suppresses evoked IPSC trains in the SON. A. Representative trace from an E18 SON neuron during the 10s glycine application. B. Expanded view of the dashed box in A showing evoked responses. Bi. Evoked responses in control, strychnine and recovery with no glycine pre-pulse. Bii. Evoked IPSCs after the glycine pre-pulse show amplitude suppression that is blocked by strychnine. C. Raw data values for the IPSC amplitudes in each condition. D. Ratio of evoked amplitudes between glycine pre-pulse and no glycine in each condition reveals a decrease in the suppression (ratio near 1) in strychnine.

NM, a result that was reduced by blockade of GlyRs with strychnine (control: $70.7 \pm 7.0\%$ suppression, $n=8$, $p<0.001$; strychnine: $26.4 \pm 8.9\%$ suppression, $n=7$, $p<0.05$ vs. no glycine condition, $p<0.001$ vs. control; recovery: $69.8 \pm 12.0\%$ suppression, $n=3$, $p=0.11$; Fig 5.2A & C). Representative traces are shown in Figure 5.2A. Raw data averages for IPSC peak amplitudes are shown in Figure 5.2B. These results suggest that activation of glycine receptors may occlude transmission through the GABA_A receptor channel.

We measured the effect of prolonged glycine application on sIPSC amplitude by comparing events pre- and post- glycine application (10s pulse). In the control condition, sIPSC amplitude was suppressed to $61.8 \pm 5.5\%$ of pre-pulse levels at 10 seconds after the pulse when the glycine currents had returned to baseline (Fig 5.3). sIPSC amplitude recovered to pre-pulse amplitude after approximately 35s. In strychnine, sIPSC amplitudes remained stable throughout the recording. After washout, sIPSC amplitude suppression during recovery mirrored that of the control condition ($64.0 \pm 6.0\%$ of pre-pulse levels).

Mechanism of suppression

In order to determine what mechanism was responsible for the observed suppression, I tested the hypotheses relating to findings from other systems. I first looked at the phosphorylation state of the receptors. Li et al. (2003) found that phosphatase 2B activity was involved in the suppression of currents through GABA_ARs by GlyR

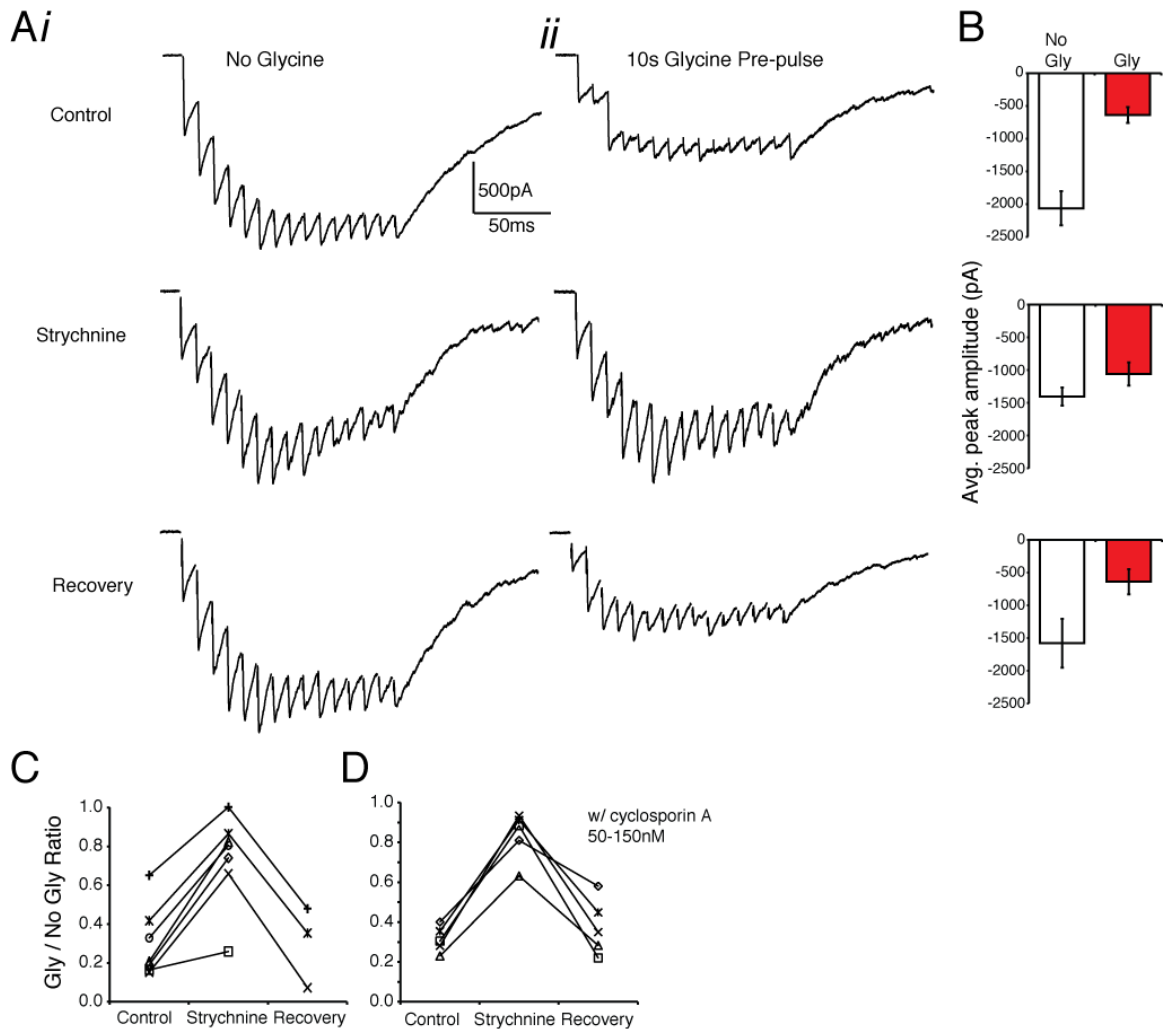


Figure 5.2: Evoked IPSCs are suppressed by glycine pre-pulse in NM. A. Representative traces from an E18 neuron showing evoked responses without glycine (Ai) and with glycine pre-pulse (Aii) in control, strychnine and recovery. B. Population data of peak amplitude comparing with vs. without glycine in each condition. C. Ratio of peak amplitude between Gly/no Gly in each condition shows an increased ratio (less suppression) during strychnine application. D. Same measurements as in C but with cyclosporin A included in the recording pipette to block phosphatase 2B activity. This manipulation yielded the same results indicating that phosphatase 2B activity does not play a role in the observed suppression.

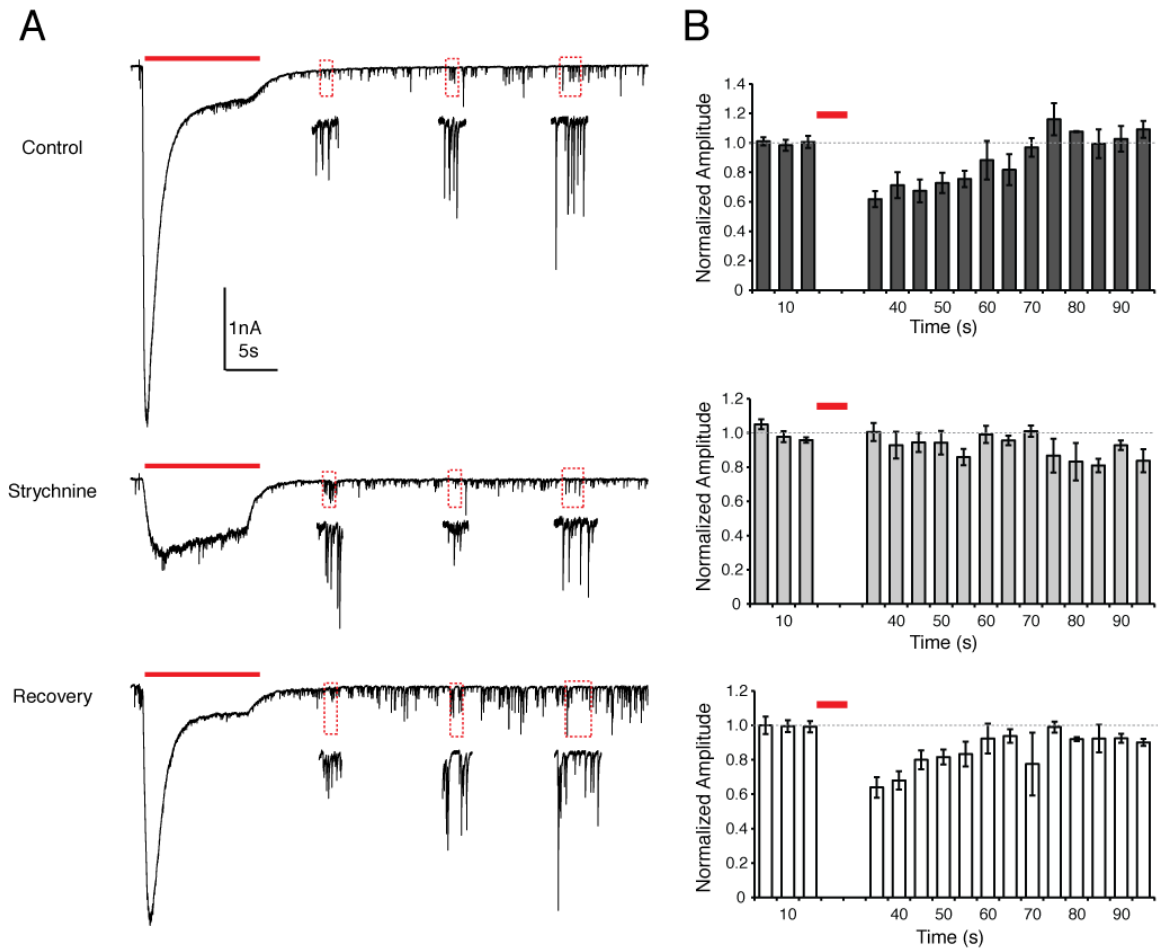


Figure 5.3: Suppression of mini IPSC amplitudes after glycine application is eliminated by strychnine. A. Representative traces from an E20 NM neuron showing miniature events recorded during a glycine puff protocol. Insets are expanded views of the minis in each dashed box which show a decrease in mini amplitude after the glycine pulse. This effect was not observed with strychnine application but recovered after washout. B. Histograms representing the normalized population data for the mIPSC amplitude analysis. Each bin represents the average mIPSC amplitude during a 5 second time window. In the control and recovery condition mIPSC amplitude recovered to baseline values after approximately 35 seconds.

activation in rat spinal cord neurons. Here, I included cyclosporin A in the recording pipette to block phosphatase 2B activity. There was no significant difference between the suppression observed with cyclosporin A when compared to the normal control ($68.4 \pm 2.9\%$, $n=5$, $p>0.05$, Fig 5.2D). Next, I aimed to determine if the suppression was a true biophysical interaction between the two receptors, or if the effect was a consequence of manipulation of driving force caused by changes in Cl⁻ ion concentration (as observed in Karlsson et al 2011). I determined whether ligand binding and receptor activation was sufficient to induce the suppression by stepping the voltage to the reversal potential of Cl⁻ during the application of glycine (protocol, Fig 5.4A; representative traces, Fig 5.4B & C; average IPSC amplitudes Fig 5.4D). I found that the suppression was greatly reduced when the flux of Cl⁻ was prevented ($4.3 \pm 6.9\%$ suppression, $n=3$, Fig 5.4E). Additionally, I employed a protocol where Cl⁻ ion flow would be in the inward direction to test whether evoked responses would be enhanced. Indeed, when the membrane voltage was held at +20mV during the glycine pulse, evoked IPSCs increased significantly (Fig 5.4F & G). These results implicate changes in the driving force of Cl⁻ ions as the mechanism of modulation for our protocols.

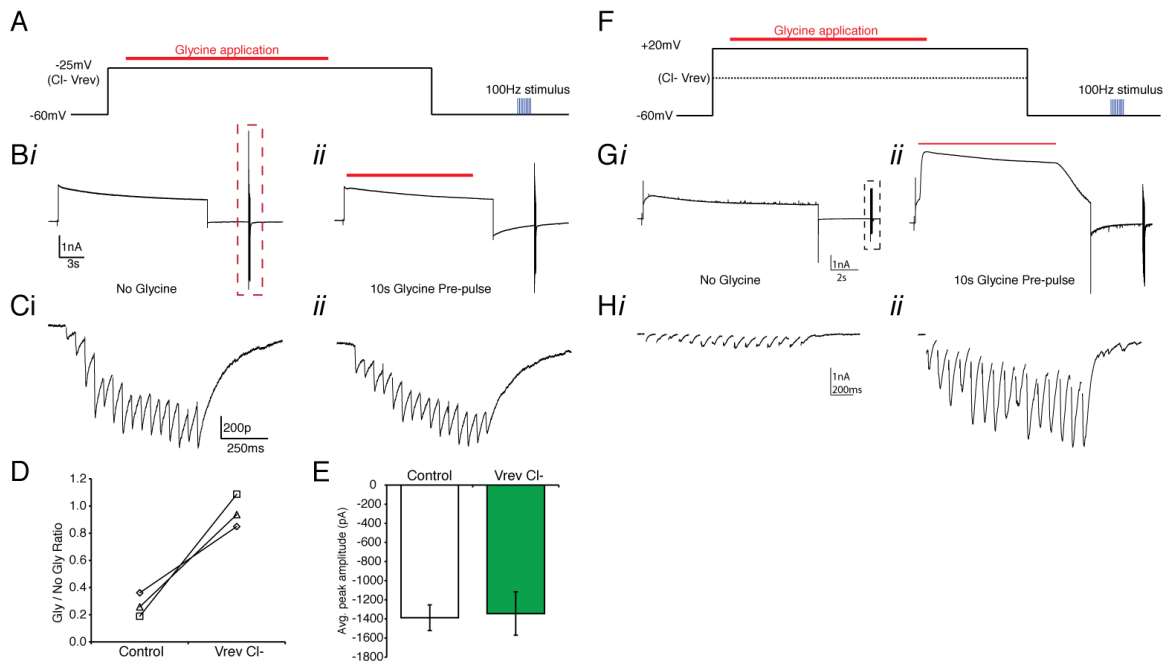


Figure 5.4: Manipulation of Cl⁻ ion flux alters the suppression profile of glycine prepulse in the NM. A. Schematic of recording protocol where Cl⁻ ion flux is minimized by clamping the membrane at the reversal potential for Cl⁻ during the glycine pulse. B. Current response from protocol in A without (B_i) and with (B_{ii}) glycine pulse (red line). Note the similarity between the traces in B_i and B_{ii}, suggesting minimal current due to glycine application. C. Expanded view of evoked current responses from the boxed region above. D. Average peak amplitude of the evoked current for the population of cells tested at Vrev Cl⁻. E. Ratio of peak amplitude between Gly/no Gly conditions in control and when glycine pre-pulse occurred at Vrev Cl⁻. Results were similar to glycine block (no suppression observed). F. Protocol for driving Cl⁻ into the neuron during glycine application. The membrane was clamped at +20mV. G. Current response from an NM cell during the protocol in F. H. Expanded view of evoked responses from G. H_{ii} shows the increase in evoked response after glycine application while holding at +20mV.

Discussion

Occlusion of GABA by GlyR activation

Our data show that preactivation of GlyRs suppressed the amplitude of synaptically evoked IPSCs in the NM and in the SON. GABA and glycine receptors both are permeable to Cl⁻ ions and interactions between the two receptors have been documented in areas where both receptor types are present and activated via presynaptic transmitter release. Several studies detail an occlusive effect that shows the amplitude of simultaneous application of GABA and glycine is less than the summed amplitude of the transmitters applied individually. Further, in some cases, pre-application of glycine occludes GABAergic currents to a greater degree than pre-application of GABA occludes glycinergic currents (Li et al. 2003). The proposed mechanisms that lead to the occlusion are diverse. A recent publication proposes that the occlusion is only an apparent cross-desensitization and that the reduction in current is not a reduction in channel conductance, but rather the result of changes in the Cl⁻ ionic concentration inside the cell (Karlsson et al. 2011). In our system, the changes in Cl⁻ ion concentration appeared to underlie the observed occlusion. I saw no suppression when Cl⁻ ion flux was prevented and driving Cl⁻ ion flux into the cell resulted in increased evoked IPSC amplitudes presumably due to increased driving force of Cl⁻. However, this does not adequately explain asymmetric cross-inhibition seen in other studies where they attribute the occlusion to the phosphorylation state of the receptors (Li et al. 2003). While I was unable to test the symmetry of the occlusion directly, I found that the signaling cascade involving phosphatase 2B was not the mechanism of the observed suppression.

Role of glycine in the avian brainstem

While a direct interaction between glycine and GABA receptors was not a conclusion of my study, the hypothesis that glycinergic activity in the brainstem shapes inhibitory transmission is still a viable one. Many studies in the avian sound localization circuit demonstrate modulatory mechanisms that dynamically alter inhibitory transmission. These mechanisms include activation of GABA_B receptors (Lu et al. 2005, Tang et al. 2009), metabotropic glutamate receptors (Lu 2007, Okuda et al. 2013) and cooperation of both tonic and phasic inhibition. Glycine receptor activation could have similar modulatory effects and the aforementioned mechanisms could also modulate glycine release.

Glycine transmission may impart changes in the kinetics of IPSCs. Postsynaptic activation of GlyRs and Cl⁻ flux would likely affect Cl⁻ concentration around the plasma membrane. Local changes in Cl⁻ ion concentration around GABA and glycine receptor channel pores can modulate the timing and voltage gating of currents (Moroni et al. 2011). In our system, the nuclei that have both GABA- and glycinergic components have IPSCs with faster kinetics. This may be relevant for providing phasic inhibition to targets, as many SON neurons were observed to phase-lock to auditory stimuli *in vivo* (Coleman et al. 2011).

Glycine activity will also affect neurons differently depending on the physiology of the target cell. Physiological heterogeneity is a characteristic of neuron in both the NA and SON. In the NA, the reversal potential for Cl⁻ (E_{Cl^-}), is neuron specific such that some neurons were found to have depolarized E_{Cl^-} , and some hyperpolarized E_{Cl^-} . (Kuo et

al. 2009). This means that the polarity of glycinergic transmission will be opposite in these groups and therefore the resulting effect will also be diverse. The E_{Cl^-} of SON neurons has not been thoroughly characterized as yet. One study using gramicidin perforated patch recordings observed an average E_{Cl^-} of -61mV from data collected in three neurons. Given the heterogeneity of response properties observed in the SON (Carr et al. 1989, Lachica et al. 1994, Coleman et al. 2011) a more thorough examination of E_{Cl^-} seems necessary.

Summary

In this report, the possible consequences of co-activation of GABA and glycine receptors on inhibitory transmission was explored. Pre-activation of GlyRs occludes evoked inhibitory transmission in the NM and SON in the avian brainstem. This occlusion was blocked when GlyRs were antagonized during glycine application. The flow of Cl^- ions out of the neuron was required for occlusion suggesting that changes in Cl^- ion concentration decreased the driving force for Cl^- resulting in less evoked current. The interplay between GABA and glycine receptors may provide an additional mechanism for fine-tuning inhibition in the avian sound localization circuit.

CHAPTER VI

Summary and Concluding Remarks

This work compares modulatory mechanisms involved in inhibitory transmission at several levels of sound localization circuits. In both the mammalian and avian circuit, modulation of inputs is critically important for the computational tasks performed and inhibition is integral.

In the mammalian system I showed that GABA_B activation provides a mechanism for gain control of inputs to coincidence-detecting neurons in the medial superior olive (MSO). I described that both excitatory and inhibitory synaptic current amplitudes are suppressed during GABA_B receptor activation. This suppression leads to a decrease in the short-term depression of these inputs as well. Also, the decay kinetics of inhibitory currents are prolonged.

In a functional test that simulated the excitatory bilateral input to the MSO, manipulation of GABA_BRs resulted in a bidirectional effect. MSO neurons had increased sensitivity to simulated interaural time disparities (sITDs) during activation of GABA_BRs and decreased sensitivity during block, suggesting that there was some endogenous GABA_BR activity evoked during our protocols.

We used a computational model to observe each GABA_BR related effect individually and in combination and I found that each effect independently increased the sensitivity of neurons to ITDs. Additionally several of the effects were cooperative. The model also showed that GABA_B dependent signaling functioned most optimally when it was positively correlated to sound intensity such that it would not be active with very low intensity inputs, but would be recruited during high intensity input.

In the avian system I described the physiology of glycinergic transmission. I demonstrated that glycine was a component of spontaneous and evoked inhibitory currents in all of the superior olivary nucleus (SON) neurons tested. The analysis of the frequency and kinetics of spontaneous events during pharmacology suggests an input arrangement where SON neurons receive some purely GABAergic inputs and some inputs that co-release GABA and glycine. Co-immunolabeling of the somas in some SON neurons for GABA and glycine provides evidence that the SON is the likely source of the co-labeled terminals seen in the avian brainstem.

The transmitter and receptor staining combined with the exogenous glycine application experiments demonstrated that glycine transmitter and functional receptors are found in each of the four avian brainstem nuclei. This result was perplexing given the findings from previous studies, which describe inhibition at the nucleus magnocellularis (NM) and nucleus laminaris (NL) as solely GABAergic. I therefore explore inhibitory transmission at the NM using physiologically relevant stimulation frequencies near the maxima of observed firing rates of the SON ($\geq 200\text{Hz}$, Coleman et al. 2011). At these rates I documented for the first time that glycinergic transmission is evoked by strong stimulation in the NM. The glycinergic response emerged over the duration of the stimulus, peaking at the last (50th) pulse. I expanded on this finding by showing that the glycinergic component was functionally relevant as the efficiency of inhibition was reduced when glycine receptors were blocked.

In the last group of experiments I described how co-activation of the GABA and glycine receptor systems could modify transmission. I determined that prolonged transmission through GlyRs suppressed the amplitude of evoked inhibition in the NM and

SON. This observation presents yet another possible mechanism by which inhibitory inputs can be regulated and fine tuned to optimize circuit function.

The research in this dissertation provides a comparative look at the role of inhibition in sound localization. In the mammalian model I demonstrate that gain control can be achieved by activation of GABA_B receptors. Gain control has been described in models and other systems (e.g. avians) as an integral part of maintaining ITD selectivity. In the avian system I expand on the recent discovery of glycine in the ITD circuit. This work shows for the first time that glycine transmission is an important feature of the timing circuit in the avian brainstem. Expanding on the role of glycine in this network necessitate substantial revision of the current models of inhibition in the avian brainstem and will be an exciting new avenue for research.

This work has provided a revised view of these circuits. Although the strategies for sound localization are different for these two model systems, there are many similarities. Here, I support the idea that one mode of transmission dominates the activity in each system, glycine in mammals, GABA in birds. But, interestingly the complementary mode plays a role in maintaining the circuit, GABA via GABA_BR activation in mammals, and glycine via recruitment during intense input. This complementary inhibitory activity is a remarkable consequence of the evolution constraints brought on by the extreme temporal precision necessary for sound localization processing.

References

- Apostolides PF, Trussell LO (2013). Rapid, activity-Independent turnover of vesicular transmitter content at a mixed glycine/GABA synapse. *J Neurosci*. 2013 Mar 13;33(11):4768-81.
- Awatramani GB, Turecek R, Trussell LO (2005). Staggered development of GABAergic and glycinergic transmission in the MNTB. *J Neurophysiol* 93:819–828.
- Backoff PM, Shadduck Palombi P and Caspary DM (1999). Gamma-aminobutyric acidergic and glycinergic inputs shape coding of amplitude modulation in the chinchilla cochlear nucleus. *Hear Res* 134: 1-2: 77-88.
- Beckius GE, Batra R, Oliver DL (1999). Axons from anteroventral cochlear nucleus that terminate in medial superior olive of cat: observations related to delay lines. *J Neurosci* 19: 3146–3161.
- Brand A, Behrend O, Marquardt T, McAlpine D, Grothe B (2002). Precise inhibition is essential for microsecond interaural time difference coding. *Nature* 417, 543-7.
- Brenowitz S, David J, Trussell, L (1998). Enhancement of synaptic efficacy by presynaptic GABA(B) receptors. *Neuron* 20, 135-41.
- Brückner S, Hyson RL (1998). Effect of GABA on the processing of interaural time differences in nucleus laminaris neurons in the chick. *Eur J Neurosci*. Nov; 10(11):3438-50.
- Burger PM, Hell J, Mehl E, Krasel C, Lottspeich F, Jahn R (1991). GABA and glycine in synaptic vesicles: storage and transport characteristics. *Neuron* 7:287–293.
- Burger RM, Cramer KS, Pfeiffer JD, Rubel EW (2005a). Avian superior olivary nucleus provides divergent inhibitory input to parallel auditory pathways. *J Comp Neurol* 481, 6-18.
- Burger RM, Pfeiffer JD, Westrum LE, Bernard A, Rubel EW (2005b). Expression of GABAB receptor in the avian auditory brainstem: ontogeny, afferent deprivation, and ultrastructure. *J Comp Neurol* 489: 11–22.
- Burger RM, Fukui I, Ohmori H, Rubel EW (2011) Inhibition in the balance: binaurally coupled inhibitory feedback in sound localization circuitry. *J Neurophysiol*. Jul;106(1):4-14.
- Cant NB, Casseday JH (1986). Projections from the anteroventral cochlear nucleus to the lateral and medial superior olivary nuclei. *J Comp Neurol* 247:457– 476.

- Cant NB, Hyson RL (1992). Projections from the lateral nucleus of the trapezoid body to the medial superior olivary nucleus in the gerbil. *Hear Res* 58, 26-34.
- Carr CE, Fujita I, Konishi M (1989). Distribution of GABAergic neurons and terminals in the auditory system of the barn owl. *J Comp Neurol* 286:190–207.
- Carr CE, Konishi M (1990). A circuit for detection of interaural time differences in the brain stem of the barn owl. *J Neurosci* 10:3227-46.
- Köppl C, Carr CE (1997). Low-frequency pathway in the barn owl's auditory brainstem. *J Comp Neurol*. Feb 10; 378(2):265-82.
- Caspary DM, Backoff PM, Finlayson PG, Palombi PS (1994) Inhibitory inputs modulate discharge rate within frequency receptive fields of anteroventral cochlear nucleus neurons. *J Neurophysiol* 72:2124–2133.
- Chaudhry FA, Reimer RJ, Bellocchio EE, Danbolt NC, Osen KK, Edwards RH, Storm-Mathisen J (1998). The vesicular GABA transporter, VGAT, localizes to synaptic vesicles in sets of glycinergic as well as GABAergic neurons. *J Neurosci*. Dec 1;18(23):9733-50.
- Chirila FV, Rowland KC, Thompson JM, Spirou GA (2007). Development of gerbil medial superior olive: integration of temporally delayed excitation and inhibition at physiological temperature. *J Physiol (Lond)* 584, 167-90.
- Clack JA (1997). The evolution of tetrapod ears and the fossil record. *Brain Behav Evol* 50:198 -212.
- Clack JA (2002). Patterns and processes in the early evolution of the tetrapod ear. *J Neurobiol* 53: 251–264.
- Code RA, Churchill L (1991). GABA_A receptors in auditory brainstem nuclei of the chick during development and after cochlea removal. *Hear Res* 54: 281– 295.
- Code RA, Rubel EW (1989). Glycine-immunoreactivity in the auditory brain stem of the chick. *Hear Res* 40: 167–172.
- Coleman WL, Fischl MJ, Weimann SR, Burger RM (2011). GABAergic and glycinergic inhibition modulate monaural auditory response properties in the avian superior olivary nucleus. *J Neurophysiol* 2011 May;105(5):2405-20.
- Conlee JW and Parks TN (1986). Origin of ascending auditory projections to the nucleus mesencephalicus lateralis pars dorsalis in the chicken. *Brain Res* 367: 1-2: 96-113.
- Cook DL, Schwindt PC, Grande LA, Spain WJ (2003). Synaptic depression in the localization of sound. *Nature* 421, 66-70.

- Couchman K, Grothe B, Felmy F (2010). Medial superior olivary neurons receive surprisingly few excitatory and inhibitory inputs with balanced strength and short-term dynamics. *J Neurosci* 30, 17111-17121.
- Darrow KN, Maison SF, Liberman MC (2006). Cochlear efferent feedback balances interaural sensitivity. *Nat Neurosci*. 9(12),1474-6.
- Dasika VK, White JA, Carney LH, Colburn HS (2005). Effects of inhibitory feedback in a network model of avian brain stem. *J Neurophysiol* 94: 1: 400-14, 2005.
- Day ML, Semple MN (2011). Frequency-dependent interaural delays in the medial superior olive: implications for interaural cochlear delays. *J Neurophysiol* 106:1985-1999.
- Dehmel S, Kopp-Scheinflug C, Weick M, Dörrscheidt GJ, Rübsamen R (2010). Transmission of phase-coupling accuracy from the auditory nerve to spherical bushy cells in the Mongolian gerbil. *Hear Res*. Sep 1; 268(1-2):234-49.
- Dugué GP, Dumoulin A, Triller A, Dieudonne S (2005). Target-dependent use of co-released inhibitory transmitters at central synapses. *J Neurosci* 25: 6490–6498.
- Dumoulin A, Rostaing P, Bedet C, Lévi S, Isambert MF, Henry JP, Triller A, Gasnier B (1999). Presence of the vesicular inhibitory amino acid transporter in GABAergic and glycinergic synaptic terminal boutons. *J Cell Sci*. Mar;112 (Pt 6):811-23.
- Ebert U, Ostwald J (1995a). GABA alters the discharge pattern of chopper neurons in the rat ventral cochlear nucleus. *Hear Res* 91: 1-2: 160-6.
- Ebert U, Ostwald J (1995b). GABA can improve acoustic contrast in the rat ventral cochlear nucleus. *Exp Brain Res* 104: 2: 310-22.
- Eulenburg V, Armsen W, Betz H, Gomeza J (2005). Glycine transporters: essential regulators of neurotransmission. *Trends Biochem Sci*. Jun; 30(6):325-33.
- Friauf E (1995). C-fos immunocytochemical evidence for acoustic pathway mapping in rats. *Behav Brain Res*. 1995 Jan 23;66(1-2):217-24
- Fukui I, Sato T, Ohmori H (2006). Improvement of phase information at low sound frequency in nucleus magnocellularis of the chicken. *J Neurophysiol* 96: 633–641.
- Fukui I, Burger RM, Ohmori H, Rubel, EW (2010). GABAergic inhibition sharpens the frequency tuning and enhances phase locking in chicken nucleus magnocellularis neurons. *J Neurosci* 30, 12075-12083.
- Funabiki K, Koyano K, Ohmori H (1998). The role of GABAergic inputs for coincidence detection in the neurones of nucleus laminaris of the chick. *J Physiol* 508: 851–869.

- Gillespie DC, Kim G, Kandler K (2005). Inhibitory synapses in the developing auditory system are glutamatergic. *Nat Neurosci* 8, 332-338, DOI: 10.1038/nn1397.
- Goldberg JM, Brown PB (1969). Response of binaural neurons of dog superior olivary complex to dichotic tonal stimuli: some physiological mechanisms of sound localization. *J Neurophysiol* 32, 613-36.
- Grothe B, Pecka M, McAlpine, D (2010). Mechanisms of sound localization in mammals. *Physiol Rev* 90, 983-1012.
- Grothe B, Sanes DH (1993). Bilateral inhibition by glycinergic afferents in the medial superior olive. *J Neurophysiol* 69, 1192-6.
- Hahner L, McQuilkin, Harris RA (1991). Cerebellar GABAB receptors modulate function of GABAA receptors. *FASEB J* 5, 2466-2472.
- Hancock KE, Delgutte B (2004). A physiologically based model of interaural time difference discrimination. *J Neurosci* 24: 7110–7117.
- Hassfurth B, Grothe B, Koch, U (2010). The mammalian interaural time difference detection circuit is differentially controlled by GABAB receptors during development. *J Neurosci* 30, 9715-9727.
- Held H (1893). Die zentrale Gehörleitung. *Arch Anat Physiol Anat Abtheil* 17: 201–248, 1893.
- Hermann, J, Pecka, M, von Gersdorff, H, Grothe, B & Klug, A (2007). Synaptic transmission at the calyx of Held under in vivo like activity levels. *J Neurophysiol* 98, 2, 807-820.
- Howard MA, Burger RM and Rubel EW (2007). A developmental switch to GABAergic inhibition dependent on increases in Kv1-type K⁺ currents. *J Neurosci* 27: 8: 2112-2123.
- Hyson RL (2005). The analysis of interaural time differences in the chick brain stem. *Physiol Behav* 86: 3: 297-305.
- Hyson RL, Reyes AD, Rubel EW (1995). A depolarizing inhibitory response to GABA in brainstem auditory neurons of the chick. *Brain Res* 677:117-26.
- Jeffress LA (1948). A place theory of sound localization. *J Comp Physiol Psychol* 41: 35–39.
- Jercog PE, Svirskis G, Kotak VC, Sanes DH, Rinzel J (2010). Asymmetric excitatory synaptic dynamics underlie interaural time difference processing in the auditory system. *PLoS Biol* 8, e1000406.

- Jonas P, Bischofberger J and Sandkuhler J (1998). Corelease of two fast neurotransmitters at a central synapse. *Science* 281: 5375: 419-424.
- Joris PX, Carney LH, Smith PH, Yin, TC (1994). Enhancement of neural synchronization in the anteroventral cochlear nucleus. I. Responses to tones at the characteristic frequency. *J Neurophysiol* 71, 1022-36.
- Joseph AW, Hyson RL (1993). Coincidence detection by binaural neurons in the chick brain stem. *J Neurophysiol* 69: 1197–1211.
- Kalinina NI, Kurchavyi GG, Amakhin DV, Veselkin NP (2009). Differences in the activation of inhibitory motoneuron receptors in the frog *Rana ridibunda* by GABA and glycine and their interaction. *Neurosci Behav Physiol*. Oct; 39(8):775-83.
- Kalloniatis M, Fletcher EL (1993). Immunocytochemical localization of the amino acid neurotransmitters in the chicken retina. *J Comp Neurol* 336: 2: 174-193.
- Kandler K, Friauf E (1995). Development of glycinergic and glutamatergic synaptic transmission in the auditory brainstem of perinatal rats. *J Neurosci* 15: 10: 6890-904.
- Karlsson U, Druzin M, Johansson S (2011). Cl(-) concentration changes and desensitization of GABA(A) and glycine receptors. *J Gen Physiol*. Dec;138(6):609-26.
- Kim G, Kandler K (2003). Elimination and strengthening of glycinergic/GABAergic connections during tonotopic map formation. *Nat Neurosci* 6: 3: 282-290.
- Konishi M (2003). Coding of auditory space. *Annu Rev Neurosci* 26: 31–55.
- Kopp-Scheinflug C, Dehmel S, Dorrscheidt GJ, Rubsamen R (2002). Interaction of excitation and inhibition in anteroventral cochlear nucleus neurons that receive large endbulb synaptic endings. *J Neurosci* 22: 24: 11004-18.
- Kopp-Scheinflug C, Tolnai S, Malmierca MS, Rubsamen, R (2008). The medial nucleus of the trapezoid body: comparative physiology. *Neuroscience* 154, 160-170.
- Köppl C (1994). Auditory nerve terminals in the cochlear nucleus magnocellularis: differences between low and high frequencies. *J Comp Neurol*. Jan 15; 339(3):438-46.
- Köppl C (1997). Phase locking to high frequencies in the auditory nerve and cochlear nucleus magnocellularis of the barn owl, *Tyto alba*. *J Neurosci* 17: 3312–3321.
- Köppl C, Carr CE (2008). Maps of interaural time difference in the chicken's brainstem nucleus laminaris. *Biol Cybern* 98: 6: 541-559.

Köppel C, Carr CE (2003). Computational diversity in the cochlear nucleus angularis of the barn owl. *J Neurophysiol* 89: 4: 2313-29.

Korada S, Schwartz IR (1999). Development of GABA, glycine, and their receptors in the auditory brainstem of gerbil: a light and electron microscopic study. *J Comp Neurol* 409, 664-81.

Kotak VC, Korada S, Schwartz IR, Sanes DH (1998). A developmental shift from GABAergic to glycinergic transmission in the central auditory system. *J Neurosci* 18: 12: 4646-55, 1998.

Kuba H, Koyano K, Ohmori H (2002). Synaptic depression improves coincidence detection in the nucleus laminaris in brainstem slices of the chick embryo. *Eur J Neurosci* 15, 984-90.

Kuenzel T, Borst JG, van der Heijden M (2011). Factors controlling the input-output relationship of spherical bushy cells in the gerbil cochlear nucleus. *J Neurosci*. Mar 16; 31(11):4260-73.

Kuo SP, Bradley LA, Trussell LO (2009). Heterogeneous kinetics and pharmacology of synaptic inhibition in the chick auditory brainstem. *J Neurosci* 29: 30: 9625-9634.

Kuwabara, N & Zook, JM (1992). Projections to the medial superior olive from the medial and lateral nuclei of the trapezoid body in rodents and bats. *J Comp Neurol* 324, 522-38.

Lachica EA, Rubsamén R, Rubel EW (1994). GABAergic terminals in nucleus magnocellularis and laminaris originate from the superior olivary nucleus. *J Comp Neurol* 348: 3: 403-18, 1994.

Leibold, C (2010). Influence of inhibitory synaptic kinetics on the interaural time difference sensitivity in a linear model of binaural coincidence detection. *J Acoust Soc Am* 127, 931-942.

Li Y, Wu LJ, Legendre P, Xu TL (2003). Asymmetric cross-inhibition between GABA_A and glycine receptors in rat spinal dorsal horn neurons. *J Biol Chem* 278, 38637-38645.

Lu T, Rubio ME, Trussell LO (2008). Glycinergic transmission shaped by the corelease of GABA in a mammalian auditory synapse. *Neuron* 57: 4: 524-535.

Lu T and Trussell LO (2000). Inhibitory transmission mediated by asynchronous transmitter release. *Neuron* 26: 3: 683-94.

Lu T, Trussell LO (2001). Mixed excitatory and inhibitory GABA-mediated transmission in chick cochlear nucleus. *J Physiol* 535: 125–131.

- Lu Y, Burger RM, Rubel EW (2005). GABA(B) receptor activation modulates GABA(A) receptor-mediated inhibition in chicken nucleus magnocellularis neurons. *J Neurophysiol* 93: 1429-38.
- Magnusson AK, Kapfer C, Grothe B, Koch U (2005). Maturation of Glycinergic Inhibition in the Gerbil Medial Superior Olive after Hearing Onset. *J Physiol* 568: Pt 2: 497-512.
- Magnusson AK, Park TJ, Pecka M, Grothe B, Koch, U (2008). Retrograde GABA signaling adjusts sound localization by balancing excitation and inhibition in the brainstem. *Neuron* 59, 125-137.
- Mathews PJ, Jercog PE, Rinzel J, Scott LL, Golding NL (2010). Control of submillisecond synaptic timing in binaural coincidence detectors by K(v)1 channels. *Nat Neurosci* 13, 601-609.
- McAlpine D, Jiang D, Palmer AR (2001). A neural code for low-frequency sound localization in mammals. *Nat Neurosci* 4: 396-401.
- McIntire SL, Reimer RJ, Schuske K, Edwards RH, Jorgensen EM (1997). Identification and characterization of the vesicular GABA transporter. *Nature*. Oct 23; 389 (6653): 870-6.
- Moiseff A, Konishi M (1983). Binaural characteristics of units in the owl's brainstem auditory pathway: precursors of restricted spatial receptive fields. *J Neurosci* 3: 12: 2553-62.
- Monsivais P, Rubel EW (2001). Accommodation enhances depolarizing inhibition in central neurons. *J Neurosci* 21:7823-30.
- Monsivais P, Yang L, Rubel EW (2000). GABAergic inhibition in nucleus magnocellularis: Implications for phase locking in the avian auditory brainstem. *J Neurosci* 20:2954-63.
- Morest DK. (1968). The collateral system of the medial nucleus of the trapezoid body of the cat its neuronal architecture and relation to the olivo-cochlear bundle. *Brain Res.* Jul;9(2):288-311
- Moroni M, Biro I, Giugliano M, Vijayan R, Biggin PC, Beato M, Sivilotti LG (2011). Chloride ions in the pore of glycine and GABA channels shape the time course and voltage dependence of agonist currents. *J Neurosci.* Oct 5;31(40):14095-106.
- Müller CM (1987) gamma-Aminobutyric acid immunoreactivity in brainstem auditory nuclei of the chicken. *Neurosci Lett* 77:272-276.

- Nabekura J, Katsurabayashi S, Kakazu Y, Shibata S, Matsubara A, Jinno S, Mizoguchi Y, Sasaki A, Ishibashi, H (2004). Developmental switch from GABA to glycine release in single central synaptic terminals. *Nat Neurosci* 7, 17-23.
- Nishino E, Yamada R, Kuba H, Hioki H, Furuta T, Kaneko T, Ohmori, H (2008). Sound-intensity-dependent compensation for the small interaural time difference cue for sound source localization. *J Neurosci* 28, 7153-7164.
- Okuda H, Yamada R, Kuba H, Ohmori H (2013). Activation of metabotropic glutamate receptors improves the accuracy of coincidence detection by presynaptic mechanisms in the nucleus laminaris of the chick. *J Physiol*. Jan 1;591(Pt 1):365-78.
- Oleskevich S and Walmsley B (2002). Synaptic transmission in the auditory brainstem of normal and congenitally deaf mice. *J Physiol* 540: Pt 2: 447-455.
- Otis, TS, Trussell, LO (1996). Inhibition of transmitter release shortens the duration of the excitatory synaptic current at a calyceal synapse. *J Neurophysiol* 76, 3584-3588.
- Osen KK (1969). Cytoarchitecture of the cochlear nuclei in the cat. *J Comp Neurol* 136:453-484.
- Overholt, EM, Rubel, EW, Hyson, RL (1992). A circuit for coding interaural time differences in the chick brainstem. *J Neurosci* 12, 1698-708.
- Parks TN, Rubel EW (1975). Organization and development of brain stem auditory nuclei of the chicken: Organization of projections from n. magnocellularis to n. laminaris. *J Comp Neurol* 164:435-48.
- Pecka M, Brand A, Behrend O, Grothe B (2008). Interaural time difference processing in the mammalian medial superior olive: the role of glycinergic inhibition. *J Neurosci* 28.
- Pecka M, Siveke I, Grothe B, Lesica NA (2010). Enhancement of ITD coding within the initial stages of the auditory pathway. *J Neurophysiol* 103, 38-46.
- Pena JL, Viète S, Albeck Y, Konishi M (1996). Tolerance to sound intensity of binaural coincidence detection in the nucleus laminaris of the owl. *J Neurosci* 16, 7046-54.
- Pfeiffer F, Simler R, Grenningloh G, Betz H (1984). Monoclonal antibodies and peptide mapping reveal structural similarities between the subunits of the glycine receptor of rat spinal cord. *Proc Natl Acad Sci U S A* 81: 22: 7224-7227.
- Price CJ, Scott R, Rusakov DA, Capogna M (2008). GABA(B) receptor modulation of feedforward inhibition through hippocampal neurogliaform cells. *J Neurosci* 28, 6974-6982.
- Ramón y Cajal, S (1909). *Histology of the Nervous System of Man and Vertebrates*. Oxford University Press. 1995.

- Raman IM, Trussell LO (1992). The kinetics of the response to glutamate and kainite in neurons of the avian cochlear nucleus. *Neuron*, Jul;9(1):173-86.
- Rautenberg PL, Grothe B, Felmy, F (2009). Quantification of the three-dimensional morphology of coincidence detector neurons in the medial superior olive of gerbils during late postnatal development. *J Comp Neurol* 517, 385-396.
- Rayleigh L. (1907). On our perception of sound direction. *Philos Mag* 13(6th Ser):214–32.
- Recanzone GH, Beckerman NS (2004). Effects of intensity and location on sound location discrimination in macaque monkeys. *Hear Res* 198, 116-124.
- Rhode WS, Greenberg S (1994). Encoding of amplitude modulation in the cochlear nucleus of the cat. *J Neurophysiol*. May;71(5):1797-825.
- Rubel EW, Fritzsche B (2002). Auditory system development: primary auditory neurons and their targets. *Annu Rev Neurosci* 25: 51-101.
- Rubel EW, Parks TN (1975). Organization and development of brain stem auditory nuclei of the chicken: tonotopic organization of n. magnocellularis and n. laminaris. *J Comp Neurol* 4: 411-33.
- Sagne C, El Mestikawy S, Isambert MF, Hamon M, Henry JP, Giros B, Gasnier B (1997). Cloning of a functional vesicular GABA and glycine transporter by screening of genome databases. *FEBS Lett*. Nov 10;417(2):177-83.
- Schroder S, Hoch W, Becker CM, Grenningloh G and Betz H (1991). Mapping of antigenic epitopes on the alpha 1 subunit of the inhibitory glycine receptor. *Biochemistry* 30: 1: 42-47.
- Schuller G, Radtke-Schuller S and Betz M (1986). A stereotaxic method for small animals using experimentally determined reference profiles. *J Neurosci Methods* 18: 4: 339-350.
- Scott LL, Mathews PJ, Golding NL (2010). Perisomatic voltage-gated sodium channels actively maintain linear synaptic integration in principal neurons of the medial superior olive. *J Neurosci* 30, 2039-2050.
- Scott LL, Mathews PJ, Golding, NL (2005). Posthearing developmental refinement of temporal processing in principal neurons of the medial superior olive. *J Neurosci* 25, 7887-95.
- Seidl AH, Rubel EW, Harris DM (2010). Mechanisms for adjusting in- teraural time differences to achieve binaural coincidence detection. *J Neurosci* 30: 70-80.

- Siveke I, Pecka M, Seidl AH, Baudoux S, Grothe B (2006). Binaural response properties of low-frequency neurons in the gerbil dorsal nucleus of the lateral lemniscus. *J Neurophysiol* 96: 1425–1440.
- Smith PH, Joris PX, Carney LH, Yin TC (1991). Projections of physiologically characterized globular bushy cell axons from the cochlear nucleus of the cat. *J Comp Neurol* 304: 387–407.
- Smith PH, Joris PX, Yin TC (1993). Projections of physiologically characterized spherical bushy cell axons from the cochlear nucleus of the cat: evidence for delay lines to the medial superior olive. *J Comp Neurol* 331: 245–260.
- Smith PH, Joris PX, Yin TC (1998). Anatomy and physiology of principal cells of the medial nucleus of the trapezoid body (MNTB) of the cat. *J Neurophysiol* 79: 6: 3127-42.
- Smith AJ, Owens S, Forsythe ID (2000). Characterisation of inhibitory and excitatory postsynaptic currents of the rat medial superior olive. *J Physiol (Lond)* 529 Pt 3, 681-98.
- Spirou GA, Berrebi AS (1997). Glycine immunoreactivity in the lateral nucleus of the trapezoid body of the cat. *J Comp Neurol* 383, 473-488.
- Su TI, Recanzone GH (2001). Differential effect of near-threshold stimulus intensities on sound localization performance in azimuth and elevation in normal human subjects. *J Assoc Res Otolaryngol* 2, 246-256.
- Sullivan WE, Konishi M (1984). Segregation of stimulus phase and intensity coding in the cochlear nucleus of the barn owl. *J Neurosci.* Jul;4(7):1787-99.
- Sullivan WE, Konishi M (1986). Neural map of interaural phase difference in the owl's brainstem. *Proc Natl Acad Sci U S A* 83:8400-4.
- Tabor KM, Wong RO and Rubel EW (2011). Topography and morphology of the inhibitory projection from superior olivary nucleus to nucleus laminaris in chickens (*Gallus gallus*). *J Comp Neurol* 519: 2: 358-375.
- Takahashi TT, Konishi M (1988). Projections of nucleus angularis and nucleus laminaris to the lateral lemniscal nuclear complex of the barn owl. *J Comp Neurol* 274: 2: 212-38.
- Tanaka I, Ezure K (2004). Overall distribution of GLYT2 mRNA-containing versus GAD67 mRNA-containing neurons and colocalization of both mRNAs in midbrain, pons, and cerebellum in rats. *Neurosci Res* 49: 2: 165-178.
- Tang ZQ, Gao H, Lu Y (2009). Control of a depolarizing GABAergic input in an auditory coincidence detection circuit. *J Neurophysiol.* Sep;102(3):1672-83.

- Thompson AM, Schofield BR (2000). Afferent projections of the superior olivary complex. *Microsc Res Tech* 51, 330-54.
- Thompson SP (1882). On the function of the two ears in the perception of space. *Philos Mag* 13: 406–416
- Tsen G, Williams B, Allaire P, Zhou YD, Ikononov O, Kondova I, Jacob MH (2000). Receptors with opposing functions are in postsynaptic microdomains under one presynaptic terminal. *Nat Neurosci* 3: 126–132.
- Viete S, Pena JL and Konishi M (1997). Effects of interaural intensity difference on the processing of interaural time difference in the owl's nucleus laminaris. *J Neurosci* 17: 5: 1815-24.
- von Bartheld CS, Code RA, Rubel EW (1989). GABAergic neurons in brainstem auditory nuclei of the chick: distribution, morphology, and connectivity. *J Comp Neurol* 287:470 – 483.
- von Békésy G. (1970). Travelling waves as frequency analysers in the cochlea. *Nature*; Mar 28;225(5239):1207-9.
- von Gersdorff H, Borst JG (2002). Short-term plasticity at the calyx of held. *Nat Rev Neurosci* 3: 53–64.
- von Gersdorff H, Schneggenburger R, Weis S, Neher E (1997). Presynaptic depression at a calyx synapse: the small contribution of metabotropic glutamate receptors. *J Neurosci* 17, 21, 8137-8146.
- Warr WB. (1966). Fiber degeneration following lesions in the anterior ventral cochlear nucleus of the cat. *Exp Neurol* 14:453–74.
- Wentholt RJ, Huie D, Altschuler RA, Reeks KA (1987). Glycine immunoreactivity localized in the cochlear nucleus and superior olivary complex. *Neuroscience* 22: 897–912.
- Westerberg BD, Schwarz DW (1995). Connections of the superior olive in the chicken. *J Otolaryngol* 24: 1: 20-30, 1995.
- Wojcik SM, Katsurabayashi S, Guillemin I, Friauf E, Rosenmund C, Brose N, Rhee JS (2006). A shared vesicular carrier allows synaptic corelease of GABA and glycine. *Neuron*. May 18;50(4):575-87.
- Yamada R, Okuda H, Kuba H, Nishino E, Ishii TM, Ohmori H (2013). The Cooperation of Sustained and Phasic Inhibitions Increases the Contrast of ITD-Tuning in Low-Frequency Neurons of the Chick Nucleus Laminaris. *J Neurosci*. Feb 27;33(9):3927-38.

Yang L, Monsivais P, Rubel EW (1999). The superior olivary nucleus and its influence on nucleus laminaris: A source of inhibitory feedback for coincidence detection in the avian auditory brainstem. *J Neurosci* 19:2313-25.

Yin TC, Chan JC (1990). Interaural time sensitivity in medial superior olive of cat. *J Neurophysiol* 64, 465-88.

Young ED, Rubel EW (1983). Frequency-specific projections of individual neurons in chick brainstem auditory nuclei. *J Neuroscience* 3: 1373–1378.

Zhang S, Trussell LO (1994). Voltage clamp analysis of excitatory synaptic transmission in the avian nucleus magnocellularis. *J Physiol* 480 (Pt 1), 123-136.

Zhou Y, Carney LH, Colburn HS (2005). A model for interaural time difference sensitivity in the medial superior olive: interaction of excitatory and inhibitory synaptic inputs, channel dynamics, and cellular morphology. *J Neurosci* 25, 3046-3058.

Vita

MATTHEW J FISCHL

Curriculum Vitae

Contact Information

<i>Address</i>	<i>Phone</i>	<i>E-mail</i>
920 W. Lehigh St. Bethlehem, PA 18018	484-515-9938	mjf206@lehigh.edu

Education

Lehigh University <i>Integrative Biology, Ph.D. program</i> 2006-Present	Bethlehem, PA
--	---------------

East Stroudsburg University <i>BS in Biology, May 2003</i> Minor: Chemistry	East Stroudsburg, PA
---	----------------------

Honors and Awards

Magna Cum Laude Graduate - East Stroudsburg University, May 2003
Marjorie Nemes Fellowship Recipient – Lehigh University, Spring 2011
Gordon C. Thorne Fellowship Recipient – Lehigh University, Spring 2012

Research Experience

PhD Dissertation

Lehigh University

Spring 2007 – Spring 2013

A comparative study on the modulatory effects of inhibition in mammalian and avian sound localization circuits

For my dissertation, I have focused on the role of inhibition in shaping the excitability of neurons involved in sound localization circuits. In the avian system, the main source of inhibitory input in the auditory brainstem is the superior olivary nucleus (SON). To date, much research has focused on the effects of the SON's inhibition on response properties of its targets with little research on the SON itself. My work utilizes *in vitro* whole cell patch clamping techniques to assay intrinsic properties and morphology of SON neurons as well as the synaptic physiology in this region. Through this work I have shown that SON neurons have a diversity of response properties during current injection protocols. I also have documented the existence of glycinergic transmission at SON synapses and have shown immunohistochemical evidence that the SON neurons themselves are the source of glycine (Coleman et al. 2011). My recent work has demonstrated that stimulation at physiologically relevant frequencies evokes glycinergic transmission in the nucleus magnocellularis, where inhibition was previously thought to be only GABAergic. I have also shown that this

glycinergic transmission is functionally relevant for the output of these neurons. My dissertation work on the mammalian circuit is detailed below.

***Howard Hughes Medical Institute Biosystems Dynamics Summer Institute Grant
Lehigh University***

Summer 2007 and Summer 2008

Modeling Local Synaptic Control in Neural Coincidence Detectors

This project focused on interdisciplinary collaboration between neurophysiology and mathematics to obtain physiological characteristics of coincidence detecting neurons in the gerbil medial superior olive (MSO) for use in a mathematical model meant to simulate coincidence detection scenarios involving both excitatory and inhibitory input to the MSO. My work here focused on the modulatory effects of GABA_B receptor activation and the functional consequences. I have showed that GABA_B receptor activation suppresses the amplitude of both excitatory and inhibitory inputs to the MSO, slows the decay timing on inhibitory currents, and decreases the amount of synaptic depression that occurs during repetitive stimulation. The net effect of these actions is that MSO neurons become more sensitive to interaural time disparities, which are cues that are used in sound localization processing. These *in vitro* results were confirmed and expanded using an *in silico* model which showed that each GABA_B dependent effect acted to improve selectivity of MSO neurons (Fischl et al. 2012).

MB Research Laboratories

Spinnerstown, PA

In Vitro Study Director

Jan. 2003 – Aug. 2006

Research here involved working on several NIH grants as well as developing *in vitro* cell and tissue culture protocols as alternatives to currently used animal tests. The grants included work on the local lymph node assay in mice, flow cytometry based analysis of mutagen induced undifferentiated DNA synthesis in various cell types, and a tissue based phototoxicity assay. I also developed, validated, and implemented a phototoxicity assay using murine 3T3 fibroblast cells.

Publications

Fischl MJ, Weimann SR, Kears MG and Burger RM. Slowly emerging glycinergic transmission enhances inhibition in the temporal processing pathway of the avian auditory system. *Submitted to Journal of Neuroscience April 2013.*

Fischl MJ and Burger RM. Transmission through glycine receptors modulates GABAergic inhibition in the avian brainstem. *In preparation*

Coleman WL, **Fischl MJ**, Weimann SR and Burger RM. GABAergic and glycinergic inhibition modulate monaural auditory response properties in the avian superior olivary nucleus. *J Neurophys.* 2011, May;105(5):2405-20. Epub 2011 Mar 2.

Fischl MJ, Combs TD, Klug A, Grothe B, Burger RM. Modulation of synaptic input by GABA_B receptors improves coincidence detection for computation of sound location. *J Physiol.* 2012 Jul 1;590(Pt 13):3047-66. Epub 2012 Apr 2.

Invited Presentations

- September 2012 Lehigh University Dept. of Biological Sciences, Bethlehem, PA
Gordon Thorne Fellowship Seminar
Glycine occludes GABAergic inhibition in the avian sound localization pathway
- February 2012 Biophysics Club, Lehigh University, Bethlehem, PA
Modulation of synaptic input by GABA_B receptors improves coincidence detection for computation of sound location
- March 2011 Lehigh University Dept. of Biological Sciences, Bethlehem, PA
Marjorie Nemes Fellowship Seminar
Sorting Synaptic Inputs: Novel Inhibitory Function in Neural Circuits for Sound Localization
- March 2011 Academic Symposium, Lehigh University, Bethlehem, PA
Exhibition of Student Research and Scholarship
Poster Presentation
Sorting Synaptic Inputs: Novel Inhibitory Function in Neural Circuits for Sound Localization

Conference Abstracts

36th Annual Midwinter Meeting of the Association for Research in Otolaryngology

February 2013

MJ Fischl, SR Weimann, MG Kearse and RM Burger. Glycine receptors expressed in “timing” neurons of the avian auditory brainstem modulate GABAergic inhibition.

Society for Neuroscience* **November 2012*

MJ Fischl, SR Weimann, MG Kearse and RM Burger. Glycine Occludes GABAergic Inhibition in the Avian Sound Localization Pathway.

Pennsylvania Network Meeting - Physics and Chemistry of Biological Systems

September 2012

MJ Fischl, SR Weimann, MG Kearse and RM Burger. Glycine Occludes GABAergic Inhibition in the Avian Sound Localization Pathway.

Society for Neuroscience* **November 2011*

MJ Fischl and RM Burger. Heterogeneity of Intrinsic Membrane Properties in the Avian Superior Olivary Nucleus

34th Annual Midwinter Meeting of the Association for Research in Otolaryngology

February 2011

MJ Fischl, S Oline, and RM Burger. GABA and Glycinergic Synaptic Transmission in the Avian Superior Olivary Nucleus

**33rd Annual Midwinter Meeting of the Association for Research in Otolaryngology
February 2010**

TD Combs, **M Fischl**, A Klug, and RM Burger. GABA_B Receptor Activation as a Mechanism for Maintaining Precise ITD Selectivity Under Varying Stimulus Conditions: an *In Vitro* Study.

WL Coleman, **M Fischl**, D Trause, and RM Burger. Physiological Heterogeneity in the Avian Superior Olivary Nucleus.

**32nd Annual Midwinter Meeting of the Association for Research in Otolaryngology
February 2009**

M Fischl, TD Combs, and RM Burger. Response Characteristics of the Avian Superior Olivary Nucleus.

American College of Toxicology Annual Meeting 2006

L Pratt, **M Fischl**, J Sallit, B Bowen, GL DeGeorge. Validation of an In Vitro Phototoxicity Test Using 3D Epidermal Tissue Models and Cytokine Endpoints

GL DeGeorge, M. Reeder, CA Kirk, T Ripper, S Litt, **M Fischl**, B Bowen, DR Cerven. Temporal Stability and Vehicle Effects on α -Hexylcinnamaldehyde Responses as a Positive Control in a Flow Cytometry-based LLNA

American College of Toxicology Annual Meeting 2005

CA Kirk, MK Reeder, TL Ripper, B Bowen, **M Fischl** and GL DeGeorge, Validation of a Non-Radioactive Flow Cytometry-based Unscheduled DNA Synthesis (FL-UDS) Assay

Teaching Experience

Teaching Assistantships at Lehigh University

Bacteriology Laboratory
Introduction to Cell and Molecular Biology Laboratory
Experimental Neuroscience Laboratory
Integrative and Comparative Biology Laboratory and Recitation

Guest Lectures

“Real life experiences with Bone Marrow Transplantation”
Immunology – Spring 2010 & 2011

Professional Affiliations and Service

Association for Research in Otolaryngology (2009 - present)
Society for Neuroscience (2011 - present)
Biological Organization of Graduate Students (Vice President 2009, President 2010)
Dean’s Advisory Council (2011-2012)

References

R. Michael Burger
Associate Professor
Department of Biological Sciences
Lehigh University
111 Research Drive
Bethlehem, PA 18015
Phone: (610) 758-5422
rmb206@Lehigh.EDU

Yong Lu
Associate Professor
Department of Anatomy and Neurobiology
Northeast Ohio Medical University
4209 St. Rt. 44, P.O. Box 95
Rootstown, Ohio 44272-0095
Phone: (330) 325-6656
ylu@neomed.edu